RECEIVED BY TIC JUL 12 1982

LBL-14278

Lawrence Berkeley Laboratory

UNIVERSITY OF CALIFORNIA

Materials & Molecular Research Division

INVESTIGATIONS OF THE POTENTIAL FUNCTIONS OF WEAKLY BOUND DIATOMIC MOLECULES AND LASER-ASSISTED EXCITIVE PENNING IONIZATION

James H. Goble, Jr.
(Ph.D. thesis)

May 1982

MASTER

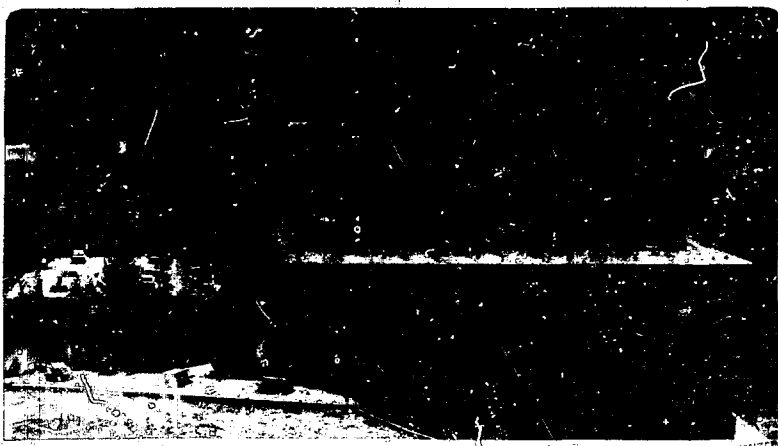

DISTRIBUTION OF THIS DOCUMENT IS UNLIMITED

Prepared for the U.S. Department of Energy under Contract DE-AC03-76SF00098

INVESTIGATIONS OF THE POTENTIAL FUNCTIONS OF WEAKLY BOUND DIATOMIC MOLECULES AND LASER-ASSISTED EXCITIVE PENNING IONIZATION

James H. Goble, Jr.

Materials and Molecular Research Division
Lawrence Berkeley Laboratory

and

Department of Chemistry, University of California
Berkeley, California 94720

LBL--14278

DE82 017259

ABSTRACT

Three variations on the Dunham series expansion function of the potential of a diatomic molecule are compared. The differences among these expansions lie in the choice of the expansion variable, λ. The functional form of these variables are $\lambda_S = 1-r_e/r$ for the Simon-Parr-Finlan version, $\lambda_T = 1-(r_e/r)^p$ for that of Thakkar, and $\lambda_H = 1-\exp(-\rho(r/r_e-1))$ for that of Huffaker.

A wide selection of molecular systems are examined. It is found that, for potentials in excess of thirty kcal/mole, the Huffaker expansion provides the best description of the three, extrapolating at large internuclear separation to a value within 10% of the true dissociation energy. For potentials that result from the interaction of excited states, all series expansions show poor behavior away from the equilibrium internuclear separation of the molecule. This property can be used as a qualitative diagnostic of interacting electronic states.

The series representation of the potentials of weakly bound molecules are examined in more detail. The ground states of $BeAr^+$, $HeNe^+$, NaAr, and Ar_2 and the excited states of $HeNe^+$, NaNe, and NaAr are best

NOTICE
PORTIONS OF THIS REPORT ARE ILLEGIBLE.
It has been reproduced from the best available copy to permit the broadest possible availability.

DISTRIBUTION OF THIS DOCUMENT IS UNLIMITED

described by the Thakkar expansion. Presumably this is because of the r^{-n} attractive forces that are responsible for the binding of these systems. Close examination of the potentials of the alkaline earth dimers suggests that covalent forces may be of importance in the bonding of these metals.

Finally, the observation of laser-assisted excitive Penning ionization in a flowing afterglow is reported. The reaction

$$Ar(^3P_2) + Ca + h\nu \rightarrow Ar + Ca^+(5p\ ^2P_J) + e^-$$

occurs when the photon energy, $h\nu$, is approximately equal to the energy difference between the metastable argon and one of the fine structure levels of the ion's doublet. By monitoring the cascade fluorescence of the above reaction and comparing it to the fluorescence from the field-free process

$$Ar(^3P_2) + Ca \rightarrow Ar + Ca^+(4p\ ^2P_J) + e^- \quad ,$$

a surprisingly large cross section of 6.7×10^3 $\mathring{A}^2$ is estimated. Mechanisms responsible for the resonant excitation and the large cross section are considered.

This is dedicated to the rest of the Gobles, and especially to my parents. It is as much their achievement as it is mine.

Acknowledgements

Except for the abstract and this acknowledgement, I consistently use the second person plural, "we", throughout this dissertation. This is not a pretense to royalty; it is an implicit acknowledgement of my research director, John Winn. For these many years he has been counselor, friend, and most important, teacher. He may have not found the burned out FET in the Baratron electronics, but he showed me how, and that I could. His support and encouragement were crucial at those times when I tended towards despair. I have benefitted from his scientific insight and chemical intuition, especially as to what is publishable material.

I want to express my gratitude to the "colleagues and co-workers" that have been as much as a family to me. Brian, Dave, Dennis, Henry, Susan, and Will provided the environment that made working there a joy. Especially appreciated are the legacy of Dennis Hartman and the assistance of Will Hollingsworth that made Chapter IV possible. The intellectual discourses with Henry Luftman, sometimes accented with raised voices, helped maintain a stimulating, academic atmosphere. A virtual member of the family, George Webber, is responsible for a feeling I have of how things on paper go together when they are made of metal.

Thanks to Howard Wood, for showing me how things are made out of metal. More important, the student shop provided a therapeutic means of working out my frustrations by making things instead of breaking them.

Special thanks go to the Mahan group for all the equipment we

borrowed and the comradery of elbow-bending at the Cheshire Cat. I am even beginning to miss the flavor of Anchor Steam on tap (a longing I did not think I would experience).

I would also like to thank Yuan T. Lee for the loan of his argon ion laser, dye laser, and the facilities for performing a series of photoacoustic spectroscopy experiments. Although this work is not reported here, the confidence- and character-building I experienced there has proven invaluable. I also thank the members of his research group for their assistance. The "can-do" attitude they enjoy continues to be an inspiration.

Thanks go to Steve Winkle, Pat Pakes, and Ken Smith for sharing, at one time or the other, their friendship and the cost of an abode. Thanks, "Wink", for inspiring me to learn how to cook. I thank Dennis and Paula Trevor for their warmth, hospitality, and the "little chickens" served on several Thanksgivings. I also thank Kate and the rest of the Lawheads for Christmas, 1980.

Thanks, Ninon, for the coffee cup with the frog inside.

I want to express my appreciation to Sheila Walsh for her work on the second virial coefficients of the Ar_2 potentials. I also thank Yuan Lee and Chris Becker for the Ar scattering data and scattering program. I also thank John Winn for the "refined Thakkar" of Ar_2 and the two Be_2 Thakkar potentials fitted to the ab initio points. I also thank Bowen Liu of IBM for his unpublished results on Mg_2.

Thanks go to Ann Weightman and Vera Spanos for turning my chicken scratchings into a readable dissertation and to Nancy Monroe and Andy Poynter for their artistic interpretation of my figures.

I also thank James Kinsey and his research group for their patience with my divided attentions while I have been writing the last three-quarters of this dissertation.

This work has been supported by the National Science Foundation, the National Resource for Computation in Chemistry, and the Division of Chemical Sciences, Office of Basic Energy Sciences, U. S. Department of Energy under Contract No. DE-AC03-76SF00098. The laser discussed in Chapter IV was borrowed from the San Francisco Laser Center, supported by NSF under Grant #CHE79-16250, awarded to the University of California at Berkeley in collaboration with Stanford University. I gratefully acknowledge the support from a University Regents' Intern Fellowship.

Finally, with all respects and reverences, I thank the Good Lord that this part of my life is completed.

TABLE OF CONTENTS

DEDICATION. i

ACKNOWLEDGEMENTS. ii

TABLE OF CONTENTS v

BIOGRAPHICAL NOTE vii

CHAPTER I. Introduction and Overview 1

References. 6

CHAPTER II. Diatomic Potential Determination and the Revival of Series Potential

A. Introduction 8

B. JWKB Solution. 10

C. The Dunham Solution. 14

D. RKR Method 18

E. The Empirical Series Strikes Back. 22

F. Further Convergence Considerations 30

G. The Program. 32

H. The Roads-Not-Taken. 35

I. General Observations 39

J. The Question of Higher a_n's. 49

K. Conclusions. 53

References 55

Tables 61

Figures. 69

CHAPTER III. Series Potentials Applied to Weakly Bound Molecules

A. Introduction 72

B. $BeAr^+$. 76

C. Other Molecular Ions 86

D. NaNe and NaAr 92

E. Ar_2 103

F. Alkaline Earth Dimers 113

G. Direct Fit 122

H. Conclusion 127

References 129

Tables 136

Figures 159

CHAPTER IV. Laser Assisted Penning Ionization

A. Introduction 176

B. Experimental 181

C. Signal Treatment and Results 185

D. Discussion 188

E. Theoretical Considerations 192

F. Future Considerations 198

G. Conclusion 200

References 201

Figures 205

Appendix I 209

Appendix II 256

James Henry Goble, Jr. was born December 16, 1952 in Longview, Texas and was raised in Fort Worth and Houston, Texas. He holds a Bachelor of Science degree in chemistry from the University of Texas, awarded in 1975. He is a member of Phi Beta Kappa, the American Chemical Society, the American Physical Society, and is a University of California Regents' Intern Fellow. He is, at this writing, a Postdoctoral Associate at the Massachusetts Institute of Technology.

Chapter I

Introduction and Overview

The main purpose of this work is to examine the nature of the bonding of weakly bound diatomic molecules. By "weakly bound", we mean binding energies of 30 kcal per mole or less. This energy regime is responsible for phenomena such as condensation, physical adsorption on surfaces, the adhesion in polycrystalline materials like ceramics, the binding in molecular crystals, the rates of ion-molecule reactions, and even the mechanism responsible for the high selectivity of enzymatic catalysis. We hope to shed some light on these kinds of forces by examining the attraction of the simplest of these systems: the weakly bound diatomic molecule.

The quantity that best describes this interaction is the intermolecular potential. Although there have been significant advances in the ab initio calculation of this potential from first principles[1], they rely on the cancellation of electron correlation errors between the molecule and those of the separated atoms. They generally tend to neglect spin-orbit interaction as well. Since such quantities are at least as large, and often larger, than the binding energies under consideration, the methods of empirically determining the potential function from experimental data, particularly spectroscopic data, must be used.

Perhaps the simplest method is the fitting of a simple, empirical potential function to spectroscopic[2], molecular beam scattering[3], or thermodynamic data[4]. Familiar examples are the Morse, Lennard-Jones 6-2, and exponential-6 functions. The drawbacks are that such functions

contain so few adjustable parameters that they may not describe the data to the accuracy known. Moreover, which functional form that seems suitable may depend upon the experiment performed.

As an example, consider the dimer of argon. Early spectroscopic work[5], dependent upon the curvature of the potential minimum, was interpreted in terms of a Morse function. In the high energy molecular beam scattering[6] the data were more sensitive to the repulsive wall, and the results were best described by a purely repulsive r^{-x} or exponential function. Thermodynamic data tend to be biased toward the long-range interactions and workers in this field[7] had found a Lennard-Jones 6-12 or the exponential-6 to be more appropriate. The situation was similar to the tale of several blind men describing the elephant.

At the other extreme of potential determinations is the Rydberg-Klein-Reese, or RKR, method[8] which does not produce an analytical potential at all. This algorithm determines the classical turning points of a potential from the spectroscopic data. The full potential is found by interpolation between the turning points. Although the method is limited to regions of the potential where data are available, new methods of extrapolation[9] have been developed for extending the potential to the dissociation limit.

The empirical technique that is examined in this work is that of J. L. Dunham[10] and the variations that have more recently appeared in the literature. Here the potential is expressed as a power series

$$V(r) = a_0\lambda^2(r)(1 + \sum_{n=1}^{\infty} a_n\lambda^n(r))$$

where the expansion coefficients are determined from the spectroscopic constants of a molecule as appropriate to the particular functional form of $\lambda(r)$. The Dunham series uses the expression

$$\lambda(r) = r/r_e - 1 \quad .$$

Because the radius of convergence of this series is limited to $r < 2r_e$,[11] the potential is unsatisfactory for the description of any but the lowest vibrational levels of the molecule. Clearly, it cannot predict the dissociation energy. Moreover, since the number of spectroscopic constants that can be determined is limited, the series must be truncated to a polynomial. Because the successive a_n's for most molecules tend to increase, the radius of convergence is even further restricted. For these reasons most workers in the past have eschewed the Dunham potential in favor of the RKR method.

It is unfortunate that the Dunham series method fails so miserably, since it not only provides a means for converting spectroscopic data into an analytical potential function but also generates potential constants that can be used to compare bonding trends among diatomic molecules[12]. Thus several workers have recently revived the series method by changing the form of $\lambda(r)$ and hence extending the radius convergence. Simons, Parr, and Finlan[13] had rearranged Dunham's expansion variable by defining $\lambda(r) = 1-r_e/r$. Thakkar[14] had generalized the rearrangement by defining $\lambda(r) = \mathrm{sgn}(p)(1-(r/r_e)^p)$. Huffaker[15] in turn had chosen the variable $\lambda(r) = 1-e^{-\rho(r/r_e-1)}$ since the leading term would be a Morse potential.

In Chapter II we review the method of Durham for determining a series potential from spectroscopic data. The RKR method and near-dissociation extrapolation are also briefly discussed since these are the methods of choice by spectroscopists and are the yard-sticks by which all other potential methods should be compared. The newer series potentials are then described and their descriptions of several molecular systems are compared. Of particular interest is the fact that the failure of these series potentials can be used as a diagnostic of interacting molecular states. This is true of even the Huffaker series, which we find superior to all other series potentials for ground state molecules bound by 50 kcal/mole or more.

Chapter III is a more selective and more detailed examination of series potentials for weakly bound molecules. In contrast to the results of Chapter II, we find that the Thakkar series gives the best description of weak binding in systems such as $BeAr^+$, NaAr, and Ar_2. We draw on our experiences from Chapter II to suggest that alkaline earth binding might be more than just van der Waals attraction. Finally, we suggest a procedure which may be more appropriate for fitting a potential to a weakly bound molecule when the amount of experimental data is limited.

Chapter IV is indirectly related to the previous two chapters in the sense that it involves very long-range interactions. Here, we report the observation of the opening of a new channel of excitive Penning ionization of calcium by absorption of a photon while colliding with a metastable ($^3P_2$) argon atom. The order-of-magnitude estimate

of this laser-assisted collisional cross section is in the neighborhood of thousands of square Ångströms, indicating some experimental support of previous theoretical speculation that this process should be long-range in nature. The laser excitation spectrum also shows resonance behavior, and this aspect is discussed as well.

REFERENCES

1. H. F. Schaefer III, Ann. Rev. Phys. Chem. 27, 261 (1976).

2. Y. P. Varshni, Rev. Mod. Phys. 29, 664 (1957); 31, 839 (1959); D. Steele, E. R. Lippencott, and J. T. Vanderslice, Rev. Mod. Phys. 34, 239 (1962).

3. H. Pauly, Atom-Molecule Collision Theory, edited by R. B. Bernstein (Plenum, New York, 1979), pp. 111-199.

4. G. C. Maitland and E. B. Smith, Chem. Soc. Rev. 2, 181 (1973).

5. Y. Tanaka and K. Yoshino, J. Chem. Phys. 53, 2012 (1970).

6. S. O. Colgate, J. E. Jordan, T. Amdur, and E. A. Mason, J. Chem. Phys. 51, 968 (1969).

7. G. C. Maitland and E. B. Smith, Molec. Phys. 22, 861 (1971); and ref. 4.

8. R. Rydberg, Z. Physik, 73, 376 (1931); O. Klein, Z. Physik, 76, 226 (1932); A. L. G. Rees, Proc. Phys. Soc. London A, 59, 998 (1947).

9. R. J. LeRoy and R. B. Bernstein, J. Chem. Phys., 52, 3869 (1970); R. J. LeRoy in Molecular Spectroscopy, 1, A Specialist Periodical Report, R. F. Barrow, D. A. Long, and D. J. Millen, eds. (Chemical Society, London, 1973) pp. 113-176.

10. J. L. Dunham, Phys. Rev. 41, 721 (1932).

11. C. L. Beckel and R. Engelke, J. Chem. Phys., 49, 5199 (1968).

12. G. V. Calder and K. Ruedenberg, J. Chem. Phys. 49, 5399 (1968); J. F. Ogilvie and D. Koo, J. Mol. Spectrosc. 61, 332 (1976).

13. G. Simons, R. G. Parr, J. M. Finlan, J. Chem. Phys. 59, 3229 (1973).

14. A. J. Thakkar, J. Chem. Phys. 62, 1693 (1975).

15. J. N. Huffaker, J. Chem. Phys. 64, 3175 (1976).

Chapter II

Diatomic Potential Determination and the Revival of the Series Potential

A. Introduction

The determination of the interatomic potential of a diatomic molecule from spectroscopic data is nearly as old as Quantum Mechanics itself. In fact, the standard RKR as well as the potential series determination procedures ultimately have their roots in the "Old Quantum Theory" (i.e. the Bohr-Sommerfeld integral), which predates the formalism of Heisenberg and Schroedinger.

In this chapter we will shake the dust from these roots and examine the semi-classical JWKB theory behind these potential determination procedures. Dunham's derivation of the relation between the series expansion parameters and the molecular spectroscopic constants is sketched and the limitations of his potential expansion are discussed. The alternative RKR method is reviewed and its limitations are considered.

These reviews set the stage for the purpose of this chapter: reconsidering the use of series expansions for describing the diatomic potential. The analytical series provides a simple yet flexible representation of a potential. Moreover, the series can be extrapolated to energy levels, including the dissociation level, which are not observed directly. The limitations associated with the Dunham expansion can be overcome by judicious choice of the expansion variable. The modifications which we will consider in particular are those of Simons, Parr, and Finlan, of Thakkar, and of Huffaker.

These modifications will be qualitatively and quantitatively compared for a wide variety of diatomic molecules.

B. JWKB Solution

Determination of the vibrational-rotational energies of a diatomic molecule begins with the solution of the Born-Oppenheimer approximation of the radial Schroedinger equation for the motion of the nuclei:

$$-B_e r_e^2 \frac{d^2\psi(r)}{dr^2} + (V(r) + B_e r_e^2 L^2/r^2)\psi(r) = E_{v,L}\,\psi(r).$$

The quantity $\psi(r)/r$ is the radial wavefunction for nuclear motion. The equilibrium rotational constant, B_e, is equal to $\frac{h^2}{2\mu r_e^2}$, where μ is the reduced mass of the nuclei and r_e is the internuclear separation at the potential minimum. The potential, $V(r)$, is the sum of the Born-Oppenheimer electron energies, internuclear repulsion, and if present, spin-orbit interactions. We define $V(r_e) = 0$ in this chapter. The eigenvalue is $E_{v,L}$, where the subscripts indicate the dependence upon vibrational and rotational quantum number, respectively.

The quantity L^2 is shorthand for the dependence of the "centrifugal repulsion" upon the angular momentum due to the rotation of the two nuclei about the center of mass. For $^1\Sigma$ molecules, $L^2 = J(J+1)$, where J is the total angular momentum of the molecule. For any other electronic state, the expression also depends upon the electronic orbital and spin momenta and how they are coupled to the nuclear rotation through the various Hund's coupling cases.[1,2] For simplicity, we assume that the molecule is $^1\Sigma$ in our discussion through this chapter.

In 1932, the above equation was solved by J. L. Dunham[7a] by means of the semi-classical JWKB method. Briefly, he assumed the form

$$\psi(r) = \exp(i\int^{r} y(x)dx/h)$$

and that y can be expanded in a power series in h:

$$y = y_0 + \frac{h}{i} y_1 + (\frac{h}{i})^2 y_2 + \ldots$$

The fact that he used h as an "expansion parameter" made this method a semi-classical one, i.e. as $h \to 0$ the system was more classical. The solution for y was

$$y_0 = \pm \sqrt{2\mu(E-U)}$$

$$y_1 = \frac{dU}{dr} / 4(E-U)$$

$$y_2 = \pm (5(\frac{dU}{dr})^2 + 4 \frac{d^2U}{dr^2} (E-U)/(32\sqrt{2\mu} (E-U)^{5/2})$$

and so on, where $U(r) = V(r) + B_e r_e^2 J(J+1)/r^2$. The general solution was

$$\psi = C_a \exp(i\int_P^r y_a(x)dx/h) + C_b \exp(i\int_P^r y_b(x)dx/h) ,$$

where the a and b subscripts referred to the choice of upper and lower signs, respectively, for y's of even subscripts. The quantity P referred to some particular value of r.

The problem with the general solution had been that it was not defined at the turning points and that values for C_a and C_b changed for different regions of the well; C_a or C_b had to be equal to zero inside or outside, respectively, of the potential well, where $E - U < 0$, and both had to be nonzero within the well. Dunham required that ψ be real and single valued and be related in the sense that the solution in the different regions have the common point P. By carrying the integration into the complex plane in order to avoid the singularities at the turning points he derived the quantization condition

$$h(v+1/2) = \oint \sqrt{2\mu(E-U)}\, dr - \frac{h}{32\sqrt{2\mu}} \oint \left(\frac{dU}{dr}\right)^2 (E-U)^{-5/2}\, dr + \ldots \quad ,$$

where $v = 0, 1, 2, \ldots$.

It is noted that if one neglects the second and higher integrals in the equation above, one has the old Bohr-Sommerfeld condition. This latter relationship can be derived from the JWKB solution through different means.[8] This condition has been the basis for the RKR method as well as the Dunham solution.

It has been pointed out[9] that Dunham's y expansion is an asymptotic series[10] in Planck's constant, h. Such a series is a sum of successive terms which at first decrease then increase and ultimately cause the series to diverge. By neglecting the successively increasing terms one obtains a polynomial which can be a good approximation to a

function one wishes to represent. Some workers[9a,b] have recommended that the third and higher JWKB terms be ignored, which would correspond to only evaluating the Born-Sommerfeld phase integral. Recently Kirschner and Leroy[11] have examined the second and third Dunham phase integrals and have found that, for all reasonable molecular states, these extra integrals provide an improved agreement between the true and semiclassical eigenvalues all the way up to the highest bound level.

C. The Dunham Solution

Having established his quantization condition, Dunham then proceeded[7b] by assuming the potential could be expanded in a power series

$$V(r) = a_o\lambda^2(1 + a_1 \lambda + a_2 \lambda^2 + a_3 \lambda^3 + \ldots) ,$$

where $\lambda = (r-r_e)/r_e$. By next assuming that the energy could be expressed in the form

$$E_{v,J} = \sum_{ij} Y_{ij}(v + 1/2)^i(J(J+1))^j ,$$

he solved for the Y_{ij}'s as functions of the a_n's. The expressions for Y_{00}, $Y_{10} - Y_{40}$, $Y_{01} - Y_{31}$, $Y_{02} - Y_{22}$, $Y_{03} - Y_{13}$, and Y_{04} are documented in his work. The validity of his method has been confirmed by Kilpatrick,[12] who obtained identical results using perturbation theory on a harmonic oscillator, treating the $a_1\lambda^3$ and higher terms as perturbations.

It should be noted that Dunham had generalized on an expression spectroscopists had customarily used at the time. The vibrational-rotational energy of a molecule is expanded as

$$E_{vJ} = G_v + B_vJ(J+1) - D_vJ^2(J+1)^2 + \ldots$$

where G_v is the vibrational energy, B_v and D_v are the rotational and centrifugal distortion constants respectively, and the subscripts indicate that these constants vary with vibrational quantum number v.

These terms are usually further expanded in the form

$$G_v = "\omega_e"(v+1/2) - \omega_e x_e (v+1/2)^2 + \omega_e y_e (v+1/2)^3 + \ldots$$

$$B_v = "B_e" - \alpha_e (v+1/2) + \delta_e (v+1/2)^2 + \ldots$$

and so on. The relationship between the Y_{i0}'s and the G_v expansion seems apparent except for some subtle differences Dunham had discovered between Y_{i0} and ω_e and between Y_{01} and B_e.

These differences can be seen from the general form (except for Y_{00}),

$$Y_{ij} = \omega_e \left(\frac{B_e}{\omega_e}\right)^{\nu} [f_{ij}(a_1, \ldots, a_\eta) + \left(\frac{B_e}{\omega_e}\right)^2 g_{ij}(a_1, \ldots, a_{\eta+4})$$

$$+ \left(\frac{B_e}{\omega_e}\right)^4 h_{ij}(a_1, \ldots, a_{\eta+8}) + \ldots] \quad ,$$

where $\omega_e = \sqrt{4B_e a_o}$, $\nu = i + 2j-1$, and $\eta = 2(i-1) + j$, such that $\nu \geq 0$ and $\eta \geq 1$. If η is -1 or 0, f_{ij} equals 1. Because $B_e << \omega_e$ for nearly all known molecules, the Y_{ij}'s tend to decrease for higher Y_{ij}'s and the functions g_{ij} and h_{ij}, the first and second order Dunham corrections, are of much less significance than f_{ij}.

It is found that although the f_{ij}'s are complicated algebraic functions of the lower a_n's, they are linear in the highest terms, the a_η's. This provides a means of solving for an a_η from its corresponding Y_{ij} and the lower a_n's. During the first iteration the g_{ij} and h_{ij} functions are neglected and a set of a_n's is determined.

When possible, the g_{ij}'s and h_{ij}'s are calculated and subtracted from their corresponding Y_{ij}'s and a new set of a_n's are determined. The process is repeated until the set converges to one's satisfaction.

Dunham's work provides enough expressions for the determination of the a_n's up to a_6 and the calculation of the first order corrections for Y_{10}, Y_{20}, Y_{01}, Y_{11}, and Y_{02}. This work has been extended by that of Sandeman[13] which permits the indirect determination of a_7 and a_8, the calculation of Y_{50}, Y_{60}, and Y_{41}, and which reports the expressions for more second order and a few third order corrections. Later Wooley[14] reported the simple expressions for a few more higher Y_{ij}'s. Niay and coworkers[15a] and Bouanich[15b] have recently published direct relations between the Y_{ij}'s and a_7 and a_8, eliminating the need for the calculation of the intermediate quantities in Sandeman's paper. Most recently, J. N. Huffaker has suggested a somewhat involved algorithm[41] for determining a set up to a_{20}. His work will be discussed in more detail later.

As mentioned in the introduction, the fatal flaw of the Dunham potential series is its poor convergence properties. It has been pointed out[16] that V(r) is infinite at r = 0 due to the Coulombic repulsion of the two nuclei. The Dunham series must therefore diverge for $\lambda = -1$. A property of any series

$$f(z) = \sum_{n=0}^{\infty} b_n z^n ,$$

for complex z, is that if the series diverges for $z = z_o$, it can only converge for values of z such that $|z|<|z_o|$, making $|z_o|$ the "radius of convergence" of the series. Thus the Dunham series must also diverge for $\lambda = +1$, meaning that the series is only useful in the region $0 < r < 2r_e$. Moreover, the values of the a_n's for nearly all molecules tend to increase as n increases. Since there can only be a finite number of Y_{ij}'s determined from a finite amount of spectroscopic data, the Dunham series must be truncated to a polynomial, and the increasing value of successive a_n's limits the usefullness of this polynomial to a region far less than the theoretical radius of convergence. Needless to say the estimation of the molecular dissociation energy by extrapolating the function at large r is out of the question.

Thus the Dunham potential was only of academic interest, except for calculating the properties of the lowest vibrational levels of a molecule whose outer turning points were well within the dreaded $2r_e$ limit. Fortunately for spectroscopists, another approach was being developed at the time Dunham was publishing his work.

D. RKR Method

Having evaluated the G_v, B_v, D_v, etc. constants from vibrational and/or electronic spectra, spectroscopists have traditionally determined the molecular potential by the Rydberg-Klein-Reese method.[17,18] For vibrational number v the classical inner and outer turning points, $r_-(v)$ and $r_+(v)$, for the rotationless (J=0) molecular potential can be found from

$$r_\pm(v) = f(v)([1+1/f(v)\cdot g(v)]^{1/2} \pm 1) \quad ,$$

where

$$f(v) = (B_e r_e^2)^{1/2} \int_{-1/2}^{v} [G_v - G_{v'}]^{-1/2} dv' \quad ,$$

$$g(v) = (B_e r_e^2)^{-1/2} \int_{-1/2}^{v} B_{v'} [G_v - G_{v'}]^{-1/2} dv' \quad ,$$

and B_e is in the same energy units as B_v and G_v. Furthermore

$$f(v) = \frac{1}{2}(r_+(v) - r_-(v)) \quad ,$$

$$g(v) = \frac{1}{2}(1/r_-(v) - 1/r_+(v)) \quad .$$

Although the physical interpretation of g(v) is not obvious, it is clear that f(v) is the width of the potential well at energy $E_{v,0}$. The f(v) and g(v) integrals are best evaluated numerically.[19,20] Although expressing $G_{v'}$ and $B_{v'}$ in terms of Y_{ij}'s can facilitate this

computation,[21] simple interpolation for non-integer v' can serve equally well.[18,20]

This latter point is of importance since the determination of a reliable set of Y_{ij}'s may not be feasible. Cashion[22] had found this to be the case for H_2. We had found a similar problem in trying to fit a set to all 20 known vibrational levels of HF.

It should be pointed out that the RKR method, like Dunham's, is based upon the semiclassical Bohr-Sommerfeld integral

$$h(v+1/2) = \frac{1}{\sqrt{2\mu}} \oint [E_{vJ}-U(r)]^{1/2} dr$$

where U(r) is the same as in Section A. Indeed, others[23] have shown the mathematical equivalence between the RKR and Dunham formulations. The main difference is the absence in the above expression of the higher order integrals Dunham had found. The most obvious breakdown is that $E_{vo} = 0$ when $v = -1/2$. This is not strictly correct since the true expression is

$$E_{vo} = G_v = Y_{00} + "\omega_e"(v+1/2) - \omega_e x_e (v+1/2)^2 + \ldots$$

Most workers shore up the RKR method by evaluating Y_{00} and setting the lower limit of the f and g integrals to that value of v so that the preceeding equation for G_v is zero. Other workers[24] have extended the RKR method to include the next Dunham integral. That such corrections are more important for HF than CO[24c] is in keeping with the premise that the semiclassical approximation is more successful for those molecules with larger reduced masses.

Although turning points can be extrapolated for vibrational levels above the highest observed level, their determination depends upon the reliability of the analytical expressions for G_v and B_v. A more physical extrapolation procedure has been suggested by Leroy and Bernstein.[25] They had assumed that the potential for the outer turning points of the upper vibrational levels can be approximated by the long-range behavior

$$V(r) = D_e - \frac{C_n}{r^n} ,$$

where D_e is the dissociation energy and where C_n and the integer n depend upon the atomic states into which the molecule dissociates. Further assuming that the inner turning point can be set to zero in the Bohr-Sommerfeld integral, they had arrived at the expression

$$D_e - G_v = [(v_D - v)\bar{H}_n/\mu^{1/2} \cdot C_n^{1/n}]^{2n/(n-2)} ,$$

where $\bar{H}_n$ is a numerical constant and v_D, corresponding to the fictitious, non-integral vibrational "quantum number" at dissociation, is a parameter which must be evaluated from the upper G_v data. The quantities D_e and C_n could either be evaluated from the G_v's or from independent determinations, although some of the most accurate D_e's have been made from the above or related expressions.

This "near-dissociation" analysis is useful for extending the potential if the upper vibrational levels are in the r^{-n} region of the potential. Recently, R. J. Leroy[26] has found that the upper levels may show near-dissociation behavior even when the limiting r^{-n} term

accounts for only a fraction of the potential in the region considered. Thus a successful near-dissociation analysis does not imply that the potential has passed into the long-range regime.

Although the inner turning points are not determined by the long-range method, the inner repulsive wall can be adequately estimated by fitting a simple function such as a Morse potential to the known inner turning points. It has been our experience that the vibrational wave-function and hence the physical properties it determines are far more sensitive to the shape of the outer attractive region than to the inner repulsive one.

E. The Empirical Series Strikes Back

Although it would seem that the RKR method is quite satisfactory for determining the molecular potential and some extoll its exclusive application over any other method,[27] there nevertheless remain some drawbacks. Since the method is numerical, the molecular information must be conveyed by tabulation of all the turning points, which can be quite lengthy. The only molecular parameters, useful for comparing bonding trends for different molecules, which can be readily determined are r_e and sometimes D_e. Even D_e must be extrapolated from the upper G_v's, a procedure which can be chancy unless a near-dissociation analysis is applied. As mentioned before, even a near-dissociation evaluation of D_e and C_n does not necessarily allow an immediately valid extension of the RKR potential (insertion of the near-dissociation expressions for G_v and B_v is not advisable since Leroy found that the ND expression for B_v to be unreliable).

Moreover, an error analysis is complicated by the numerical procedure and would require the reporting of individual standard deviations for the turning points (increasing the amount of information to be conveyed in literature), hence it is rarely performed or reported by most workers. Systematic errors of course remain hidden since the method is semiclassical, and first order at that. The numerical nature is itself inconvenient; many workers continue to determine dipole moment functions using the Dunham potential a_n's to evaluate perturbed harmonic oscillator wavefunctions.[11,28]

Thus the analytical potential function enjoys many advantages over the RKR potential. It is easy to work with. The number of parameters and associated errors that need to be reported are less than the number of turning points necessary. Moreover, the parameter errors yield uncertainty in the potential at a particular value of r, whereas the reverse is true of RKR; the former is more useful to users of a reported potential. The parameters themselves can have physical meaning and can be compared to establish relationships in bonding. Calder and Ruedenberg[29] have examined the Dunham a_1 and a_2 for 160 diatomics and were able to establish empirical relationships among ω_e, $\omega_e x_e$, B_e, and α_e for any atom-pair in the periodic table. Frost and Musulin also have examined a_1 and a_2 in search of a universal reduced diatomic potential curve, discovering that $(a_0 a_2)^{1/2}/a_1$ was equal to 0.86 within 10% for 23 different molecules. When an analytical function has a physical basis, extrapolation of the potential in undetermined regions is more reliable than RKR.

Of all analytical potential functions the series function is most suitable since it can be systematically improved with new data by adding higher order terms. Moreover, a series which is evaluated in the spirt of the Dunham method automatically incorporates the higher order WKB corrections missed by RKR. The problem with the Dunham series is that the leading term, $a_0\lambda^2$, is a harmonic oscillator. Thus one does not have to resort to a mathematical analysis to see why the series fails; the higher order terms can hardly be corrections in order for the series to simulate a realistic diatomic potential.

Simons, Parr, and Finlan[31] (hereafter known as SPF) suggested the modification $\lambda_s = 1 - r/r_e$, for the series

$$V(r) = b_0\lambda_s^2(1 + \sum_{n=1} b_n \lambda_s^n)$$

would extend the radius of convergence, since the pole in the true V(r) at r = 0 does not correspond to a finite λ_s. By requiring that all derivatives of their series be equal to all derivatives of the Dunham series at $r = r_e$, they established the relationship

$$b_n = a_n - \sum_{i=1}^{n-1} (-1)^i \binom{n+1}{i} b_{n-i} - (-1)^n (n+1)$$

for $n \geq 1$ and $b_0 = a_0$, where $\binom{m}{j}$ is the binomial coefficient $\frac{m!}{(m-j)!j!}$. Thus having determined a set of Dunham a_n's, they could successively determine a set of b_n's quite easily. By requiring that the series have the correct r^{-m} behavior at long range, i.e. setting the boundary conditions

$$\lim_{r \to \infty} (r^2 \frac{d^k}{dr^k} V(r)) = 0 \quad , \qquad k < m \quad ,$$

they could easily generate up to m - 1 extra coefficients.

This series expansion has been applied to not only diatomic molecules, but to linear[32] and bent[33] triatomic molecules as well. Moreover it has been used to model chemisorption interactions.[34] Bickes and Bernstein have fitted the SPF expansion to pre-determined van der

Waals potentials[35] and have used it to invert molecular beam elastic scattering data.[36] The series' improved theoretical convergence radius, its versatility, and SPF's assertion that *it had a theoretical basis made the SPF* expansion seem very promising.

From a pragmatic point of view, the leading term of the series is the Kratzer-Fues[37] potential, which had been used as a model potential by early spectroscopists. It is generally recognized,[13,38] however, that the Kratzer-Fues function is not a very good representation of true molecular interactions. This may explain why the SPF series, although having a range of convergence larger than that of Dunham's, tends to diverge before $3 \cdot r_e$, going to very, very large or sometimes even very negative values at $\lambda_s = 1$, or as $r \to \infty$. Although Simons and Finlan found[31b] that adding a few "boundary condition" coefficients improved convergence, the number of extra terms taken is somewhat arbitrary.

Thakkar[39] generalized the Dunham and SPF series by defining

$$\lambda_r = \mathrm{sgn}(p) \cdot (1 - (\frac{r_e}{r})^p)$$

where

$$\mathrm{sgn}(p) = \begin{cases} +1, & p > 0 \\ -1, & p < 0 \end{cases} ,$$

so that the Dunham variable corresponds to $p = -1$ and the SPF variable

to $p = +1$. Thakkar then related the e_n's of his expansion

$$V(r) = e_o\lambda_r^2(1 + \sum_{n=1} e_n\lambda_r^n)$$

to the a_n's of Dunham in the same manner SPF had solved for their b_n's. His algebraic relations were much more complex and tedious than those of SPF and will not be reproduced here, except for the simplest relations

$$e_o = a_o/p^2$$

and

$$e_1 = (a_1 + p + 1)/(p\cdot\mathrm{sgn}(p)) \quad .$$

The remainder are to be found in Thakkar's paper. Since there was one extra parameter, p, in this series expansion compared to those of Dunham and SPF, there was some ambiguity as to the choice of p. Thakkar argued that the optimal choice for p would be one that would eliminate the first correction term in the series, i.e. $e_1 = 0$, or

$$p = -a_1 - 1 \quad ,$$

which of course led to nonintegral values. Nevertheless, Thakkar found that the behavior of this series for CO and HF was better than that of SPF. Moreover, the potential tended to a constant value at $\lambda_r = 1$, <u>i.e.</u> it extrapolated to dissociation energies within 10% of the true values.

It should be noted that the leading term,

$$e_o\lambda_T^2 = e_o((\frac{r_e}{r})^{2p} - 2(\frac{r_e}{r})^p) + e_0$$

is the same as the Lennard-Jones (2p,p) potential. Since the latter, especially for p = 6, has been very successful in describing very weakly bound molecules, we should expect the Thakkar series to be a very promising tool for studying those systems. Indeed we have found this to be the case and will discuss it in greater detail in Chapter 3.

Following this trend of using a simple potential function as an expansion variable, one would wonder how useful a series could be using a Morse potential, namely

$$\lambda_H = 1 - e^{-\rho(r-r_e)/r_e} \quad .$$

Point of fact, Dunham himself had made just such a speculation in his original work.[7b] Because the Morse function had been so simple and so popular among spectroscopists, it is curious that no one had seriously investigated the series representation before the publication of J. N. Huffaker's first article in 1976.[40] Using perturbation theory, Huffaker derived the relationships among the Y_{ij}'s and the c_n's of the expansion

$$V(r) = c_o\lambda_H^2(1 + \sum_{n=2}^{\infty} c_n\lambda^n) \quad .$$

By further requiring equality of the derivatives at r_e between his and

Dunham's series, as SPF and Thakkar had, and substituting the resulting expressions into his Y_{ij} formulations, Huffaker obtained Dunham's original equations between the Y_{ij}'s and the a_n's, thus showing the internal consistency of the method. More recently, by adopting the JWKB approach, Huffaker has developed an algorithm[41a,d] for calculating higher order c_n's, where the highest value of n is limited only by the amount of available data and the machine precision of the computer. Most recently,[41e] he has developed a generalized formula for finding the a_n's and b_n's from c_n's (unfortunately, the relationship to the e_n's was not so obvious and hence not reported).

There are several similarities between the Thakkar and Huffaker expansions. First, the expansion variables contain two parameters, r_e and p or ρ. By hopefully optimizing the second parameter of the variable the first correction term in the series can be eliminated. Although the Huffaker-Dunham coefficient relations are not quite as complex as those of the Thakkar-Dunham, we only list the simplest ones, which are

$$\rho^2 c_o = a_o$$

$$\rho = -a_1$$

$$= p + 1$$

These equations make Huffaker's lead ng term a Morse-Pekeris function, <u>i.e.</u> p is determined from α_e rather than $\omega_e x_e$.

With a few exceptions, which we will note later and in Chapter 5, the Huffaker series appears to offer the most accurate description of a molecular potential of the four series we have discussed so far. We have found that the higher order correction terms are usually small (<0.2) and tend to decrease for increasing n. Even though the series must be truncated to a polynomial of order N, we have found that the extrapolated dissociation energy

$$D_e \cong c_o \left(1 + \sum_{n=2}^{N-2} c_n\right)$$

is almost always positive and approximates the known value within 10%. There remains, however, a convergence problem to be addressed.

F. Further Convergence Considerations

Although it seemed that the new expansion variables had extended the region of series convergence to the domain $0 < r < \infty$, certain anomalies in the truncated polynomials became apparent. SPF noted that their function tended to converge slowly at $r \sim \frac{1}{2} r_e$ and sometimes had an artifice at $r < r_e$, quickly becoming negative at smaller values. We have seen these artificial maxima for many molecular states for the Thakkar and Huffaker series as well. It appeared that these new series expansions tended to diverge for some $r < r_e$.

Thakkar speculated that his and the SPF series had a smaller convergence radius of $-1 < \lambda_T < 1$ because the theoretical justification for these expansions had been that λ_T be a perturbation variable on the electronic Born-Oppenheimer Hamiltonian evaluated at r_e.[39] Beckel[42] pointed out that if the potential $V(r)$ has a term of the form $\exp(-\alpha r)$, α being some constant, then $V(r)$ has, for $p > 0$, an essential singularity at $\lambda_T = +1$, i.e. for $\lambda_T(r) = 1 - (r_e/r)^p$, the expansion in λ_T of the function

$$\exp(-\alpha r) = \exp\left(-\frac{\alpha\, r_e}{(1-\lambda_T)^{1/p}}\right)$$

has a singularity at $\lambda_T = 1$. This therefore restricted the radius of convergence to $|\lambda_T| = 1$, or rather the series ceased to be convergent at $\lambda_T = -1$ and $r = r_e/2^{1/p}$ (with $r = \frac{1}{2} r_e$ for the SPF case of $p = 1$). Although this particular problem can not occur for Huffaker's expansion,

$\lambda_H = 1 - \exp(-\rho(r/r_e - 1))$, since

$$\exp(-\alpha r) = \exp(-\alpha r_e)\cdot(1-\lambda_H)^{\alpha r_e/\rho}$$

is analytic for positive α and ρ, we propose that any potential that has an r^{-n} term (which is sure to occur at longe range) is not analytic at $\lambda_H = 1$ with respect to the Huffaker variable, because

$$r^{-n} = [r_e(1-\rho^{-1}\ln(1-\lambda_H))]^{-n}$$

has an essential singularity at $\lambda_H = 1$. This sets a radius of convergence of $|\lambda_H| = 1$ and explains why we have seen truncated Huffaker polynomials reach non-physical maxima and become negative for decreasing r, and why these maxima have appeared to correspond roughly to $\lambda_H = -1$.

Since these convergence restrictions are in the region $r < r_e$ they are not nearly as serious as the one placed on the Dunham series. Usually the artificial maxima occur at V(r) values of $\frac{1}{2} D_e$ or greater, so we can fit a simple repulsive function to the inner wall to extend the potential function for $V(r) > D_e$. As mentioned before the eigenvalues and eigenfunctions of the potential are more sensitive to the outer portion than to the inner wall, so the point of concern is the accuracy of these series representations for $r > r_e$.

G. The Program

In order to investigate the behavior of the truncated polynomials of these series expansions for various molecular states, we have written a FORTRAN program which will invert a set of Y_{k0}'s and $Y_{\ell 1}$'s, where $1 \leq k \leq 4$ and $0 \leq \ell \leq 3$, to give Dunham, SPF, Thakkar and Huffaker polynomials up to the sixth order correction to the leading term, i.e. up to a_6, etc. Although this program is listed and described more fully in Appendix A, a brief description of the general algorithm will be given here.

Using Sandeman's notation, the Y_{ij}'s can be expressed as

$$Y_{ij} = x_{ij} + y_{ij} + z_{ij} + \ldots$$

where the x_{ij}, y_{ij}, z_{ij} correspond to the f_{ij}, g_{ij}, and h_{ij}, respectively, of Section II, with the appropriate factor of (B_e/ω_e). As suggested in Section II, the assumption $Y_{ij} \cong x_{ij}$ is made and a set of a_n's is sequentially calculated. The order of calculation is illustrated in Fig. 1, which shows that the a_n's for even n are determined from the Y_{k0}'s and those of the odd n are determined from the $Y_{\ell 0}$'s (if B_e, or rather r_e, may be considered "a_{-1}"). If a particular Y_{ij} is not available it is set equal to zero and the corresponding a_n is determined (a practice we consider risky and we tend to avoid). If the set of a_n's is sufficient to determine a particular y_{ij}, the latter is calculated, subtracted from Y_{ij}, and the new set of x_{ij}'s is used to

determine the next iterative set of a_n's. The process is repeated until the change in the next set is negligible. We have found that ten to twenty iterations are needed to give an average relative error of $\sim 7 \times 10^{-15}$. Out of over one hundred cases, we have found only two cases (a set of very non-physical Y_{ij}'s for Be_2 and Ar_2) in which the iteration actually diverged.

The x_{ij}'s and y_{ij}'s can be computed from Dunham a_n's or Huffaker's c_n's. Earlier, we had computed the former quantities with separate programs using these authors' equations and found the x_{ij} and y_{ij} sets to agree within machine precision. Thus we are confident that these equations are faithfully coded.

Since this program was written, the articles by Bouanich and Huffaker had appeared which permitted the calculation of higher a_n's. We have not tried to recode our work for the following reasons:

1. The higher equations are algebraically very complex and their transcription to computer code would be subject to error. Indeed, Huffaker's formulas are a convolution of several sets of intermediate quantities requiring calculation.
2. Our main interest is in weakly-bonded molecules which have only a few number of bound vibrational levels, hence the higher Y_{ij}'s needed by the higher a_n's cannot be determined for lack of experimental information.
3. Because the relative standard deviations of the a_n's and Y_{ij}'s increase with n and i respectively, the higher a_n's may be calculated in principle but will remain indeterminate in practice.

4. The relationships between the a_n's and Thakkar's higher e_n's have not been published and we have found their derivation to be too tedious (in short, we tried but ran out of patience).

We were thus less interested in making the program a state-of-the-art instrument and more interested in spending the time examining more molecular systems with the tools at hand. We felt we could calculate enough expansion parameters to determine several trends for the different potential series.

H . The Roads-Not-Taken

It should be mentioned that there are two other series approximations which we have not considered in detail. The first is the Ogilvie-Tipping,[43] or OT, expansion, where

$$\lambda(r) = (r-r_e)/(r+r_e) \quad .$$

As has been pointed out by Beckel[42] and Engelke,[44] for $0 < r < \infty$, $-1 < \lambda < 1$ and hence the OT series should in principle be convergent for all $r \neq 0$. In fact Engelke has found[44] that the OT series and his modifications are quite good in describing the ground and excited states of H_2^+. Although he gave a formulation for determining the OT coefficients from the a_n's up to the fourth order correction, we have found a general formula and will report it here. Given the OT expansion

$$V(r) = d_o\lambda^2(1 + \sum_{n=1} d_n\lambda^n) \quad ,$$

we have

$$d_o = 4a_o$$

$$d_n = 1 + n + \sum_{m=1}^{n} 2^m \binom{n+1}{n-m} a_m \quad ,$$

where $\binom{n+1}{n-m}$ is the binomial coefficient.

Because the d_n calculation was so straightforward we examined the OT polynomials for $HF(X^1\Sigma^+)$, $HF(B^1\Sigma^+)$, HI, CO, $I_2(B^3\Pi_{0^+u})$, $Li_2(A^1\Sigma^+u)$, $BeAr^+$, BeH^+, Ar_2, Mg_2, Ca_2, and $NaAr(A^2\Pi_{3/2})$. Despite Engelke's work, we have found that for $r > r_e$ the OT polynomial in general performed more poorly than that of SPF, Thakkar, or Huffaker. In none of the cases examined did the $r \to \infty$ extrapolation give a value within a factor of +2 of the known dissociation energy. It had the highest propensity over the other three to reach a non physical maximum and become negative for increasing r. It did demonstrate superior behavior for $r < r_e$, i.e. if the OT polynomial showed an artificial maximum along the inner wall of a particular molecule along with the SPF, Thakkar, or Huffaker function, the OT maximum was at smaller r and V(r) was largest. This last point was not as important for describing a true potential, as mentioned earlier. For these reasons, we did not investigate the OT expansion any further.

It is curious that our observations vary so markedly with Engelke's. It may be that H_2^+ is unique; it has only one electron so that the only interatomic repulsion effects are the Coulombic repulsion of the two nuclei and the electron's average kinetic energy due to particle-in-a-box type shrinkage.[45] In terms of the reduced variables r/r_e and $V(r)/D_e$, H_2^+ has one of the broadest wells. We tend to think that H_2^+ is a chemical singularity and that the OT series has a smaller radius of convergence in the empirical sense.

The other approach we have neglected is the [N,N] Padé approximant.[46] The form for this function is

$$V(r) = f_o\lambda^2\left(1 + \sum_{n=1}^{N-2} f_n\lambda^n\right)/\left(1 + \sum_{n=1}^{N} g_n\lambda^n\right) ,$$

where λ is the Dunham variable, $r/r_e - 1$. The desirable qualities are that for small λ it is a harmonic oscillator (which some workers prefer for the latter's familiarity), it extrapolates to a finite value $f_o f_{N-2}/g_N$ as $r \to \infty$, and, by choosing $N = m$ for r^{-m} asymptotic behavior, has a chance at recovering the long-range part of the potential. Jordan and coworkers have applied this approximant to H_2^+ [47] and the alkali halides.[48] The latter work had determined the f_n's and g_n's by expanding the denominator in a binomial expansion, multiplying the two series together and equating the coefficients of λ^{n+2} to Dunham's a_n's.

The problem with this approach is that the relationships of the f_n's and g_n's to the a_n's change for different N. This makes the algorithm inconvenient; the introduction of one higher Y_{ij} allows the calculation of one higher a_n and the iterative correction of the lower a_n's from the one set of Dunham equations whereas a completely different set of equations must be employed to find the new set of f_n's and g_n's. The systematic improvement of the Padé approximants with new data is not as straightforward as with the other series mentioned.

Moreover, Bickes[49] has demonstrated that he can fit an SPF polynomial more accurately and over a wider region of H_2^+ than Jordan's [2,2] or [3,3]'s. Similar observations were made by Engelke concerning his expansions vs. the [2,2] and [3,3]. An examination of these approximants for $BeAr^+$, discussed in Chapter 3, showed the extrapolated

dissociation energies to be a factor of two too large. For these reasons we have not pursued the Padé approximants.

I. General Observations

We have examined the behavior of the SPF, Thakkar, and Huffaker potentials for 31 molecules and 43 of their electronic states. Because the list is not exhaustive and is weighted by our own interests and prejudices we have not attempted a careful, systematic examination of the coefficients or the extrapolated dissociation energies. Nevertheless we feel the list is fairly representative of the different kinds of molecular states known and that we can safely draw some qualitative conclusions. To our knowledge, no other work as extensive has appeared in print for these three potential series.

The program described in Appendix A was run on the Lawrence Berkeley Laboratory's CDC 7600 and 6600 computers using single precision (approximately 14 significant digits). The output of this program and plots of the potential polynomials and RKR tie-lines can be found on the microfiche attached to this publication. A few comments concerning output are in order:

1. The first line is a title which identifies the data set and the corresponding plot.
2. The second line is an abbreviated reference of the form: First Author/Journal and Volume/Pg. No./Year/Y_{ij} Status. where the Journal code is CJP: Canadian Journal of Physics, CPL: Chemical Physics Letters, CRASB: Comptes Rendus de l'Académie des Sciences B, JCP: Journal of Chemical Physics, JMS: Journal of Molecular Spectroscopy, PR: Physics Review, PRA: Physics Review A, and PRL: Physics Review Letters. The Y_{ij} status is "Y" if Y_{ij}'s

appeared in the reference, "N" if only G_v and B_v data are available.

3. The dissociation energy need only be an estimate, since it is only used for scaling the vertical axis of the plot.
4. Technically speaking, the Born-Oppenheimer approximation requires that one use the mass of the nuclei rather than the atomic masses. Hence the atomic masses are corrected for mass of the electrons. This fine point only shows up in calculating r_e.
5. The expression "CUT OUT AT IT = " indicates the iteration at which the a_n's converged (maximum allowed = 30). This printing feature is removed from the latest version of the program.
6. The X's and Y's refer to Sandeman's notation for the Y_{ij}'s and the first Dunham correction. The leading integers correspond to i and j respectively.
7. The first parameter for each series is the a_o, b_o, etc. The second is r_e for all of them. The third corresponds to a_1, b_1, p, and ρ respectively. The rest are the succeeding correction terms, extrapolated D_e for all but Dunham's series, and the last Huffaker parameter is the σ described in his first paper.
8. For the first seven runs, the standard deviations for the Thakkar and Huffaker D_e's and Huffaker's σ were not calculated in the strictly correct, mathematical sense and therefore tend to underestimate the true standard deviations. The calculation of the standard deviation of the SPF D_e is programming-error ridden and

is therefore meaningless. These errors are corrected in the final version of the program and all standard deviations for those molecules in the eighth run are correct.

9. Ignore the "WMIN FAILED TO CONVERGE" message for NAH/X SIGMA+/; it really did converge.

A few comments concerning the plots are:

1. The code for the potential polynomials are Dunham: long dash, SPF; dot-dash, Thakkar: short dash, Huffaker: dots (or very short dashes).
2. RKR tie lines correspond to the vibrational energies and their classical turning points. The highest level corresponds to the highest level to which Y_{ij}'s were fitted.
3. The horizontal tie line running across the center of the plot from $r = 0$ to $5\ r_e$ corresponds to the estimated dissociation energy.
4. The horizontal lines that occasionally appear crossing the $r = 0$ axis and running the length of the plot seem to be due to bugs in the LBL Computer Center's IDDS interface with the microfiche plotter; they did not appear in plots on other devices.
5. For the molecular hydrides and $HeNe^+$ in the first seven runs, the divisions along the r-axis should be in units of either 0.2 Å or 0.5 Å. Because of a formatting error in the plotting

portion of the program, the r-axis labels are rounded to the nearest Å and thus for HF, for example, two tick marks each are labelled "1." Å, "2." Å, etc.

The overall organization of the output is broken into 9 sets which can be identified by the "LOAD MAP" that precedes each. The sets are: van der Waals' molecules, the hydrogen halides and carbon monoxide, alkaline earth dimers, molecular ions, alkali hydrides, alkali dimers, an unclassified group of various molecular states, and a set containing correction runs of the former sets plus HD and D_2, respectively. The correction run had been made in order to generate plots that had been scaled incorrectly for $HeNe^+$ and the two O_2^+ states or to correct for mispunched cards on the $A^1\Sigma^+$ states of KH and CsH. The data set for I_2 $B^3\Pi_{0^+u}$, which also had a mispunched entry, was replaced with a data set containing newer, more accurate Y_{ij}'s. Certain minor bugs in the program were fixed for the last run and a final listing is included. A complete listing of all molecules and states are to be found in Table I.

From these results we can make several qualitative, intuitive observations. Most noteworthy is that for molecules that are chemically bonded, i.e. have well depths of greater than 30 kcal/mole or 10,000 cm^{-1}, the Huffaker series is superior to any of the others. It generally converges uniformly, i.e. no non-physical maxima, to a positive value for increasing internuclear separation. The extrapolated dissociation energy is frequently within 10% of the true value. On those occasions

when it fails by running over 10% above or below the true dissociation or by reaching a maximum and going negative, the other series have also failed and have done so for smaller r. For $r < r_e$, the Huffaker series occasionally turns over, but since these maxima tend to be well above D_e this is no great problem. Moreover, the correction terms of the Huffaker series are the smallest. This last point is a little ambiguous since Huffaker's λ approaches one for increasing r more rapidly than the variables of SPF or Thakkar, i.e. the Huffaker correction terms are smaller but are called into play earlier.

The Thakkar series potential has a greater tendency to turn over. For $r < r_e$, its maximum tends to be lower than Huffaker's. Although Thakkar's series also occasionally turns over for $r > r_e$ whereas Huffaker's does so only rarely, when the former does turn over its maximum is closer to the true dissociation energy than Huffaker's extrapolated value. In these cases it would seem that the Thakkar function collapses at the finish line. When the Thakkar function does not go through a large r maximum its D_e overestimates the true value where the Huffaker D_e is too low. This can be explained by the fact that the Thakkar potential has a long-range r^{-p} term built into it, but we find p to be smaller than the true long-range n, and hence the potential rises too quickly and past the dissociation limit. On the other hand, if the Huffaker potential faithfully follows the RKR curve, it will asymptotically approach the same value as a Birge-Sponer[49] extrapolation.[50] The latter extrapolation is already known[25] to

underestimate the true value due to the neglect of long-range forces. These forces are neglected by the Huffaker potential as well.

The SPF potential is, for large r, the poorest of the new series potentials; it diverges from the RKR curve first and turns over most often. When SPF and Thakkar both turn over, SPF flips over first. Clearly, the SPF series needs to include extra terms from the boundary conditions mentioned earlier.

On the short range, repulsive wall side the SPF may be slightly better in the sense that, when it does turn over, it does so well above the 2.5 D_e maximum of the plotting range. For that matter, in this region the Dunham potential is superior to all the others, since it turns over the least and always above the viewpoint of the plot. This may be because the Dunham series is well within its radius of convergence while the others are fast approaching theirs. It may, in fact, be a worthwhile study to compare the repulsive wall of the spectroscopically determined Dunham series to those potentials derived from elastic scattering work.

As far as spectroscopic work is concerned, the new series are definite improvements over the Dunham expansion. A visual inspection of the plots indicates that they agree fairly well with the RKR turning points up to the highest level. On closer examination, however, they do not provide as stringent quantitative agreement as demanded by the experimental accuracy of the original data. As an example, the G_v's for HI have been calculated for the Huffaker and Thakkar expansions

by the Numerov-Cooley method.[50] The corresponding B_v's have then been determined from the resulting wavefunctions by the equation

$$B_v = B_e r_e^2 \int \psi_v^2/r^2 \, d\tau$$

The results are tabulated in Tables II and III.

Of particular note is the quantity δY_{ij} given in Table II. Although an accurate description of the upper $G_o(v)$, where $G_o(v) = G_v - G_o$, requires Y_{50}, this last quantity is not used in the determination of the Thakkar and Huffaker potentials. Thus if these two series were to represent faithfully the input data, δ(Thakkar) and δ(Huffaker) should be equal to $\delta(Y_{ij})$ rather than Y_{ij}. In any case, the deviations of these two potentials are well outside experimental tolerances for the upper levels. In this rare case, the Thakkar potential shows better agreement with the true values than does the Huffaker one. This is probably due to the fact that the former reaches a maximum at 3.8 Å that is <1% of the true D_e, coming closer to simulating the true potential within this range (see Fig. 2). The decreasing portion of the potential is insignificant here, since the wavefunction is not calculated past 3.8 Å.

Despite the quantitative shortcomings the newer expansions provide at least a good approximate agreement in the range where the true potential is known and, with a few exceptions, a reasonable qualitative description over the entire range. Examination of these exceptions proves instructive and should be discussed briefly.

One is the Ca_2 $A^1\Sigma_u^+$ state, which is one of the few cases where Huffaker turns over. Although workers had, by analogy to Mg_2, correlated this state to the ^1P level of Ca,[52,53] Vidal[54] correctly pointed out that an avoided crossing occurs and that Ca_2^* dissociates into a ground and an excited ^1D atom. Thus this curve may be shallower due to this premature adiabatic termination.

Another case of avoided crossing is the $A^1\Sigma^+$ state of the alkali hydrides recently studied by Stwalley and coworkers.[55] Here a moderately weak diabatic covalent state of ground state atoms crosses a more strongly bonding ionic curve, creating a uniquely shaped, flat bottom A state.[56] As a result the values of $\omega_e x_e$ and α_e are negative, making this a very unique molecular state. This also leads to a Thakkar $p < 0$, which invalidates the higher coefficients since the Thakkar relations change with change of sign in p (the computer code assumes $p > 0$ always).[57]

The anomalous behavior of the series for the HF $B^1\Sigma^+$ state may derive from two sources. Similar to the alkali hydride $A^1\Sigma^+$ case, the $B^1\Sigma^+$ correlates to the ions H^+ and F^- (although the adiabatic $A^1\Sigma^+$ state should avoid another crossing and dissociate into ground state hydrogen and an excited ^2P alkali atom). For example we find the Thakkar p to be very small, around 0.2, and would expect poor behavior for this function. DiLonardo and Douglas,[58] who reported the Y_{ij}'s we have used, have noted that the value $D_e - G_v$ is very close to $e^2/r_+(v)$ for v = 14-26, where $r_+(v)$ is the outer RKR turning. They

have also observed that above v = 26 the $B^1\Sigma^+$ state is strongly perturbed by the $b^3\Pi$ and other higher Rydberg states intersecting the B state along the inner wall. This is the second factor that could account for the series poor behavior.

A further example of a perturbed state not lending itself to a series potential analysis is the N_2 $C^3\Pi_u$ level examined by Huffaker,[41b] where the higher order Morse terms are as high as 800 for the tenth order correction. He attributes this[41e] to the fact that the C state tends toward predissociation, i.e. is perturbed by other states. By the same token, predissociation[59] into the $^1\Pi_{1u}$ state probably perturbs the I_2 $B^3\Pi_{o^+u}$ state badly enough to explain why we have seen all of the series functions fail to represent the potential of the latter. Furthermore, Huffaker had found[41a] that even higher order corrections than we have calculated became increasingly large and only degraded his series.

All these cases where even the Huffaker potential fails correspond to excited electronic states which strongly interact with neighboring excited states or undergo avoided curve crossings. This failure is perhaps ultimately based on the fact that the leading term, or the primal function, is a Morse potential, which has been used primarily for describing ground state interactions. Thus the Huffaker series is from the outset prejudiced toward ground state potentials and this is probably the reason that it does so well for the case where valence bonding forces are at work.

When, in contrast, the bonding is dominated by the weaker long-range forces, as will be considered in Chapter 3, the Thakkar function is superior. This success may again be rationalized by the fact that the leading Thakkar term has a built in prejudice for long-range interactions. Along this line of reasoning the SPF and Dunham expansions, based upon the unrealistic harmonic oscillator and Kratzer-Fues potentials, respectively, cannot be expected to give equally good results in any case and, point of fact, do not.

Thus for ground state potentials and those of excited electronic states which do not interact with neighboring excited states the Huffaker and/or Thakkar expansions provide a good qualitative description and a reasonable quantitative description. Quantitative improvement can be made by employing still higher order corrections as Huffaker has done. Moreover the parmeters in these expansions can be subjected to physical interpretation and be used in denoting and diagnosing bonding trends such as will be done in the next chapter.

J. The Question of Higher a_n's

A point made earlier which we should address here is whether any of the higher order correction coefficients are meaningful. The question had arisen when J. K. Cashion studied the potential for H_2.[22] He had found that the higher Y_{ij}'s, such as Y_{31} and Y_{40} needed in order to find a_5 and a_6, respectively, could not be meaningfully determined. This was in accord with the observations of Herzberg and coworkers,[61] who found that these higher terms varied considerably with the number of vibrational levels used in their fit. The a_5 and a_6 coefficients could hence not be calculated with any reliability, and Cashion questioned whether these or higher coefficients ever could be, forming what today appears to be a concensus of doubt.

The problem with using H_2 as a model potential is that, with the smallest reduced mass and the smallest known value of r_e, it has an exceptionally large B_e of 60.864 cm^{-1}. The ratio (B_e/ω_e) is therefore exceptionally high as well. This is a crucial ratio since it scales the values of the Y_{ij}'s. As noted in Section III, for fixed j each succeeding Y_{ij} is smaller by (B_e/ω_e) so that, all other things being equal, molecular hydrogen's Dunham's Y_{ij} expansion in (v+1/2) should converge the slowest of all molecules. This situation can conceivably make the calculation of the Y_{ij}'s impossible.

Consider the extreme case of the ground state of NaAr; there are only two observed vibrational levels which give only a rough estimate of ω_e and no determination of $\omega_e x_e$ at all, although the latter and

higher Y_{no}'s are most likely significant. We propose that this may be the case for H_2, though less severe. There may simply be too few vibrational levels known to too low an accuracy to determine the number of Y_{ij}'s necessary to describe the former. Ideally, one could use larger, fictitious masses to derive the "correct" Y_{ij}'s, and in fact Cashion had used this approach for the various isotopic species of H_2 to find the true a_0, a_1, and a_2. This restriction to the naturally occurring isotopes may still be too limited as can be seen from Table IV for the (B_e/ω_e) ratios of H_2 to T_2 compared to other, more "typical" molecules. Also listed is the Harrison and Bernstein "well capacity" parameter, $B_z \equiv D_e/B_e$, which has been shown to be related[62] to the number of bound vibrational levels of a potential, which is relevant since it indicates how much experimental information could possibly be available for a molecule.

Herzberg and coworkers have also noted that the lower vibrational levels of H_2, HD, and D_2 are also unusual in the sense that the ΔB_v and $\Delta^2 G_v$ functions have positive curvature. For these reasons we feel that Cashion's "model calculation" was far too unique a model and that his conclusions concerning higher order coefficients need <u>not</u> apply to other, "normal" molecules.

Perhaps the most compelling arguments for determining higher a_n's are the recent results of several workers toward this end. J. P. Bouanich[15b] has fitted a set up to a_8 for CO, finding only a_7 and a_8 to be indeterminant, pointing out that this could be entirely due to experimental errors (Y_{41} was unknown and he had assumed to be zero in

order to calculate a_7 and a_8). Niay and coworkers have circumvented the problem of determining the intermediate Y_{ij}'s by developing a non-linear least-squares method[15a] of calculating the a_n's directly from the measured absorption lines. Although this procedure required taking the derivative of the analytical expressions of the Y_{ij}'s as a function of the a_n's (hence the need to know the number of Y_{ij}'s was still present implicitly), they could bring the expressions for Y_{02}, Y_{12}, etc. into play, which had not been done before, as well as enjoying the application of the original off-the-chart-paper data. They had found that they could derive a consistent set of a_n's through a_6 for $H^{79}Br$,[15a] through a_5 for HI,[63] and through a_6 for DI,[64] that agreed with the same a_n's determined by the traditional method. In those cases where the higher a_n's for the two methods disagreed (a_7 and a_8 for HBr, a_6-a_8 for HI, and the difference between a_5 for HI and a_5 for DI), they had found that in some cases these a_n's were indeterminate due to experimental errors. In the other cases they had speculated that even higher a_n's not determined interferred with the calculation of those a_n's which had been found to be inconsistent.

It is also important to note that the relative standard deviations of the expansion coefficients of the newer series tend to be smaller than those of the a_n's. A casual glance of the output microfiche (under appropriate magnification) will reveal that even when Dunham's a_6 has a standard deviation that makes it completely indeterminate, the values of e_6 and c_6 remain statistically significant. We therefore

conclude that determination of higher corrections for these series is still with merit and should be encouraged. We will also, at the end of Chapter 3, propose a method of determining higher a_n's which will completely eliminate the need for the Y_{ij}/a_n relationships.

K. Conclusions

From the various molecular systems examined and the discussion of higher order coefficient determination the following observations can be made:

1. The newer series representations of a molecular potential have an extended range of good behavior over the old Dunham series.
2. The Thakkar and Huffaker series, whose expansion variables are themselves based upon realistic molecular potentials, show the best behavior and are capable of describing the potential at least qualitatively for very large internuclear separation. For molecules bonded by more than 30 kcal/mole the Huffaker series appears to give the best representation, extrapolating to a constant value for large r that lies very close to the true dissociation energy.
3. The series show the poorest representation for electronically excited molecular states that interact with neighboring states. Even in these cases the series serve as a diagnostic of the extent of the interaction. (For example, we had suspected a pecularity in the assignment of the $A^1\Sigma_u^+$ state of Ca_2 when the Huffaker representation failed, two years before C. R. Vidal pointed out the obvious concerning the correct correlation to excited atomic states). As far as seeking an accurate description of such states, one must resort to RKR methods, which are not biased by an assumed potential form.

4. It appears, that, in principle, quantitative improvement in the series can be had by deriving relations for the higher correction terms which, despite J. K. Cashion's doubts, <u>can</u> be determined reliably.

REFERENCES

1. G. Herzberg, Spectra of Diatomic Molecules, 2nd Edition, (Van Nostrand Reinhold, New York, 1950) pp.219-226.
2. M. Mizushima, The Theory of Rotating Diatomic Molecules, (John Wiley, New York, 1975) pp.132-135, 307-317.
3. G. Wentzel, Z. Physik 38, 518 (1926).
4. L. Brillouin, Comptes Rendus 183, 24 (1926).
5. H. A. Kramers, Z. Physik 39, 828 (1926).
6. H. Jeffries, Proc. London Math. Soc. 23 (Series 2), 428 (1925).
7. J. L. Dunham. Phys. Rev. 41, 713 (1932), b) ibid. 41, 721.
8. a) D. Landau and E. M. Lifshitz, Quantum Mechanics, 2nd Revised Edition (Pergamon, Oxford 1975) pp.161-165. b) E. Merzbacher, Quantum Mechanics, 2nd Edition (Wiley, New York, 1970) pp.118-125. c) M. L. Goldberger and K. M. Watson, Collision Theory, (Wiley, New York, 1965) pp.324-330. d) M. S. Child, Molecular Collision Theory, (Academic Press, London, 1974) pp.249-262.
9. A. Messiah, Quantum Mechanics Vol. I (Wiley, New York) p.233.
10. J. Heading, An Introduction to Phase-Integral Methods (Wiley, New York, 1962) pp.1-9.
11. S. M. Kirschner and R. J. Leroy, J. Chem. Phys. 68, 3139 (1978).
12. J. E. Kilpatrick, J. Chem. Phys. 30, 801 (1959).
13. I. Sandeman, Proc. R. Soc. Edinburgh 60, 210 (1940).
14. H. W. Wooley, J. Chem. Phys. 37, 1307 (1962).

15. a) P. Niay, P. Bernage, and C. Coquant, Can. J. Phys. 55, 1829 (1977); b) J. P. Bouanich, J. Quant. Spectrosc. Radiat. Transfer 19, 381 (1978). Bouanich also claimed to have formulas for a_9 a_{10} which were too lengthy to publish, but which he could make avialable upon request.

16. C. L. Beckel and R. Engelke, Chem. Phys. 49, 5199 (1968).

17. R. Rydberg, Z. Physik 73, 376 (1931); O. Klein, Z. Physik 76, 226 (1932); A. L. G. Reese, Proc. Phys. Soc. London A 59, 998 (1947).

18. J. T. Vanderslice, E. A. Mason, W. G. Maisch, and E. R. Lippincott, J. Mol. Spectrosc. 3, 17 (1959).

19. J. Tellinghuisen, J. Mol. Spectrosc. 44, 194 (1972).

20. R. N. Zare and J. K. Cashion, UCRL Report 10881 (1963).

21. M. E. Kaminsky, J. Chem, Phys. 66, 4951 (1977); ibid. 73, 3520 (1980).

22. J. K. Cashion, J. Chem. Phys. 45, 1037 (1966).

23. W. R. Jarmain, Can. J. Phys. 38, 217 (1960); A. C. Hurley, J. Chem. Phys. 36, 1117 (1962).

24. a) R. H. Davies and J. T. Vanderslice, Can J. Phys. 44, 219 (1966); b) S. M. Kirschner and J. K. G. Watson, J. Mol. Spectrosc. 31, 321 (1973); c) J. N. Huffaker, J. Mol. Spectrosc. 65, 1 (1977).

25. R. J. LeRoy and R. B. Bernstien, J. Chem. Phys. 52, 3869 (1970); R. J. LeRoy, Molecular Spectroscopy 1 (a Specialist Periodical Report of the Chemical Society of London), edited by R. F. Barrow, D. A. Long and D. J. Millen (Chem. Soc. London, 1973) pp.113-176.

26. R. J. LeRoy, J. Chem. Phys. 73, 6003 (1980).

27. J. A. Steinfeld, Molecules and Radiation (Harper and Row, New York, 1974) p.109.

28. P. Niay, P. Bernage, C. Coquant, and R. Houdart, Can. J. Phys. 56, 727 (1978).

29. G. V. Calder and C. Ruedenberg, J. Chem. Phys. 49, 5399 (1968).

30. S. S. Frost and B. Musulin, J. Am. Chem. Soc. 76, 2045 (1954).

31. a) G. Simons, R. Parr, and J. M. Finlan, J. Chem. Phys. 59, 3229 (1973); b) J. M. Finlan and G. Simons, J. Mol. Spectrosc. 57, 1975)

32. G. Simons, J. Chem. Phys. 61, 369 (1974).

33. G. D. Carney, L. A. Curtiss, and S. R. Langhoff, J. Molec. Spectrosc. 61, 371 (1976).

34. G. D. Carney and G. Wolken Jr., Chem. Phys. Lett. 41, 347 (1976).

35. R. W. Bickes, Jr. and R. B. Bernstein, Chem. Phys. Lett. 26, 457 (1974).

36. R. W. Bickes, Jr. and R. B. Bernstein, J. Chem. Phys. 66, 2408 (1977).

37. S. Kratzer, Z. Physik 3, 289 (1920); E. Fues, Ann. Phys. (Leipzig) 80, 367 (1926).

38. Y. P. Varshni, Rev. Mod. Phys. 29, 664 (1957); Rev. Mod. Phys. 31, 839 (1959).

39. A. J. Thakkar, J. Chem. Phys. 62, 1693 (1975).

40. J. N. Huffaker, J. Chem. Phys. 64, 3175 (1976).

41. a) J. N. Huffaker, J. Chem. Phys. 64, 4564 (1976); b) P. H. Dwivedi and J. N. Huffaker, J. Chem. Phys. 66, 1726 (197); c) P. H. Dwivedi and J. N. Huffaker, J. Chem. Phys. 68, 1303 (1978); d) J. N. Huffaker, J. Mol. Spectrosc. 71, 160 (1978); e) J. N. Huffaker, J. Chem. Phys. 70, 2720 (1979).

42. C. L. Beckel, J. Chem. Phys. 65, 4319 (1976).

43. J. F. Ogilvie, Canadian Spectroscopy Symposium, Ottawa, Canada, October 1974; Paper ES4, Symposium on Molecular Spectroscopy, Columbus, Ohio, 18 June 1976.

44. a) R. Engelke, J. Chem. Phys. 68, 3514 (1978); b) R. Engelke, J. Chem. Phys. 70, 3745 (1979).

45. J. S. Winn. J Chem. Phys. 74, 608 (1981); M. Karplus and R. N. Porter, Atoms and Molecules (Benjamin, Menlo Park, California, 1970) pp.292-296.

46. G. A. Baker and J. L. Gammel, The Padé Approximant in Theoretical Physics (Academic, New York, 1970).

47. K. D. Jordan, J. Mol. Spectrosc. 56, 329 (1975).

48. K. D. Jordan, J. L. Kinsey, and R. Silbey, J. Chem. Phys. 61, 911 (1974).

49. R. W. Bickes, Jr., J. Mol. Spectrosc. 59, 153 (1976).

50. R. T. Birge and H. Sponer, Phys. Rev. 259 (1926).

51. J. W. Cooley, Math. Comp. 15, 363 (1961); J. K. Cashion, J. Chem. Phys. 39, 1872 (1963).

52. W. J. Balfour and R. F. Whitlock, Can. J. Phys. 53, 472 (1975).

53. K. Sakurai and H. P. Broida, J. Chem. Phys. 65, 1138 (1976); J. C. Wyss, J. Chem. Phys. 71, 2949 (1979).

54. C. R. Vidal, J. Chem. Phys. 72, 1864 (1980).

55. a) K. C. Li and W. C. Stwalley, J. Mol. Spectrosc. 69, 294 (1978); b) F. B. Orth and W. C. Stwalley, ibid. 76, 17; c) F. B. Orth and W. C. Stwalley, ibid. 79, 314; d) S. C. Yang, Y. K. Hsieh, K. K. Verma and W. C. Stwalley, ibid. 83, 304 (1980); e) Y. K. Hsieh, S. C. Yang, A. C. Tam, K. K. Verma, and W. C. Stwalley, ibid. 83, 311 (1980); f) Y. K. Hsieh, A. C. Tam, and W. C. Stwalley, J. Chem. Phys. 68, 1448 (1978).

56. G. Herzberg, ibid. pp.367-377.

57. Another curiosity is that for the $A^1\Sigma^+$ state of all the isotopic species of LiH, the second order Dunham correction to $Y_{11}(\alpha_e)$ runs from 30%-58% of Y_{11}, which is extraordinarily large. This suggests that one should consider the second order effects on the RKR curve.

58. G. DiLonardo and G. E. Douglas, Can. J. Phys. 51, 434 (1973). For a more recent examination of the perturbing excited states see: A. E. Douglas and F. R. Greening, Can. J. Phys. 57, 1650 (1979).

59. J. Tellinghuisen, J. Chem. Phys. 57, 2397 (1972) and references therein.

60. One exception to this generalization is the $X^1\Sigma_g^+$ state of Be_2. There appears to be some "unusual behavior" in the ground state and will be discussed in more detail in Chapter 3.

61. a) G. Herzberg and L. L. Howe, Can. J. Phys. 37, 636 (1959); b) H. Bredohl and G. Herzberg, ibid. 51, 867 (1973); c) I. Dabrowski and G. Herzberg, ibid. 54, 525 (1976).

62. H. Harrison and R. B. Bernstein, J. Chem. Phys. 38, 2135 (1963).

63. P. Niay, P. Bernage, C. Coquant, and A. Fayt, J. Mol. Spectrosc. 72, 168 (1978).

Table I. Enumeration of Molecular States that have been Calculated

Molecule	State	Set	Number of Variations	References
Ar_2	$X^1\Sigma_g^+$	1	9	1
NaAr	$A^2\Pi_{1/2}$	1	3	2
NaAr	$A^2\Pi_{3/2}$	1	3	2
NaNe	$A^2\Pi_{3/2}$	1	2	3
HF	$X^1\Sigma^+$	2	2	4
HCl	$X^1\Sigma^+$	2	1	5
$H^{79}Br$	$X^1\Sigma^+$	2	1	6
$H^{81}Br$	$X^1\Sigma^+$	2	1	6
$D^{79}Br$	$X^1\Sigma^+$	2	1	7
$D^{81}Br$	$X^1\Sigma^+$	2	1	7
HI	$X^1\Sigma^+$	2	2	8,9
CO	$X^1\Sigma^+$	2	1	10
Be_2	$X^1\Sigma_g^+$	3	7	11
Mg_2	$X^1\Sigma_g^+$	3	2	12,13
Mg_2	$A^1\Sigma_u^+$	3	3	12,13
Ca_2	$X^1\Sigma_g^+$	3	3	14,15,16
Ca_2	$A^1\Sigma_u^+$	3,8	2	14,16
$BeAr^+$	$X^2\Sigma^+$	4	1	17
BeH^+	$X^1\Sigma^+$	4	1	18
HF^+	$A^2\Sigma^+$	4	1	19
H_2^+	$X^2\Sigma_g^+$	4	1	20

$HeNe^+$	$X^2\Sigma^+$	4,8	1	21
$HeNe^+$	$B^2\Sigma^+$	4	1	21
O_2^+	$b^4\Sigma_g^-$	4,8	1	22
O_2^+	$a^2\Pi_u$	4,8	1	22
^6LiH	$X^1\Sigma^+$	5	1	23
^7LiH	$X^1\Sigma^+$	5	3	23,24
^6LiD	$X^1\Sigma^+$	5	1	24
^7LiD	$X^1\Sigma^+$	5	1	24
NaH	$X^1\Sigma^+$	5	1	25
KH	$X^1\Sigma^+$	5	1	26
RbH	$X^1\Sigma^+$	5	1	27
^6LiH	$A^1\Sigma^+$	5	1	23
^7LiH	$A^1\Sigma^+$	5	1	23
^6LiD	$A^1\Sigma^+$	5	1	23
^7LiD	$A^1\Sigma^+$	5	1	23
NaH	$A^1\Sigma^+$	5	1	25
KH	$A^1\Sigma^+$	5,8	1	26
RbH	$A^1\Sigma^+$	5	1	27
C_sH	$A^1\Sigma^+$	5,8	1	28
Li_2	$X^1\Sigma_g^+$	6	1	29
Li_2	$A^1\Sigma_u^+$	6	1	29
Na_2	$A^1\Sigma_u^+$	6	1	30
NaK	$X^1\Sigma^+$	6	2	31
IbR	$X^1\Sigma^+$	7	2	32
I_2	$B^3\Pi_{o+u}$	7,8	2	33,34

XeF	$X^2\Sigma^+$	7	1	35
OH	$X^2\Pi$	7	1	36
OH	$A^2\Sigma^+$	7	1	36
HF	$B^1\Sigma$	7	3	37
LJ	6-12 Model	7	4	38,39
HD	$X^1\Sigma_g^+$	8	2	40
D_2	$X^1\Sigma_g^+$	8	2	41

Set 1 = van der Waal's molecules; Set 2 = Hydrogen halides and CO; Set 3 = Molecular ions; Set 4 = Alkaline earth dimers; Set 5 = Alkali hydrides; Set 6 = Alkali dimers; Set 7 = Various unclassified molecules; Set 8 = Correction run.

References:

1. E. A. Colbourn and A. E. Douglas, J. Chem. Phys. 65, 1741 (1976).

2. R. E. Smalley, D. A. Auerbach, P. S. H. Fitch, D. H. Levy, and L. Wharton, J. Chem. Phys. 66, 3778 (1977).

3. R. Ahmad-Bitar, W. P. Lapatovich, D. E. Pritchard, and I. Renhorn, Phys. Rev. Lett. 26, 1657 (1977).

4. D. W. Webb and K. N. Rao, J. Mol. Spectrosc. 28, 121 (1968).

5. D. H. Rank, B. S. Rao, and T. A. Wiggins, J. Mol. Spectrosc. 17, 122 (1965).

6. P. Bernage and P. Niay, C. R. Acad. Sci. Paris Ser. B 282, 243 (1976).

7. P. Bernage and P. Niay, J. Mol. Spectrosc. 63, 317 (1976).

8. P. Bernage, P. Niay, and L. Houdart, C. R. Acad. Sci. Paris Ser. B 278, 235 (1974).

9. P. Niay, P. Bernage, C. Coquant, and H. Bocquet, J. Mol. Spectrosc. 68, 329 (1977).

10. A. W. Mantz, J.-P. Maillard, W. B. Roh, and K. N. Rao, J. Mol. Spectrosc. 57, 155 (1975).

11. B. Liu and S. D. McLean, J. Chem. Phys. 72, 3418 (1980).

12. W. J. Balfour and G. E. Douglas, Can. J. Phys. 48, 901 (1970).

13. C. R. Vidal and H. Scheingraber, J. Mol. Spectrosc. 65, 46 (1977).

14. W. J. Balfour and R. F. Whitlock, Can. J. Phys. 53, 472 (1975).

15. J. C. Wyss, PhD. Dissertation, University of California at Santa Barbara (1979).

16. C. R. Vidal, J. Chem. Phys. 72, 1864 (1980).

17. K. V. Subbaram, J. A. Coxon, and W. E. Jones, Can. J. Phys. 54, 1535 (1976).

18. W. W. Watson and R. F. Humphreys, Phys. REv. 52, 318 (1937).

19. S. Gewurtz, H. Lew, and P. Flainek, Can. J. Phys. 53, 1097 (1975).

20. C. L. Beckei, B. D. Hansen III, and J. M. Peek, J. Chem. Phys. 53, 3681 (1970).

21. I. Dabrowski and G. Herzberg, J. Mol. Spectrosc. 73, 183 (1978).

22. P. C. Cosby, J.-B. Ozenne, J. T. Moseley, and D. L. Albritton, J. Mol. Spectrosc. 79, 203 (1980).

23. K. C. Li and W. C. Stwalley, J. Mol. Spectrosc. 69, 294 (1978).

24. F. B. Orth and W. C. Stwalley, J. Mol. Spectrosc. 76, 17 (1979).

25. F. B. Orth, W. C. Stwalley, S. C. Yang, and Y. K. Hsieh, J. Mol. Spectrosc. 79, 314 (1980).

26. S. C. Yang, Y. K. Hsieh, K. K. Verma, and W. C. Stwalley, J. Mol. Spectrosc. 83, 304 (1980).

27. Y. K. Hsieh, S. C. Yang, A. C. Tam, K. K. Verma, and W. C. Stwalley, J. Mol. Spectrosc. 83, 311 (1980).

28. Y. K. Hsieh, S. C. Yang, A. C. Tam, and W. C. Stwalley, J. Chem. Phys. 68, 1448 (1978).

29. P. Kusch and M. M. Hessel, J. Chem. Phys. 67, 586 (1977).

30. M. E. Kaminsky, J. Chem. Phys. 66, 4951 (1977).

31. E. J. Breford and F. Engelke, Chem. Phys. Lett. 53, 282 (1978).

32. E. M. Weinstock and A. Preston, J. Mol. Spectrosc. 70, 188 (1978).

33. J. Tellinghuisen, J. Chem. Phys. 58, 2821 (1973).

34. J. Wei and J. Tellinghuisen, J. Mol. Spectrosc. 50, 317 (1974).

35. P. C. Tellinghuisen, J. A. Coxon, J. E. Velazco, and D. W. Setser, J. Chem. Phys. 69, 5187 (1978).

36. J. A. Silver, W. L. Dimpfl, J. H. Brophy, and J. L. Kinsey, J. Chem. Phys. 65, 1811 (1976).

37. G. DiLonardo and A. E. Douglas, Can. J. Phys. 51, 434 (1973).

38. J. Goble, see Chapter 3.

39. J. K. Cashion, J. Chem. Phys. 48, 94 (1968).

40. H. Brehdohl and G. Herzberg, Can. J. Phys. 51, 867 (1973).

41. I. Dabrowski and G. Herzberg, Can. J. Phys. 54, 525 (1976).

Table II. Vibrational levels of HI calculated from series potentials.

v	$G_o(v)/cm^{-1}$ Observed[a]	$\delta(Y_{ij})$[b,c]	δ(Thakkar)[b]	δ(Huffaker)[b]
1	2229.581	.007	.006	.001
2	4379.225	.074	.045	.067
3	6448.036	.405	.276	.490
4	8434.720	1.433	1.040	1.896
5	10337.487	3.917	2.920	5.366
6	12153.971	9.026	6.777	12.540
7	13881.140	18.420	13.777	25.721

a) Calculated from constants of P. Niay, P. Bernage, C. Coquant, and A. Feyt, J. Mol. Spectrosc. 72, 168 (1978). Uncertainties are not less than 0.003 cm^{-1}.

b) $\delta(x) = G_o(v)$ (calculated by method x) $- G_o(v)$ (observed).

c) $\delta(Y_{ij})$ corresponds to "truncated" set of Y_{ij}'s; i.e. Y_{50} was known but not used in calculation of $G_o(v)$ in order to remain consistent with the fact it was not used in the calculation of the Thakkar or Huffaker series. Reference: P. Niay, P. Bernage, C. Couquant, and H. Bocquet, J. Mol. Spectrosc. 68, 329 (1977).

Table III. Rotational constants of HI calculated from series potentials.

v	B_v/cm^{-1} Observed[a]	$\delta(Y_{ij})^{b,c}$ $\cdot 10^3$	δ(Thakkar) $\cdot 10^3$	δ(Huffaker) $\cdot 10^3$
0	6.42636	.99	-.02	-.01
1	6.25528	-.27	-.19	-.12
2	6.08296	-.28	.00	.30
3	5.90878	-.51	.32	1.23
4	5.73187	-1.08	.84	3.02
5	5.55115	-1.93	1.83	6.36
6	5.36528	-2.72	3.79	12.25
7	5.17271	-2.93	7.34	22.00

a) Same reference as Table I(a). Uncertainties less than 0.0005 cm^{-1}.

b) $\delta(x) = B_v$ (calculated by method x) $- B_v$ (observed).

c) Y_{ij}'s taken from same reference as Table I(c).

Table IV. Some $\left(\frac{B_e}{\omega_e}\right)$ and B_z Values.

Molecule	μ (amu)	B_e/ω_e	D_e (cm^{-1})	$B_z \cdot 10^{-3}$
H_2	0.5036	.0138221	38292.7	0.6293
HD	0.6714	.011969	38292.7	0.8388
HT	0.7551	.011286	38292.7	0.9433
D_2	1.0068	.0097737	38292.7	1.2574
DT	1.2074	.0089245	38292.7	1.5079
T_2	1.5078	.0079857	38292.7	1.8831
HF	0.9565	.003672	49380.0	2.3564
Ar_2	19.9763	.001914	99.545	1.6655
Be_2	4.5050	.002358	813.825	1.2829
H_2^+	0.5036	.012893	22525.694	0.7517
CO	6.8543	.0008901	90541.7	46.882
N_2	7.0015	.0008472	79890.0	39.980
NO	7.4664	.0008780	53340.0	31.903
O_2	7.9975	.0009098	42039.0	29.241

FIGURE CAPTIONS

Fig. 1. Schematic procedure for determining Dunham series parameters from spectroscopic Y_{ij}'s.

Fig. 2. Series potentials and RKR turning points for HI. --- Dunham, ····SPF, — — — — Huffaker, ——Thakkar. Horizontal bars are the RKR tie lines calculated from the same Y_{ij}'s used to determine the analytical potentials.

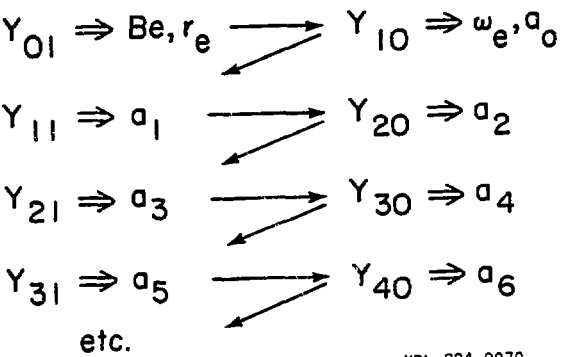

XBL 824-8979

Figure 1

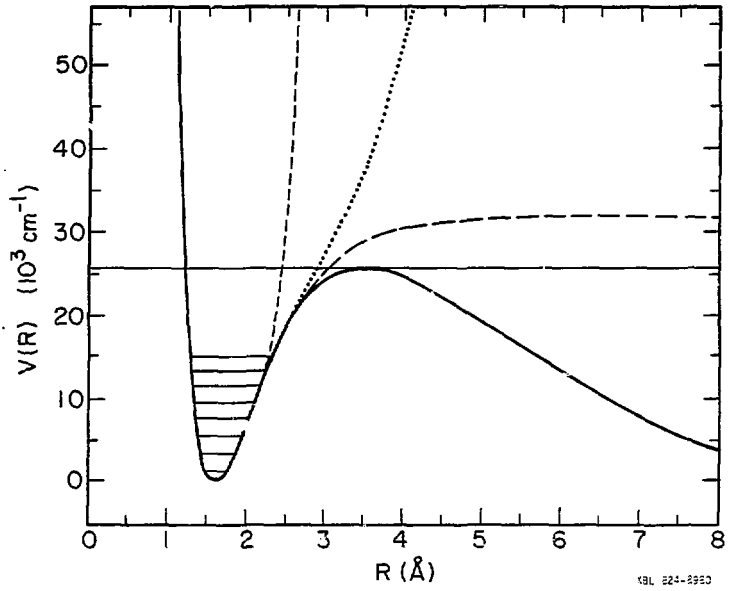

Figure 2

Chapter III.

Series Potentials Applied to Weakly Bound Molecules

A. Introduction

In this chapter we will examine those diatomic molecules whose only sources of binding are the so-called long-range forces. In a nutshell, the elements in the Born-Oppenheimer Hamiltonian that account for one atom's electrons' interaction with the other atom as well as the repulsion between the two nuclei are all perturbations of the Hamiltonians for the individual atoms. These interactions can thus be expanded in powers of r^{-1}, where r is the internuclear separation. First order perturbation for identical atoms, one of which is in an excited state, leads to the resonance interaction:

$$V(r) - D_e \sim C_3 r^{-3} \quad ,$$

and for two atoms neither of which are in an S state, the quadrupole-quadrupole interaction is obtained:

$$V(r) - D_e \sim C_5 r^{-5} \quad ,$$

where $V(r_e) = 0$, the "~" means "is approximated by a large enough r," and C_3 and C_5 can be positive or negative. When these first order terms are zero, second order effects become apparent, such as charge-induced dipole attraction:

$$V(r) - D_e \sim -\frac{1}{2} Z^2 e^2 \alpha r^{-4} \quad ,$$

where Z is the charge on the ion and α is the static polarizability of the neutral atom, and the induced-dipole-induced dipole attraction (also known as van der Waals or London dispersion forces)

$$V(r) - D_e \sim -C_6 r^{-6} \quad ,$$

where C_6 is always positive. Derivations of these expressions as well as evaluation schemes for the C_n's are well covered by Hirschfelder, Curtiss, and Bird[1].

The last interaction, the van der Waals force, is responsible for the "physical" properties of matter, i.e. condensation and freezing, the structure of molecular crystals, properties of glasses, and of course the "nonideal" behavior of gases. The attractive r^{-6} potential is present in all atoms and molecules, whether they be in open or closed shells and in the absence of chemical interactions. Traditionally, these forces have been studied by means of the temperature dependence of thermodynamic and transport properties of gases such as second virial coefficients, viscosities, and thermal conductivities. Since these quantities are convoluted over a Boltzmann energy distribution of a particle temperature, one had been hard pressed to obtain a very detailed description of the potential. Generally, the data had allowed the adjustment of only a small number of parameters of a simple model potential function. The advent of crossed molecular beam elastic scattering has permitted finer control of energy and energy distribution

of the colliding particles[2]. Perhaps the crowning achievement of this technique is the direct inversion of the differential cross section for He-Ne scattering to yield a numerical potential, free of the prejudice of any empirical potential function[3].

The spectroscopic investigation of these weak, long-range interactions has until recently been limited to the analysis of the topmost vibrational levels of chemically bound systems where the asymptotic part of the potential dominates in the region of the outer turning point. The study of diatomic molecules whose binding is entirely due to long-range forces has been limited by a number of practical experimental difficulties. The concentration of dimers is necessarily low compared to that of the monomers, requiring high pressures, low temperatures, and long absorption path lengths in order to achieve a detectable signal. Because the potential minimum lies at relatively large separations, the rotational constant is very small yielding rotational spacings small enough to challenge the dispersion limit of most monochromators. Couple this aspect with the small separation of vibrational levels and the high degree of vibrational and rotational excitation at even low temperatures and one is left with a very complex spectrum. The analysis is further plagued by presence of the ubiquitous atomic transition lying nearby from which the molecular transition is derived.

The recent development of rare gas-halogen laser systems and the prospect of developing other rare gas excimer systems has stimulated interest in understanding these van der Waals molecules and their spectroscopic properties[4]. The wish to understand further the line

broadening mechanisms of high pressure atomic lamps has also encouraged workers to study the diatomic potentials responsible for the broadening despite the cited difficulties. Moreover, the introduction of laser-induced fluorescence with tunable dye lasers[5] has provided the high resolution and high sensitivity necessary for those dimers with a visible absorption spectrum. The development of supersonic molecular beam sources has further aided study of these dimers by producing them in a collision free environment (eliminating the problem of pressure broadening) and with an effective internal excitation of ca. 10 K, greatly simplifying the spectrum[6].

Our own motivation for examining weak diatomic molecules is twofold. One is to coordinate bonding trends for these systems in a systematic manner and hopefully arrive at some simple formulations for predicting their characteristic properties. Our second motivation is that this work is to complement the experimental work in progress in this laboratory. The Molecular Beam Electric Resonance project is a powerful tool for determining the structure and properties of van der Waals molecules, and thus any insight in these weak interactions is certain to be useful. The other project is the investigation of the excitative Penning and the excitive associative ionization of alkaline earths in a flowing afterglow of metastable rare gases. The observation of the almost diffuse chemiluminescence of $CaAr^+$ inspired us to examine the potential and spectroscopic properties of the analogous $BeAr^+$ in order to facilitate the analysis of the data for the former ion[7,8].

B. $BeAr^+$

Upon exciting with a microwave discharge $BeCl_2$ or $BeBr_2$ vapor in a buffer gas of 200 torr of Ar or Kr, Subbaram and co-workers[9] observed in emission a series of closely spaced, violet shaded vibrational bands around 4000 Å. Because the bands showed an intensity dependent upon the pressure of the rare gas and whose band positions and spacings changed when changing from Ar to Kr and because the band showed $^2\Pi$-$^2\Sigma$ transition structure, they concluded that the source of the emission was from $BeAr^+$ and $BeKr^+$. Subsequent high resolution studies[10,11] permitted the evaluation of vibrational and rotational constants for the two states of these molecular ions. In both cases they found B_e and ω_e to be larger for the excited $A^2\Pi$ state.

The $BeAr^+$ $X^2\Sigma^+$ vibrational and rotational constants had been determined up to Y_{30} and Y_{21}, respectively, providing enough information to make a reasonable potential series analysis. We would expect the binding of this molecule to be primarily due to the ion-induced dipole attraction and relatively free of interfering chemical interactions. This would make $BeAr^+$ a "long-range molecule" in the sense that the long-range r^{-4} potential should still be the predominant attractive interaction near r_e where the vibrational-rotational data and hence the series cofficients are determined, making this a likely first test-case for the different potential series.

The $BeAr^+$ spectroscopic constants are listed in Table I, permitting the determination of the a_0 to a_4 Dunham coefficients, listed in Table II. The [3,3] Padé approximant (PA) potential could be determined

as well, and its coefficients are listed in Table III along with those of the SPF, Thakkar and Huffaker potentials. The simple [2,2] PA expression

$$V(r) = a_0\lambda^2/(1-a_1\lambda + (a_1^2 - a_2)\lambda^2) \quad ,$$

does not require listing of its coefficients.

By evaluating these potentials at the RKR turning points reported by Subbaram[10], we find the [2,2] and [3,3] PA's to be a little lower than G_v, by no more than 10 cm^{-1} for v = 4, which is good compared to a 30 cm^{-1} underestimation by the Thakkar and Huffaker potentials. The situation is reversed for the v = 4 outer turning point, where the PA's are 39 cm^{-1} high while the Thakkar and Huffaker values are only over by 11 and 5 cm^{-1}, respectively. We expect this problem of PA overestimation to grow worse for higher vibrational levels, since the dissociation limits,

$$D_e^{[2,2]} = a_0/(a_1^2 - a_2)$$

and

$$D_e^{[3,3]} = a_0 f_2/g_3 \quad ,$$

are 8967.5 and 8971.2 cm^{-1}, respectively, which is more than twice Subbaram's estimate of 4100 cm^{-1}, indicating there is no hope for recovering the long-range portion of the potential with the [2,2] or

[3,3] approximants. In principle, one would require a [4,4] PA to stimulate r^{-4} behavior, but the similarities of the [2,2] and [3,3] approximants do not suggest the [4,4] would be drastically different. In any case, there is simply not enough data to construct a [4,4] for this test problem.

In Fig. 1 we show the Dunham, SPF, Thakkar and Huffaker potentials plotted against the reduced coordinate r/r_e. Tie lines connecting the RKR turning points are also shown for comparison. The Dunham potential was not expected to perform very well, and, in fact, it failed to reproduce the v" = 3 and 4 levels on the outer branch. This failure is perhaps to be expected in molecules which have a strong long-range interaction, causing the outer turning points of even the lowest few vibrational states to extend well beyond r_e. The SPF potential recovers the RKR data somewhat better, being low by 61 cm^{-1} at the outer turning point of v" = 4. This potential rapidly fails at larger r, however, converging to a negative energy at $r = \infty$. For $BeAr^+$ n = 4, and we can generate up to four additional SPF coefficients by requiring the terms in r^{-1} through r^{-3} to have zero coefficients and by requiring the r^{-4} term to have a coefficient given by the ion-induced dipole interaction between a unit charge (Be^+) and a polarizable sphere (Ar). One need not impose all constraints, of course, and thus four additional SPF potentials can be generated. As Table II shows, the highest-order SPF correction, b_4, is very large and negative. This value may be poorly determined due to truncation of the series, to insufficiently precise spectral data, or to both factors. Neglecting b_4, but imposing one to four boundary conditions will generate four

more SPF potentials (for a grand total of nine).

We have generated all eight extended SPF potentials (in addition to the direct inversion potential shown in Fig. 1) based on boundary conditions and/or neglect of the b_4 correction. Although the addition of each new coefficient extended the range of good behavior, none of the eight additional SPF potentials showed remarkable improvement over the initial SPF potential of Table III and Fig. 1. Including b_4 and adding one to four constraints yielded potentials which continue to show negative values for the potential in the region plotted in Fig. 1. As successive constraints are employed to generate additional terms, the nonphysical maximum at $r > r_e$ moves to larger r and attains a greater value for V before turning over. In contrast, neglecting b_4 and adding successive constraints yield four potentials which continually rise over the $r > r_e$ range, but to unphysically large values. These eight potentials do not exhibit reasonable long-range behavior and are, therefore, not significant improvements over the simplest SPF function. More quantitative comparisons of these potentials are presented later.

Clearly, the Thakkar and Huffaker potentials have the greatest claim to validity at large r among these potentials. In order to examine their long-range behavior in detail, we have plotted in Fig. 2 the quantity $[V(\infty) - V(r)]/V(\infty)$ versus r/r_e on a log-log scale. The Huffaker potential, being based on Morse functions, does not yield a straight line. This function rises too quickly to yield the long-range form dominated by a single term of the type r^{-n}. Within the experimental errors of the spectroscopic constants (as indicated by the

dashed lines), the Thakkar potential yields very nearly a straight line of slope -3.74 at $r/r_e = 1.3$ and -3.27 at $r/r_e = 5$. This behavior is reinforced by comparison in Fig. 2 to the function

$$[V(\infty) - V(r)]/V(\infty) = \frac{\alpha e^2}{2r^4 D_e}$$

where $\alpha = 1.6421$ Å^3, the polarizability of Ar, and $D_e = 4536.6$ cm^{-1}, the dissociation energy of the Thakkar potential. It is also important to point out that the outer turning point of the v" = 4 level is at $r/r_e = 1.239$. The Thakkar potential is thus able to express the long-range nature of the potential from limited information localized about the potential minimum. Such an ability is an important feature of any empirical potential for species which are weakly bound; the long-range behavior becomes a particularly telling feature of any derived potential, as other quantities, such as the dissociation energy, are usually not well-known.

It is in fact, the estimation of the dissociation energy that is the most useful feature of these potentials. The estimated dissociation energies for the X-state of $BeAr^+$ are 3778±68 and 4537±250 cm^{-1} for the Huffaker and Thakkar potentials, respectively. Subbaram and co-workers had fitted their RKR points to two model potentials: a difference between two exponentials and an (exp, n) function finding D_e's of 3900 and 4300 cm^{-1}, respectively, with n = 4.4±0.5. By taking an average, they had declared an estimate of 4112±200 cm^{-1}. Since the average of our estimates, 4157±380 cm^{-1}, only increases the uncertainty of D_e, it would seem that our analysis is a step backwards in the search for a better

estimate.

Recently, however, LeRoy and Lam[12] have made a new estimate, indicating that the Thakkar value should be the preferred one. Performing a variation on the old near-dissociation analysis, they had fitted the $BeAr^+$ G_v values to the formula

$$G_v = D_e - H_n(v_D-V)^{2n/(n-2)} \times F(v)$$

where

$$F(v) = 1 + A_1(v_D-v) + A_2(v_D-v)^2 + \ldots$$

or

$$F(v) = [1 + B_1(v_D-v) + B_2(v_D-v)^2 + \ldots]^{2n/(n-2)} .$$

By varying the number of coefficients in each expansion, they had arrived at a common value of 4500±50 cm^{-1} for D_e and 40.8±0.5 for v_D. What is most notable is that the Thakkar D_e of 4537 cm^{-1} lies comfortably within the limits of LeRoy and Lam's uncertainty, which is <u>five times smaller</u> than the standard deviation of the Thakkar value. This further indicates that the Thakkar function is the best choice for a weakly bound molecule.

The most rigorous test of a potential derived from spectral data is the ability of the potential to reproduce the spectral constants observed. The proper way to apply this test is to find the eigenvalues of the potential. We have found the lowest five eigenvalues of the vibra-

tional motion for all the ground state potentials reported here (except the Dunham and PA potentials, but including a model potential discussed later), by integration of the radial Schrödinger equation as outlined by Cooley [13]. The results are presented in Table IV as the differences between the calculated and observed eigenvalues. The superiority of the Huffaker and especially the Thakkar potentials is evident. The fact that the Huffaker potential consistently and increasingly underestimates the successive eigenvalues further indicates that its dissociation energy estimate should be too small. Table IV also quantitatively demonstrates that the successive improvement of the SPF potential through added boundary-condition coefficients still does not bring the latter potential into line with the two former ones.

We should remark upon the misbehavior of the Huffaker and Thakkar potentials and just how serious this failure is. It is obvious from Fig. 1 that both reach nonphysical maxima at 0.791 r_e for the potential of Huffaker and 0.806 r_e for that of Thakkar. For this reason integration of the Schrödinger equation must begin at no value smaller than 0.80 r_e lest the wave function should begin to "feel" the attractive artifact of the potential. This proves to be no severe constraint as illustrated by the fact that, for $v = 4$ of the Huffaker potential, the wave function at 0.80 r_e is only 0.68% of its first maximum inside the well, suggesting that the wave function should be well characterized within the inner wall given that the grid size is sufficiently small. For higher vibrational levels it will be necessary to attach smoothly a simple repulsive function such as an r^{-m} or a Morse function. This practice is, of course, standard procedure for extending the inner portion of the RKR curve above the

dissociation limit. Moreover, misbehavior of the inner wall is not unique to the series potentials; Tellinghuisen[14] has noted that the inner RKR turning points near dissociation have a tendency to flair in or out and has discussed the necessary remedies for this problem. Thus, if we find a series potential turning over along the inner region, we are in no worse shape than with an RKR curve.

It is also worth noting the Thakkar maximum occurs for $\lambda_T = -0.979$, very close to the theoretical convergence radius. Although the Huffaker maximum corresponds to $\lambda_H = -1.384$, the critical value of r is only 0.015 r_e closer in than that of Thakkar. An improved radius of convergence in λ-space does not necessarily imply an overwhelmingly improved radius of convergence in r-space.

Since we regard the overall success of the Thakkar function as evidence of the importance of the r^{-4} attraction in the region of the potential minimum, we will consider a simple model potential

$$F(r) = Ae^{-\beta r} - (Z^2e^2\alpha/2r^4)$$

where A and β are adjustable parameters, Z represents the "effective" charge of the beryllium ion as seen by the rare gas atom, and α is the polarizability of the rare gas. By requiring that this potential have a minimum at r_e and that it possess the same curvature at the minimum as all other potentials, we secure the values of A and β through the relations

$$\beta = (\omega_e^2 r_e^3/4B_e Z^2 e^2 \alpha) + (5/r_e)$$

and

$$A = (2Z^2e^2\alpha/\beta r_e^5)$$

We now vary Z in order to reproduce the Thakkar dissociation energy of 4537 cm^{-1}, obtaining Z = 1.29 for the X state. From Table IV it is apparent that the calculated eigenvalues for this model potential are comparable in their agreement with experiment to those of the best SPP modifications.

Although there are not enough data known for the $A^2\Pi_r$ state to permit an adequate series inversion analysis, there are enough for the evaluation of model potential parameters. From the Thakkar D_e of the X state, the T_e from Table I, and the Be($^2P_{1/2}$-^2S) transition energy[15] of 31928.8 cm^{-1}, (since the $A^2\Pi_{1/2}$ state correlates to the Be^+ $^2P_{1/2}$ state) we derive a dissociation energy for the A state of 1189 cm^{-1}, which in turn yields a value of Z_Π of 1.88.

The values of the two Z's and the relative binding energies of the two states can be rationalized in terms of the screening effect of the remaining valence electron of the beryllium ion. The $X^2\Sigma^+$ state corresponds to the outer Be^+ electron being in a 2sσ molecular orbital, placing it between the Be^{2+} core and the Ar atom's electron, screening the core by 71%. The excited state places this electron into a 2pπ m.o., which is mostly pure 2p and placed mainly on the beryllium ion, thus providing a poorer screen between the core and the Ar electrons. The strength of polarization is thus larger, and because the outer "repulsive" valence electron is more out of the way, the ion-neutral approach is closer, and hence the well depth for the excited state is

larger.

It is also probable that $Z > 1$ atomes for the sins of omission of the hyperpolarizability and higher order induction terms that are certainly important for field strengths on the order of 10^8 Volt cm^{-1}. The simple model potential nevertheless provides a chemist's qualitative description of the binding and a surprisingly good quantitative description of the ground state.

In summary, the Thakkar potential augers well in this initial test of its description of a weakly bound diatomic molecule, recovering the long-range r^{-4} behavior from spectroscopic data centered about the potential minimum. Moreover, it extrapolates to a limiting value that compares very well to recent, careful determinations of the dissociation energy. This latter value can be used to evaluate a simple model potential for the ground and excited states of $BeAr^+$, which in turn gives a fair quantitative description of the ground state and an interesting qualitative explanation for the bonding of both states.

C. Other Molecular Ions

Although $BeKr^+$ has also been observed[11] under high resolution, like the A $^2\Pi_r$ state of $BeAr^+$ not enough vibrational levels are observed to warrant a decent potential inversion analysis. The three parameter model potential, however, requires only the experimental quantities ω_e, B_e (hence r_e), and D_e. The last piece of data is not known for either state, but Hartman[7,16] has argued that, since the value of Z is a property of the beryllium ion alone, the Z_Σ and Z_Π quantities should be transferable from $BeAr^+$ to $BeKr^+$, permitting an evaluation of the latter's D_e's. One therefore finds $D_e'' = 5511$ cm^{-1} for the X $^2\Sigma^+$ state and $D_e' = 13656$ cm^{-1} for the A $^2\Pi_{1/2}$ state of $BeKr^+$. Since

$$T_e = \Delta E + D_e'' - D_e' \quad ,$$

where $\Delta E = 31928.8$ cm^{-1} is the $^2P_{1/2}$–^2S energy of Be^+ [15], one predicts a T_e of 23784 cm^{-1} which compares well to the observed value of 23782.18 cm^{-1}. Some of this good agreement stems from the luck of rounding the Z's to three significant figures, but even so only a rounding error of ±50 cm^{-1}, or 0.2%, is present.

Because of the success of this model Hartman[7,8] has applied this potential to the complex chemiluminescence of the A $^2\Pi_r$ state of $CaAr^+$ with some success.

It is intriguing to consider the application of this model to $BeXe^+$, which has also been observed in emission by Coxon and coworkers[17]. Unfortunately, because of blending of the rotational lines due to the several isotopes of xenon and the limited amount of

run time they had due to the cost of xenon (they used a flow system for their microwave discharge), a high resolution rotational analysis and a determination of r_e was not possible. We can, however, take their values of the ω_e's and estimate the model parameters in the following manner. The value of β can be estimated from the Zener approximation:[18]

$$\beta = ((I_1/R_\infty)^{1/2} + (I_2/R_\infty)^{1/2})/a_0$$

where I_1 and I_2 are the ionization potentials of the rare gas and the beryllium ion in either the ^2S or $^2P_{1/2}$ state as applicable, R_∞ is the Rydberg constant for infinite nuclear mass, and a_0 is the Bohr radius. Table V compares the Zener approximation to the model potential evaluations of β for $BeAr^+$ and $BeKr^+$, indicating an average error of 0.05 $\mathring{A}^{-1}$. By estimating the β's for $BeXe^+$ and using the curvature equation, we find

$$r_e^6 = ha_0R_\infty Z^2\alpha(\beta r_e-5)/(\mu\omega_e^2\pi^2c) \quad ,$$

where h is Planck's constant, ω_e and the Rydberg constant, R_∞, are expressed in cm^{-1}, $\alpha = 4.0444\ \mathring{A}^3$ for xenon, and we take μ to be the reduced mass for the 131 isotope of xenon. We find for the X state: $r_e = 2.458\pm.016\ \mathring{A}$ and $D_e = 6308\pm90\ cm^{-1}$, and for the A state: $r_e = 2.348\pm.020\ \mathring{A}$ and $D_e = 14870\pm250\ cm^{-1}$, where the uncertainties are quoted only for the $\pm0.05\ \mathring{A}$ uncertainty of the β's. These values follow the expected trend apparent from Table VI. The estimated T_e for

$BeXe^+$ is 23367 cm^{-1}, about 5.8% higher than Coxon's observed value of 22096 cm^{-1}, but not unreasonable considering the assumptions made.

In order to determine the range of applicability of the model potential, we list the Z values of various simple ion molecules in Table VII. We assume the polarizabilities of the rare gases to be 0.2051, 0.3946, 1.6421, and 2.4794 Å for He, Ne, Ar, and Kr, respectively.

For the homonuclear rare gas ions, where exchange and chemical forces are important, the Z-values are obviously too large to be explained by any deshielding arguments and prove, as expected, that the model provides an inadequate description of the bonding. Similar is the case for the rare gas-proton pairs where the long-range force can only correspond to a bare proton, i.e. $Z \equiv 1$. Again, one expects chemical forces to be important in the region of the potential minimum. It appears that the model potential, like the Thakkar series, is useful for bound energies of less than 40 kcal mol^{-1}.

The mixed rare gas ion pairs, on the other hand, show fairly reasonable Z-values that can be rationalized. In contrast to beryllium ion-rare gas cases, the molecular orbital angular momentum is derived not from a "repulsive" electron but rather from an "attractive" electron hole. For example, the X $^2\Sigma^+$ and A $^2\Pi$ state of $HeAr^+$ both correlate to the ^2P state of Ar^+. (Since the data for this system are from an ab initio calculation[19], we do not concern ourselves with spin-orbit interactions.) The X state has only one electron in the argon 3σ orbital, and hence the helium atom sees an unscreened neon nucleus to the tune of $Z = 1.20$. The A state has two electrons in the $3p\sigma$ orbital,

and hence the helium is more effectively screened from the neon charge, although Z = 0.95 is only a rough estimate since ω_e must be evaluated from the Kratzer formula using the rotational and centrifugal distortion constants of the ground vibrational level. The value of Z = 1.07 for B state of $HeNe^+$, which correlates to $Ne(^1S)$ and $He^+(^2S)$ is most reassuring, since the remaining, very tightly bound electron of helium should quite effectively shield its alpha particle from the approaching electrons of neon. The importance of the ion-induced dipole interaction has been confirmed in the study by Dabrowski and Herzberg[20]. The Z-value for the observed $HeNe^+$ A $^2\Pi_{1/2}$ state is, again, a rough estimate due to lack of data but nevertheless compares well to the corresponding A state of $HeAr^+$.

The Z for the X state of $HeNe^+$ seems unusually large for Ne^+ and casts a shadow of doubt on the exponential-4 model, which is especially disappointing since the binding energy is comparable to that of $BeAr^+$. There are several differences between these two molecular ions worth pointing out. First, only the top 15% of the well has been observed in Dabrowski and Herzberg's emission studies, subjecting ω_e and D_e to errors of extrapolation, whereas 34% of the bottom of the vibrational well is observed for $BeAr^+$. Second, the A $^2\Pi_{1/2}$ state of $BeAr^+$, is well separated energetically from the ground state and does not interact through Hund's case (c) coupling perturbations, whereas the X and A states correlate to different spin-orbit states of $Ne^+(^2P)$, the latter being split by only 780.5 cm^{-1}[15]. This coupling is seen through the "borrowing of intensity" from the X state, making the B $^2\Sigma^+$ to A $^2\Pi_{1/2}$ emission

possible in contrast to the complete lack of emission to the A $^2\Pi_{3/2}$ state, which does not couple. Examination of Fig. 8 of Dabrowski and Herzberg's paper reveals that the region of closest interaction between the A and X states is the long-range portion of the X state. It is possible, then, that the A state perturbations are distorting the shape of the X state potential in the region where data are available.

We have examined the X and B states of $HeNe^+$ more closely through a potential series inversion. We list the Y_{ij}'s and potential coefficients in Table VIII. The potential plots, shown in Figs. 3 and 4, further demonstrate that the Thakkar series is superior to the Huffaker series for qualitatively describing weakly bound systems, even more so in this case, since the values of the dissociation energies are less at issue than with $BeAr^+$. Of particular note is the successively decreasing correction coefficients for the B state, indicating that the Thakkar function is well suited for describing this potential. A more quantitative test is in Table IV: the reproduction of vibrational and rotational data. The results for the B state appear tolerable, but the Thakkar values for the X state tend to be too large. These deficiencies may be attributed to the A state interactions and possibly the extrapolation problems cited earlier. Overall, however, the Thakkar series is the best available one for both states since that of Huffaker cannot even reproduce the bound states that were initially observed.

One unique point definitely worth mentioning is the matter of p for these states. In general, we have observed that for most weakly bound molecules which have an r^{-n} attraction dominating their binding,

the value of p is on the order of n-1, such as 3.16 for $BeAr^+$. This is not the case for the X and B states of $HeNe^+$, where the p-values are 4.65 and 4.41, respectively. Although we might try to dismiss the X state anomaly as before, we remain perplexed with the case of the B state. To illustrate further the long-range deviation we plot $[V(\infty)-V(r)]/V(\infty)$ versus r in Fig. 5 as we have done in Fig. 2. For $BeAr^+$, the fact that p was one integer too small was compensated for by the higher order correction coefficients, yielding a reasonable long-range behavior. This is not possible for the smaller correction terms of the $HeNe^+$ B state. It might be that the $HeNe^+$ B state is so close to a pure r^{-4} molecule, having the least chemical interaction, that it is the exception that proves the rule and causes the Thakkar potential to overestimate the exponent of the long-range behavior.

D. NaNe and NaAr

The line broadening mechanisms of the sodium D lines and the interatomic interactions between ground state and excited sodium atoms is of practical interest. One application is the high pressure sodium vapor street lamp which is fast replacing the familiar mercury vapor lamp, changing the nightime urban landscape from blue to pinkish orange. Another application is the suggested[21] combination of alkali metal atoms and $^1S_0$ atoms to form excimer laser systems. One such set of candidates is the sodium-rare gas (Rg) pair. For these reasons the sodium-rare gas interactions have received quite a bit of theoretical and experimental attention.

The analysis of NaRg pairs was our next logical step, since they are isovalent to the $BeRg^+$ molecules we have discussed thus far. Indeed, the spectroscopic properties of $BeRg^+$ resemble those of NaRg more than the other isovalent series, BeX, where X is a halogen, since the binding is through weak long-range physical forces rather than short-range chemical ones. The interesting difference here is that the nature of the long-range attraction for NaRg is the even weaker London dispersion r^{-6} reaction.

The experiments that concerned us most were the supersonic molecular beam laser induced spectroscopy studies of NaNe by Ahmad-Bitar, Lapatovich, Pritchard, and Renhorn (ALPR)[22] and of NaAr by Smalley, Auerbach, Fitch, Levy, and Wharton (SAFLW)[23]. Using Campargue-type nozzle sources[24], which are capable of producing internal molecular temperatures <1°K, they had formed, or "condensed", a reasonably high concentration of NaRg in a cold, collision-free environment. Crossing

this beam at right angles with a narrow bandwidth tunable cw dye laser permitted very high resolution, high sensitivity laser-induced fluorescence studies of the dimer. The resulting spectral constants in turn allowed us to make a potential series inversion, at least for the A $^2\Pi_r$ state. We had, in fact, done so and reported our results for the A $^2\Pi_{3/2}$ state of NaNe and X $^2\Sigma^+$, A $^2\Pi_{1/2}$, and A $^2\Pi_{3/2}$ states of NaAr. Since that time there have been more careful and definitive experimental studies on NaNe and on NaAr.

Rather than repeat our earlier results, which are readily attainable in the literature[25], we will simply summarize and critique them with respect to the more recent experimental studies.

In our original study we had found for the A $^2\Pi_{2/3}$ state of NaNe, like the X and B states of $HeNe^+$, the Thakkar function to be the best series representation of the potential. The Huffaker series had severely underestimated the well-depth and had again failed to reproduce the vibrational levels used to determine it. The Thakkar potential had ten bound levels with a dissociation energy of 149.70 cm^{-1}, or 7% higher than ALPR's original estimate. Since we have already reported the G_v's, B_v's, and the RKR turning points, we only list the deviations between the observed and calculated quantities in Table X. The consistently larger $\Delta G(v+1/2)$'s and larger B_v's for the higher levels reaffirm our suspicion that the Thakkar potential probably overestimates D_e; the fact that p=4.18 whereas the long-range n=6 suggests that the Thakkar potential should rise past the true dissociation limit, but probably not by the ten wave number discrepancy between our value and that of ALPR.

The initial report of ALPR was followed by Lapatovich, Ahmad-Bitar, Moskowitz, Renhorn, Gottscho, and Pritchard (LAMRGP)[26], yielding accurate values of D_e and r_e for the X, A, and B states. By means of a LeRoy and Bernstein near-dissociation analysis they obtained a dissociation energy of 140±5Å. In an even more careful analysis by Gottscho, Ahmad-Bitar, Lapatovich, Renhorn, and Pritchard (GALRP)[27], a Thakkar potential was fitted to the RKR turning points of the A $^2\Pi_{3/2}$ state, yielding a dissociation energy of 144.4 cm^{-1}. This latter value is probably more realistic since the former was obtained by extrapolating the near-dissociation formula to $v = -1/2$, which is in a regime where the formula could not possibly be valid. We are, of course, reassured that their latter value agrees more closely (3.7%) to our original estimate. In Table XI we list the spectroscopic constants, our Thakkar coefficients and those of GALRP. The RKR turning points are also given there.

GALRP have found the A $^2\Pi_{1/2}$ state to be badly perturbed by the B $^2\Sigma^+$ state and, anticipating poor behavior due to interacting states, we therefore do not consider fitting a Thakkar function to their data. In fact, GALRP have already performed an extensive deperrurbation calculation of the adiabatic A and B states, yielding results we consider instructive. In particular, they have found a shallow secondary minimum of 0.04 cm^{-1} at 7.1 Å of the A $^2\Pi_{1/2}$ state, lying between the outer turning points of $v = 5$ and $v = 6$ (see Fig. 7 of ref. 27). Although an RKR analysis would not have shown this minimum, the effects appear in the values of B_v and Franck-Condon factors. Any series potential function would be hard-pressed to reproduce faithfully this phenomenon

with only a few terms. We feel this may suggest why the series potentials fail to represent an excited, interacting state which, from a casual glance at the RKR curve, appears to be "normal".

One other excited state interaction GALRP have studied more closely is the predissociation of the $v = 4$ and 5 rovibronic levels of the A $^2\Pi_{3/2}$ state into the A $^2\Pi_{1/2}$ continuum. It would be tempting to blame this effect on the fact that the deviation of B_4 in a least-squares fit of $Y_{k'}$'s is exceptionally large, as we had noted earlier[25], but this would not explain why B_5 is so well-adjusted while the predissociation line broadening of $v = 5$ is no less than that of $v = 4$. Unless further evidence indicates that the broadening should be asymmetric for $v = 4$, yielding an incorrect B_4, there is no physical justification for the exclusion of B_4 in a least-squares fit of GALRP's newer, more accurate data.

As for the X $^2\Sigma^+$ state, there is only one bound vibrational level observed. Using the rotational data and the isotopic shift observed for $Na^{22}Ne$, GALRP have fit a function

$$V(r) = C_8/r^8 - C_6/r^6 \quad ,$$

yielding a dissociation energy 8.0±0.3 cm^{-1} and an internuclear equilibrium separation 5.3±0.1 Å. Although their fitted value of $C_6 = 7.092\times10^5$ cm^{-1} Å^6 is considerably larger than Dalgarno and Davidson's estimate of 2.3×10^5 cm^{-1} Å^6 [28], the overall physical description of the potential is probably well within the uncertainties cited.

The same is true for the B $^2\Sigma^+$ state. Only two vibrational levels

are observed. Since this state is also strongly perturbed by the A state, a reliable Thakkar fit would be as unlikely as for the X state. GALRP's values for r_e and D_e are 7.9±0.5 Å and 4.5±0.5 cm^{-1}.

In GALFW's original analysis of NaAr laser-induced fluorescence, there was an uncertainty of the vibrational level assignment of the A $^2\Pi_r$ states, the lowest for the A $^2\Pi_{1/2}$ being either 6, 7, or 8, so we considered all three possibilities in our Dunham constants/series potential analysis. Since that time Tellinghuisen, Ragone, Kim, Auerbach, Smalley, Wharton, and Levy (TRKASWL)[29] have dispersed the laser-induced fluorescence of the A state to the X $^2\Sigma^+$ state and have established that the lowest observable level is v = 7 by analyzing the bound-free fluorescence (which, incidentally, showed that the vibrational assignment of the excited state <u>could</u> be established by counting the number of nodes in the bound-free fluorescence and assigning them to the nodes of the excited state's vibrational wave function). We will therefore restrict ourselves to recording only the "x = 7" results of our paper.

The mechanical constants for the A $^2\Pi_{1/2}$ and A $^2\Pi_{3/2}$ state are listed in Table XII and the Thakkar potential coefficients in Table XIII. Since there are not enough data to perform a nominal least-squares fit (<u>i.e.</u> no degrees of freedom), it is impossible to establish an error bounds on the reliability of the individual constants, as was the case for NaNe. Moreover, we question whether the coefficients for the A $^2\Pi_{1/2}$ state are very reliable at all due to 1) the possible interaction with the (unobserved) B $^2\Sigma$ state and 2) the fact that the values for Y_{21} and Y_{31} were set to zero in order to calculate a coefficient

set up to e_6. The equal and opposite values of the e_3/e_4 and e_5/e_6 pairs hint that the higher order e_n's may be nonphysical. Despite these problems, the Thakkar dissociation energy of 572.2 cm^{-1} compares well with TRKASWL's latest evaluation of 568.2 cm^{-1}, indicating that the Thakkar potential's gross description of the state remains satisfactory. The Thakkar D_e is also within the limits of the value of 550±30 cm^{-1} from the argon pressure-broadening studies of York, Scheps, and Gallagher[30]. All these results confirm our earlier suspicion that the theoretical SCF-CI calculations of Saxon, Olsen, and Liu[31] had determined a dissociation energy ~15% too small, which is not a terrible indictment considering their project.

The A $^2\Pi_{3/2}$ state enjoyed a more quantitative success in reproducing the experimental values of SAFLW despite the fact that there was one fewer vibrational level observed. Part of the success may be attributed to the fact that, with one fewer observed level, we had not been tempted to overextend the degree of the Thakkar polynomial, but surely the lack of B $^2\Sigma_{1/2}$ interaction made a series description of this potential more appropriate[32]. The agreement between this potential and experimental results is better than that of the $^2\Pi_{1/2}$ state as is apparent in Tables XIV and XV. The Y_{ij}'s used to compute the $^2\Pi_{2/3}$ Thakkar function also determine an RKR potential which shows remarkable agreement - ' is illustrated in Figure 6. Also shown is the Huffaker series and its repeated failure to reproduce the overall potential form.

Some of this agreement may be due to a fortuitously good set of G_v Y_{ij}'s; the derivative of G_v with respect to v is zero in the neighborhood of the dissociation level, which is equivalent to saying that

the Birge-Sponer plot crosses the $\Delta G_v = 0$ axis near dissociation. The RKR exprapolation therefore shows "dissociative" behavior at and above $v = 17$. (By comparison, the G_v expansion for the $^2\Pi_{1/2}$ state increases monotonically for positive v, indicating no dissociation.) However, when we compare our value with the D_e's obtained by others, we are encouraged. For the A $^2\Pi_{2/3}$ state, TRKASWL determine D_e to be 558.6 cm^{-1}. Düren, Gröger, Hasselbrink, and Liedtke[33], studying elastic scattering of argon with laser-excited sodium in the $^2P_{3/2}$ state, have recently derived 562 cm^{-1} for their pseudopotential and 551 cm^{-1} for the Lennard-Jones (8,6) model.

The most significant development in NaAr since our original publication is a better spectroscopic determination of the ground state. TRKASWL had observed fluorescence bands past $v'' = 4$ into the continuum of the ground state, whereas only $v'' = 0$ and 1 were observed in SAFLW's work. Although the resolution of the dispersed fluorescence was not good enough to permit a rotational analysis of the vibrational levels, the accuracy of the determined vibrational energies permitted a near-dissociation analysis evaluation of the dissociation energy, which was found to be 40.4±1 cm^{-1}. Using this value, TRKASWL derived a potential for describing the bound-free Franck-Condon intensities. Since they were primarily interested in the repulsive part of the potential, they found a modified Morse to be an adequate description.

The new vibrational data also made a determination of ω_e and $\omega_e x_e$ possible. We have used these values to determine a new Thakkar function, yielding $p = 4.0517$, $e_2 = -0.07770$ and $D_e = 55.668$ cm^{-1}. Using $p = 6$,

we have found $e_2 = 0.13431$, $e_1 = 0.32472$, and $D_e = 40.158\ cm^{-1}$. We have examined this latter function more closely. The appropriate vibrational and rotational constants are reported in Table XVI and the p = 6 Thakkar function is plotted along with TRKASWL's modified Morse function and Duren and Groger's (DG)[34] modified Lennard-Jones potential in Fig. 7.

Examining the plot, one can see that in the bound region of the potential the Thakkar function follows the TRKASWL potential faithfully up to 6.5 Å, where it switches over and coincides with the long-range portion of the DG potential. (Our C_6 coefficient is 1.5 $cm^{-1}\ Å^6$ compared to 1.4 $cm^{-1}\ Å^6$ for the DG potential, both of which are ca. 50% larger than the theoretical one[28].) Above dissociation the slowly ascending TRKASWL potential is to be preferred since it was fitted to continuum fluorescence up to 2500 cm^{-1} above dissociation, where DG's scattering data employs collision energies of only 625 cm^{-1}. Not apparent in Fig. 7 is the crossing between the Thakkar and DG functions above 100 cm^{-1}. The steepness of the Thakkar function is a tragic flaw which is not easily remedied.

The RKR turning points using TRKASWL's Y_{ij}'s are also illustrated. The poor behavior of the inner turning points can probably be blamed on an inadequate description of B_v for high vibrational levels, casting doubt on B_e and α_e. This in turn casts an aspersion on the Thakkar constants derived from these values.

A closer, quantitative examination of the vibrational energies and rotational constants in Table XVII in fact reveals that the p = 6 Thakkar potential to be, rather than the best of both worlds (i.e. TRKASWL and DG potentials), a weak compromise. We have calculated experimental

$G_0(v)$'s from the band measurements of TRKASWL's Table I. The uncertainties are the standard deviations of the average $G_0(v)$'s listed. The experimental B_v's are those of SAFLW. It is apparent that the TRKASWL and DG potentials show considerable difference in Fig. 7, yet their vibrational energies are within experimental error. Although the p = 6 function is fairly close, the fact that its vibrational energies are still outside the error limits is a direct result of the compromise; as the Thakkar function follows TRKASWL's repulsive wall and switches over to DG's potential for $r > r_e$, the Thakkar function is wider than the other two potentials. Since the vibrational energies are determined solely by the potential width (cf. the RKR f(v) expression), the Thakkar $G_0(v)$ values will lie lower than those of DG and TRKASWL. The B_v data, more dependent upon the centering of the potential at the correct r_e, shows the Thakkar potential to be a little better than that of DG, but still outside SAFLW's error estimates.

It is worthwhile revisiting our original technique of fitting the Thakkar potentials to the data of SAFLW. We had taken the band shift measurements from the $^2P_{1/2}$ line of Na for the rotationless vibrational levels of the v' = 7 level of the $^2\Pi_{3/2}$ state and the v" = 0 and 1 levels of the $^2\Sigma^+$ state. Using our values from the integrated Thakkar potential for the upper state, we computed $D'_v \equiv D'_e - G'_v$ and determined the constants D''_0 and D''_1 from the formula

$$D''_v = D'_7 + \Delta(v'',7) \quad ,$$

where $\Delta(v'',7)$ is the (negative) band shift from the $^2P_{3/2}$ line of sodium[15]

at 16973.379. By constraining $\omega_e x_e''$ such that for any ω_e'' SAFLW's ΔG was reproduced, ω_e'' was iteratively varied so that resulting Thakker D_e'', ω_e'', and $\omega_e x_e''$ yielded our computed values for D_0'' and D_1''. This was done for Thakkar functions of variable p(TI) and p ≡ 6 (TII), as well as several other model potentials[35].

The reported D_e's for the Thakkar functions are, in light of TRKASWL's results, about one wave number high. Closer examination shows that our calculated values of D_0'' and D_1'' of 34.91 and 23.65 cm^{-1}, respectively, are 0.96 cm^{-1} higher than those calculated from TRKASWL's derived values. This can be further traced to an error in our extrapolated D_7' and, in fact, our D_7' of 145.625 cm^{-1} is 0.95 cm^{-1} higher than that predicted by Table II of TRKASWL's work.

Repeating our iterative algorithm on the D_0'' and D_1'' of Tellinghuisen et al., we find the ω_e'', $\omega_e x_e''$, and D_e'' of the standard, variable p Thakkar (TIII) and p ≡ 6 Thakkar (TIV) to be identical! This is in marked contrast to the preceding results using the "standard" Y_{ij} potential determination. The spectroscopic quantities derived from these potentials and the Thakkar constants for TI - TIV are listed in Tables XVII and XIX, respectively. Most notable is that the adjustment of D_0'' and D_1'' does bring the D_e'' of the Thakkar potentials into agreement with Tellinghuisen's value.

This exercise illustrates more than just internal consistency. First, it reiterates the success of representing the A $^2\Pi_{3/2}$ state with a Thakkar function since our original, relative accuracy of better than 5% for the X state hinged upon the 1 cm^{-1} absolute accuracy of D_7'.

It shows that, given the right data and fitting procedure, the Thakkar function is also an appropriate one for the ground state as well, yielding fairly good quantitative results. The agreement between TIII and TIV when compared to the disagreement between Thakkar functions using our tradiitional fitting procedure indicates that, when dealing with limited data, newer means of potential fitting incorporating all data available should be invoked. This point will be considered in more detail towards the end of this chapter.

We also find a certain paradox in Table XIX. Although TI and TII overestimate D_e by 1 cm^{-1}, their G's are better than those of the corresponding TIII and TIV. While this may warrant further study, we suspect that the expansion to e_2 is too limited to accommodate all the data.

A final point to be made is the apparent ambiguity of choice of variable-p over p = 6 Thakkar functions. Our earlier experience with $BeAr^+$ lead us to conclude that the variable-p was to be preferred. In light of NaAr X $^2\Sigma^+$ and the results of Gottscho <u>et al</u>. for A $^2\Pi_{3/2}$ of NaNe, it may be that the two kinds of Thakkar functions should be examined on a case-by-case basis. As a matter of consistency, however, we will stay with our choice of variable-p for the remainder of this chapter.

E. Ar_2

We consider now the dimer of argon. The interaction and binding of this nobel gas, 0.3 kcal mol^{-1} at 3.8 Å, should be considered the model system for studying van der Waals attraction. Argon, obtained by liquification of air, is readily available and has been the subject of extensive study in the past, and the thermodynamic and transport properties are well documented[36]. Still another of its properties in nature that lends itself for microscopic study is the fact that it occurs almost exclusively (99.6%) as the 40-isotope: a boson. The Pauli Exclusion Principle requires that only even angular momentum quantum numbers can occur for the ground state of the dimer, permitting a unique and detailed study of the differential elastic scattering cross section and the resolution of the rotational structure by vacuum ultraviolet absorption spectroscopy.

As a result, a great number of potential functions have been derived of varying degrees of complexity. Recent examples are the numerical functions of Dymond and Alder[37] and of Colbourn and Douglas [38], the piecewise continuous functions of Parsons, Siska, and Lee[39], of Aziz and Chen[40], and of Koida and co-workers[41], and the function of Barker, Fisher, and Watts[42] which is analytic for all r, if somewhat unwieldy. Results of earlier and simpler potential functions are reviewed by Smith[43]. Probably the best functions for describing the combined spectroscopic and thermodynamic data are the HC-D potential of Aziz and Chen and potential 4 of Koida et al. We might also infer that their potentials could reproduce the elastic scattering data satisfactorily, but this test is yet to be made in

the literature.

In light of this, no systematic study of potentials applicable to van der Waals molecules is complete without considering Ar_2. Our purpose is not to propose a potential superior to any in print but rather to deterime whether the Thakkar potential is suitable for this system. We find, in fact, that our standard procedure produces a potential function that does not describe the argon-argon interaction to the accuracy that the true potential is known. This is not an indictment of the potential form so much as it is for the method of determining the potential; Colbourn and Douglas (CD)[38] found that the RKR method failed to produce a potential adequate for predicting the higher vibrational and highly excited rotational levels. In order to improve the Thakkar function we incorporate into the fit the elastic scattering data of Parsons, Siska, and Lee (PSL)[39], from which we derive a potential that is suitable for describing the spectroscopic, scattering and thermodynamic data available. Towards the end of this chapter we will describe a method for systematically varying a Thakkar or any other function using spectroscopic data alone which is more in the spirit of how CD derived their numerical potential from their initial RKR estimate.

We find our initial, or nominal, Thakkar by first fitting a set of Y_{ij}'s to the $G_0(v)$ and B_v values reported by Colbourn and Douglas. Since data are available for v = 0 to v = 5, we have enough values to perform a least-squares Y_{ij} fit. This proves helpful since we can estimate the standard deviations of the Y_{ij}'s and hence the standard deviations of the Thakkar constants, which are reported in Table XX. Because of the relative uncertainties in the data, discussed in ref. 38,

and the low number of degrees of freedom (*i.e.* the differences between number of data and number of fitted parameters) in the least-squares fit, even a minimal set of Y_{ij}'s had fairly high standard deviations[44]. In turn, the nominal Thakkar constants inherit large uncertainties; the well depth, D_e, is uncertain by 18% and in fact is 10% higher than the best determinations of the Ar_2 bond energy. Because of these uncertainties, the nominal Thakkar cannot reproduce the dimer's potential to the known degree of accuracy or even accurately reproduce the spectroscopic data from which the potential is derived.

There are three reasons why our standard procedure failed to produce an agreeable potential. One, as mentioned before, is the uncertainty in the measured spectroscopic constants. Although listing their $G_0(v)$'s to 0.001 cm^{-1}, CD expressed an actual confidence of 0.1 cm^{-1} up to 0.25 cm^{-1} for v = 5. Relative to the dissociation energy, this means an uncertainty of 1 to 2.5 parts per thousand. This is slightly less than the 2.5 parts per thousand from TRKASWL's measurements of the X state of NaAr, where our standard Thakkar procedure produced a potential whose dissociation energy was in error by 38%. By comparison, our more presentable results for $BeAr^+$, $HeNe^+$, NaNe, and NaAr involved relative errors in the range of 20 to 77 parts per million.

A second reason for the Ar_2 failure is the fact that we could only employ an expansion up to Y_{30} and Y_{21} with any confidence, although the data encompassed almost the entire potential well. While a low order expansion may be appropriate for extracting the "true" Y_{ij}'s when only a fraction of the potential is sampled (such as with $BeAr^+$ and the

A $^2\Pi_{3/2}$ state of NaAr), the need of describing the entire potential will require a higher order expansion in Y_{ij}'s. This is the same problem we cited for HF in Chapter II, and is endemic to the molecular system being considered. In all fairness, we should report that we have, in fact, examined higher order Y_{ij} and hence Thakkar expansions (at the price of even higher standard deviations due to fewer degrees of freedom) and found no improvement in the nominal Thakkar function. We nevertheless feel that lack of available molecular information remains a source of error.

To substantiate further this point, we come to the third reason. There is, in fact, "extra" information available which we do not employ: the D_v's. As discussed in Chapter II, our procedure does not employ the information available from the highly excited rotational states, except to derive more accurate B_v's and hence Y_{i1}'s. This point is equally true of the RKR procedure and, point of fact, is the reason that CD had scrapped the RKR method. Citing the lack of $G_0(v)$'s and B_v's as well as the semiclassical approximation as the reasons their RKR potential could not satisfactorily reproduce their observed levels, CD manually adjusted their initial RKR potential in order to reproduce the energies of the high J levels, thus arriving at their final numerical function. As mentioned before, we will discuss how to use this "extra" information later in this chapter.

We have taken another tack for increasing our data set. Using the nominal potential to generate the differential elastic scattering cross section for Ar for comparison with the high resolution data of

PSL, we have systematically varied the nominal constants throughout their calculated uncertainties in an attempt to improve the differential cross section. This adjustment was not done in a least-squares fitting sense; rather a set of calculations was made for various parameter values, and the RMS deviation of the calculation from the experimental data was iteratively lowered until the agreement was significantly improved. Thus, it is possible that these refined constants could be more highly refined by methods such as suggested by Bickes and Bernstein[45], but the rapid convergence of our iterative method made further refinement unwarranted.

We give the refined potential constants in Table XXI, and plot the differential cross sections computed from the nominal and refined Thakkar potentials as well as the Morse-Spline-van der Waals (MSV III) potential of PSL in Fig. 8. All calculations shown were done with the same degree of angular and velocity averaging to allow easy visual comparison among the fits. As a result, the symmetry oscillations at large angles (due to the even J parity property of Ar_2) are somewhat enhanced by incomplete averaging.

A qualitative glance at this figure shows that the nominal Thakkar provides an unsatisfactory description; the calculated rainbow scattering appears too large an angle, indicative of too deep a potential well. Although the constants of the refined Thakkar are remarkably similar to those of the nominal, the improvement in the calculated cross section is dramatically evident. While the MSV III potential gives better agreement at scattering angles slightly less than the primary rainbow, the overall fits of the refined Thakkar potential and the

MSV III potential are comparable.

As a final check of the validity of the refined Thakkar potential, we have calculated the second virial coefficient using the standard expression including the first quantum correction[46]. The results of these calculations for the nominal Thakkar, the refined Thakkar, the MSV III and the Colbourn and Douglas potentials are shown in Fig. 9, as a plot of differences from the experimental data of Levalt Sengers et al.[47] For this calculation we have connected the table of points given by Colbourn and Douglas with spline functions and extended the potential in regions outside of their table with a Morse function and with the expression

$$V(R) = -\frac{C_6}{R^6} - \frac{C_8}{R^8}$$

at short and long ranges, respectively. The average RMS deviations, evaluated every 100K, of the refined Thakkar, MSV III, and Colbourn and Douglas potentials are 2.06, 2.34, and 1.17, respectively. When calculated every 2K from 80K to 120K the average RMS deviations are 3.84, 8.41, and 4.46. The low deviations for the potential of Colbourn and Douglas are of no surprise, since they had adjusted their values of D_e and C_8 to improve agreement between experimental and calculated second virial coefficients.

In Fig. 10, we plot the four potentials for Ar_2 of immediate concern. These are the nominal and refined Thakkar potentials, the MSV III potential, and the CD potential. We have chosen these latter two poten-

tials since the authors, who have taken the data sets we have employed, have found these potentials best represented their respective data sets[48]. The refined Thakkar has a well depth of 100.37 cm^{-1}. Other Ar_2 potentials have well depths only slightly less than this. PSL report 97.83 cm^{-1} for MSV III, CD as well as Aziz and Chen employ 99.55 cm^{-1}, and Koida et al. find 99.58 cm^{-1} as their optimum. While both Thakkars employ an r_e value of 3.758 Å, the other values are MSV III: 3.760 Å, Koida et al.: 3.7545 Å, and CD and Aziz and Chen: 3.759±.005 Å.

Therefore, these most recent and elaborate functions, including the refined Thakkar potential, are in excellent agreement regarding these two main parameters of the interatomic potential. They disagree mainly in the shape of the repulsive wall at energies several times the well depth. The Thakkar potential rises much more steeply than a Morse function, while both the MSV and the Colbourn and Douglas potentials have single Morse function repulsive walls. The repulsive portion of Aziz and Chen's potential, adjusted to fit the Hartree-Fock potential calculated by Wahl and co-workers, may be equally good, but we have not examined this.

It is noteworthy that the MSV and Thakkar functions begin to deviate only at energies of ~300 cm^{-1}. The collision energy used in the scattering measurements of Ref. 39 was only 500 cm^{-1}. Colgate, et al.[49] reported high energy Ar-Ar scattering results which are in much better agreement with the exponential (Morse-like) repulsion of the MSV potential than with the Thakkar potential. We conclude that the repulsive

wall of the Thakkar function is in serious error, but only at energies of several times the well depth.

While the repulsive wall is not well determined above some energy (and probably so for all the potentials discussed here), it is interesting that the refined Thakkar function gives the best calculated second virial coefficient at high temperatures (Fig. 9). The repulsive wall tends to dominate B(T) more at these temperatures, which are well above the Boyle temperature of ca. 400K. This indicates that the repulsive wall misbehavior of the Thakkar is not serious enough to prevent prediction of high temperature thermodynamic properties.

Finally, we list in Table XXII the energies of the bound vibrational levels, G_v, and the corresponding rotational constants, B_v, for the potentials. The G_v's were computed by numerical solution of the radial Schroedinger equation. Using the resulting wave functions for each vibrational level, the B_v's were calculated by the expression

$$B_v = B_e r_e^2 \langle v | r^{-2} | v \rangle$$

The MSV III potential has been similarly analyzed by Docken and Schafer[50]. We have repeated their calculation in order to have a consistent evaluation of the B_v's and to extend their precision.

The experimental quantities are for the Colbourn and Douglas (CD) potential for v = 0-5. The refined Thakkar and MSV III B_v values agree with the CD values to better than 0.001 cm^{-1}, well within the spectroscopic uncertainty. The G_v values, or more correctly, the

level spacings ($\Delta G_{v+1/2}$) are in similarly good agreement. THE MSV III $\Delta G_{v+1/2}$'s are uniformly smaller than the CD values by, on average, -0.29 cm^{-1}. The refined Thakkar $\Delta G_{v+1/2}$'s are both greater and smaller than the CD values. The average error is only -0.01 cm^{-1}. More comprehensive examinations of the spectroscopic constants of other potentials are available in references 40 and 41.

One point well worth noting is that, in Table XXII, B_5 for the CD potential (0.0289 cm^{-1}) differs from the one listed in Table I of their paper (0.0298 cm^{-1}). This is not a typographical error; we have found that CD's reported B_5 and D_5 fit the eight observed rotational lines in the least-squares sense. This does not mean that their B_5 is the true mechanical constant and reiterates the problem we cited earlier concerning one's ability to extract good spectroscopic constants from a limited set of data[51].

An important question is whether B_v is a reliable parameter for measuring rotational energies at these higher vibrational levels. Our definition of B_v, as a quantum mechanical average of r^{-2}, is correct if the centrifugal potential is a perturbation on the vibrational Hamiltonian. For J = 10, v = 5, the rotational energy becomes comparable to the splitting between the rotationless v = 5 and v = 6 levels. Under these conditions perturbation theory becomes a poor approximation, and hence B_v alone provides an inadequate description of the potential under the influence of angular momentum. We thus report the higher B_v's merely as a stylized comparison of potentials. A more rigorous comparison should report the rotational energies themselves.

Returning to our discussion of the Ar_2 potential, we feel it is

important to note that this potential does not behave solely as r^{-6} in the region where the spectroscopic data are pertinent. Indeed, the r^{-8} contributions to the binding at the outer turning points of $v = 4$ and 5 are 18% and 15%, respectively. We are therefore not particularly troubled that the refined Thakkar potential approaches its asymptotic value as $r^{-5.6}$ instead of r^{-6} as long as the potential shows the correct behavior in the region of interest. In this region the higher order terms correct for any deficiency in the true asymptotic behavior in the same manner that the r^{-8} and higher terms correct for the erroneous assumption that the potential is purely r^{-6}.

It is clear, then, that the Thakkar function is a suitable functional form for describing the dimer of argon and, by implication, most van der Waals' molecules. Although there are some inherent weaknesses in the potential, such as "impure" r^{-6} behavior and a repulsive wall that ultimately rises too sharply, such weaknesses do not prevent the potential from predicting available experimental quantities. The derived vibrational and rotational energy levels, differential elastic scattering cross sections, and second virial coefficients are reliable at temperatures from 0°K to 500°K. What is apparent is that one may have to use potential-determining algorithms other than the Dunham method, which in this case has a tendency to amplify experimental uncertainties. Further improvement of the Ar_2 Thakkar potential may be possible in order to improve further agreement with spectroscopic and scattering data, but at this point our goal has been achieved.

F. Alkaline Earth Dimers

Up to this point we have only considered weakly bound diatomic molecules where one or both partners are rare gas atoms. With all its valence orbitals filled, the rare gas atom should see no "chemical" forces in effect and only simple polarization, long-range forces should contribute to the binding. A similar situation exists for the dimers of the alkaline earths, where the outer ns valence orbitals have been filled and mimic the helium configuration. The measured dissociation energies[52a,b] of these homonuclear dimers (1-3 kcal per mole) are characteristically smaller than those of the neighboring alkali dimers (9-24 kcal per mole) or those of the transition element dimers (10-120 kcal per mole). Most workers therefore consider the alkaline earth, or Group II A, dimers to be bound only by van der Waals forces[52]. This claim is further substantiated by the similar binding energies of the Group II B dimers Zn_2, Cd_2 and Hg_2 (4, 2, and 1.8 kcal per mole, respectively[52a,b],) indicating that the filled $ns^2(n-1)d^{10}$ configuration leads to no chemical binding, either.

Despite these trends, we expect the nature of the bonding in the bulk solid to be due to more than dispersion forces. The solids have cohesive energies twenty times that of argon[53], are metallic, and melt above 650°C[54]. Some of these properties must ultimately be derived from the vacant, nearby np orbitals and, for calcium and higher, (n-1)d orbitals that participate in the covalent and metallic bonding. We will show that there are subtle indications that there is mixing of these vacant orbitals in the ground state of even the dimers, a quality not readily apparent from dissociation energies.

The spectroscopy and diatomic potentials for the ground states of Mg_2 and Ca_2 are now well-determined quantities. The original high resolution Mg_2 absorption data of Balfour and Douglas[55] has been augmented by the analysis of Li and Stwalley[56] and the dispersed fluorescence of the argon ion laser excitation data of Scheingraber and Vidal[57]. The ensuing analysis by Vidal and Scheingraber[58] establishes the dissociation energy, 430 cm^{-1}, to within one wave number and provides an accurate set of Dunham Y_{ij} constants. Similar laser excitation-dispersed fluorescence experiments by Wyss[59] and by Vidal[60] have extended Balfour and Whitlock's (BW)[61] absorption work on Ca_2. Vidal's data analysis for Ca_2 is as careful and thorough as that for Mg_2, yielding a very good set of Y_{ij} constants and a value for D_e of 1095.0±0.5 cm^{-1}.

In recent years a small controversy has erupted concerning the ground state of Ca_2. Sakurai and Broida[61] observed an anti-Stokes continuum in their laser-excited fluorescence of Ca_2 and Wyss[59] observed molecular fluorescence far to the red of BW's band system. These workers concluded that the green band of BW was originating from an excited state, with the true ground state being the source of the red band. Failing to reproduce Wyss' band system, Vidal[60] has since concluded that the red band was an experimental artifact. Liao[62] and Scheingraber and Vidal[57] have also explained the blue continuum as free-bound-free excitation/fluorescence. It appears, then, that the original assignment of BW has been confirmed and the argument laid to rest[63].

Returning to our own studies of these systems, we have taken the Y_{ij} constants of Vidal and Scheingraber and of Vidal for Mg_2 and Ca_2, respectively, and have performed our usual series-inversion procedure. The constants are listed in Tables XXIII and XXIV. These functions, along with the smoothly connected turning points of Vidal's IPA potentials, are plotted in Figs. 11 and 12, illustrating the success of the Huffaker series over those of Thakkar in the region of $r > r_e$ (the artificial maxima at small r is of less concern here). As we have noted in Chapter II, the Huffaker series potential provides a better description for those molecules bound by chemical forces. Although it does not seem that such forces could be responsible for the small binding energies, we suggest that they still may be influential enough to shape the potential in the region of the equilibrium internuclear separation. We reiterate that it is this region which is the most strongly weighted in our series-determination routine.

Further examination of Tables XXIII and XIV indicates the reason for the Thakkar deficiencies. For both dimers $p \sim 3.58$. This is much smaller than the anticipated exponent of 6 for van der Waals attraction and smaller than any of the p's encountered for neutral molecules in this chapter. This explains the Thakkar tendency to "overshoot" the dissociation energy by so much. The relatively large correction constants with oscillatory signs for both Ca_2 potentials also indicate some convergence problems and are probably responsible for the artificial maxima at small r.

The low value of p is also further evidence of incipient covalency. A. Thakkar[64] and J. S. Winn[65] have listed a variety of

p-values for chemically bound diatomics, ranging from 1.0 - 2.5. For our van der Waals systems, we have observed values from 4.2 - 5.6. The magnesium and calcium dimers thus have p-values that show more favor toward a chemically bound system.

The level of analysis of the spectroscopy of Sr_2 is not as detailed as that of the preceding dimers. No high resolution absorption data of the quality of Balfour and co-workers have been taken, and the situation is further complicated by the fact that the rotational constant is less than half that of Ca_2 due to the mass alone. Working with half the dispersion of Vidal and colleagues, Bergeman and Liao[66] could only resolve the vibrational progressions and bound-free undulations from their laser-excitation/dispersed fluorescence spectra of strontium dimer.

Despite these limitations, they have carefully adjusted two Morse potentials for the ground and excited states in order to duplicate the observed vibrational progressions and Franck-Condon intensities. They derived the quantities $\omega_e = 36.9 \pm 1\ cm^{-1}$ and $D_e = 1100 \pm 100\ cm^{-1}$ for the ground state. If we accept their extrapolated r_e of 4.5±0.2, we can derive an effective p of 3.4±0.30 through second derivative relations between simple Morse and Thakkar functions. Considering the suitability of the Huffaker series for Mg_2 and Ca_2, Bergeman and Liao's Morse potential and hence our derived value of p are not far from reality, and we therefore see that Sr_2 follows the same trend in p-values set by Mg_2 and Ca_2.

It is unfortunate that no data at present exist for the barium dimer. There have been suggestions[52b,67,68] that Ba_2 should be

bound more strongly than the other Group II A dimers due to interactions other than van der Waals forces; the participation of the nearby 6s5d and 6s5p configurations in a more covalent bond. Because of the still larger mass and the multiplicity of natural isotopes, we should not impatiently await a forthcoming analysis.

We save our analysis of the beryllium dimer for last. It is unique among the alkaline earths, possessing nearly double the cohesive energy in the solid and hence a very high melting point with a correspondingly low vapor pressure at high temperatures. Couple these properties with its known toxicity and one has a dearth of experimental information on this element. On the other hand, the small number of electrons makes the dimer amenable to accurate theoretical calculations.

The state-of-the-art calculations for Be_2, are unfortunately, contradictory. Chiles and Dykstra[69] have recently considered a number of configuration interaction (CI) approaches to the problem, comparing their results to previous work in the literature. Their results span the array of reported values, which can be broken into two groups: those with a minimum of ca. 0.15 kcal/mole at 4.5 Å and those binding Be_2 by 2-8 kcal/mole at 2.5 Å. Of these references we carefully choose the interacting correlated fragments (ICF) results of Liu and McLean[70]. Their companion results for He_2 and Mg_2 predict values for D_e and r_e that agree with experimental results within 2%. Chiles and Dykstra also point out that the 7s5p4d2f Slater type atomic orbital set used in the Be_2 ICF calculation is the largest set used to date. The well depth of the ICF potential is 0.23 ± 0.02 kcal/mole (807 cm^{-1}) and r_e = 2.49 ± 0.02 Å, making this one of the more

strongly bound of the theoretical potentials.

We begin our analysis by smoothly connecting Liu and McLean's reported potential points with a spline fit and solving Schrodinger's equation for the vibrational levels and rotational constants, which we report in Table XXV. For this potential, we extrapolate 813.825 cm^{-1} for D_e and 2.49114 Å for r_e. We plot the interpolated potential in Figure 13 along with the determined Huffaker and Thakkar potentials. The results are, besides disappointing, unusual. Both the Thakkar and Huffaker potentials recover only 50% of the potential before reaching their asymptotic limit. The exceptionally high Thakkar p of 8.76 indicates a very high reduced curvature.

To ascertain that this phenomenon is not due to the lack-of-information problem with Ar_2, i.e. too few levels to get the true Y_{ij}'s, we increase the nuclear isotopic mass of Be to values of 543 and 5433 amu, which conveniently correspond to a B_e of 0.01 and 0.001 cm^{-1}, respectively. The results show no quantitative improvement of the series potentials, although the Thakkar p seems to converge to a value of 4.7, giving a reduced curvature of 6.5. The reduced curvatures of Mg_2, Ca_2, and Sr_2 are 33, 42, and 38, respectively. The values of the various Be_2 potential coefficients and their plots can be found on the attached microfiche.

To be sure that our procedure is not in error, we have repeated the same calculations on Liu and McLean's potential for Mg_2[71]. Even though the number of theoretical points is fewer, we obtain results that are substantially in agreement with the experimental values.

We conclude that the problem lies with the Be_2 potential itself.

The probable cause of this ill series-potential behavior can be attributed to the near-zero convexity of the potential between 3.3 and 5 Å apparent in Figure 13. As we have shown in Chapter II, any "true" Born-Oppenheimer potential that shows some discontinuous change in shape due to interaction with other states, such as curve-crossing, will cause the fitted series potentials to behave erratically. To investigate further the "kinks" at 3.3 and 5 Å, we least-squares fit simple Thakkar functions to the inner and outer regions of the Liu and McLean points. For the equilibrium region of $r<3.4$ Å, with r_e and D_e constrained to Liu and McLean's values, we obtain the constants $p = 4.939$, $e_0 = 993.400\ cm^{-1}$, and $e_2 = -0.18$. For the outer tail region, a very simple Thakkar function with $p = 5.69$, $e_0 = D_e = 230\ cm^{-1}$ and $r_e = 3.7$ Å proved sufficient. These two functions, along with the <u>ab initio</u> points employed, are illustrated in Figure 14.

The fact that the p of the "tail" fit Thakkar function is close to 6 indicates that Liu and McLean points follow the correct long-range behavior. Moreover, the C_6 of $0.975\times10^6\ cm^{-1}\ Å^6$ we find by fitting the outer two <u>ab initio</u> points to a C_6/C_8 expansion compares well with the semi-empirical value of $1.06\times10^6\ cm^{-1}\ Å^6$ calculated from oscillator strengths[72], further reinforcing this point.

It is the inner portion of this potential that makes Liu and McLean's work unique among all other calculations and, if correct, Be_2 unique among alkaline earth dimers. Although the Be_2 binding energy is nearly twice that of Mg_2 and is hence out of step with the

trend of increasing D_e of the dimers with increasing atomic number and polarizability, so is the cohesive energy of bulk beryllium as well. The enhanced bonding of Be_2 is no doubt due to admixture of the 2p orbital to the (bonding) $2\sigma_g$ molecular orbital. It would be tempting to invoke curve-crossing by the A $^1\Sigma_g^+$ state, analogous to the case of BeH[73], to explain the radical change in shape of the ab initio curve, but the very high energy of the $^1P^0$ state discourages this.

Another point that also contributes to the increased bonding is the "late" occurence of the repulsive wall. The r_e of 2.49 Å of Be_2 is remarkably smaller than the 3.9 - 4.5 Å distances that characterize the other dimers. This anomaly is similar to the unusually small nearest-neighbor distance[53] of 2.20 Å in crystalline beryllium compared to the 3.2 - 4.4 Å values of the other alkaline earths. The smaller hard-sphere diameter permits the two Be atoms to approach each other close enough for the covalent forces to take effect, a feature that also distinguishes the chemistry of the Be^{2+} ion from that of the Group IIA ions[74]. The rapid rise of this hard, compact wall is the major source of the large reduced curvature. This in turn gives rise to the relatively large p of 4.94 (which incidentally agrees with our "converged" value for large isotopes) and not the usual long-range effects.

The preceding discussion is based upon the assumed accuracy of the ab initio potential. Chiles and Dykstra feel that the system is not yet a closed book. Since Liu and McLean's value of -29.23 Hartrees for the asymptotic energy has a correlation energy of 1.4 eV from the

known ionization energies of two Be atoms[15], there is some room for doubt. To date, the only observation of Be_2 in absorption is in rare gas matrices, as reported by Brom, Hewett, and Weltner[75]. They observe a vibrational progression at 350 nm which is much narrower than that of Mg_2, indicating a smaller difference between the r_e' and r_e'' for Be_2. If similarities in r_e imply similarities in potential curves, then the fact that they estimate $D_e' \geq 14360\ cm^{-1}$ ($D_e' = 9412.5\ cm^{-1}$ for Mg_2) augers well for a more strongly bound ground state.

G. Direct Fit

As we have mentioned several times in this chapter, our standard procedure for finding series potential parameters for weakly-bound molecules leaves something to be desired, especially when the available data are limited. Three steps are involved in going from the raw spectroscopic data to the final potential function. First, the basic constants G_v, B_v, D_v, etc., must be calculated for the ground and excited states from the observed spectral lines. This compounds the initial uncertainty in the line frequency with the inherent uncertainties of the fitting procedure. The next step is to fit a set of Y_{ij}'s to the G_v's and B_v's, further compounding the error. By the time we determine the final potential, the honest uncertainty of the derived parameters makes the potential a poor predictor of the original data. This is best illustrated by Ar_2, where the $\pm 11\ cm^{-1}$ error of e_0 is a far cry from the $0.1\ cm^{-1}$ precision of the vibrational-rotational levels reported by Colbourn and Douglas[38].

Besides the multi-stage amplification of error, there is the problem of limited amounts of data. In the cases of the ground states of NaNe and NaAr, the problem is one of technology; only one excited vibrational state at most is populated in a supersonic nozzle expansion/condensation. The other problem is endemic to the molecular system itself, where there are simply too few vibrational levels to "interrogate" the shape of the potential. This problem has been discussed for Ar_2, demonstrated for Be_2, and is best illustrated by NaNe, which has only two vibrational levels. When there is a deficiency of vibra-

tional data, one must examine the rotational data for high J more closely. As we have pointed out, the Dunham equations do not lend themselves as easily to a B_v/D_v fit as for a G_v/B_v fit. There is the strong correlation between B_v and D_v such as for $v = 5$ of Ar_2 that also makes the Dunham approach less attractive.

What we propose is a means of fitting the potential function directly to the vibrational-rotational energy levels of the molecule. This eliminates at least one step, the Y_{ij} determination, and the uncertainties that go with it. The $G_v/B_v/D_v$ set can simply be treated as a set of numerical fitting constants, and one need not worry about whether they are the "true" mechanical constants. In many cases the relative energy levels of each of the electronic states can be deter- directly from the spectral line positions through the combination relations[76,77], thus eliminating the $G_v/B_v/D_v$ determination step.

The fitting method is simply a nonlinear least-squares refinement[78] of a set of potential parameters, $\{\theta_k\}$. The observed relative energy levels are denoted by y_i and the energy levels calculated from the potential by $f_i(\theta_k)$, where subscript i refers to the vibrational and rotational quantum numbers involved. We take an approximate set of potential parameters, $\{\theta_k^0\}$, and the approximate energies and parameter derivatives to be f_i^0 and $(\partial f_i/\partial\theta_k)^0$, respectively. We can show that a refined set of parameters, $\{\theta_k\} = \{\theta_k^0\} + \{\Delta\theta_k\}$, can be found by solution of the matrix equation:

$$\Sigma_k[\Sigma_i(\frac{\partial f_i}{\partial\theta_k})^0(\frac{\partial f_i}{\partial\theta_j})^0]\Delta\theta_k = [\Sigma_i(\frac{\partial f_i}{\partial\theta_j})^0(y_i-f_i^0)] \quad .$$

The refinement is iterated until one has a convergent $\{\theta_k\}$ set or the $y_i - f_i^0$ differences are less than the experimental error.

In order to find the coefficients of $\{\Delta\theta_k\}$, we must evaluate the derivatives $(\partial E(v,J)/\partial\theta_k)^0$. This can be done by employing the Hellmann-Feynman[79] Theorem:

$$\left(\frac{\partial E_i}{\partial \theta_k}\right)^0 = \langle \psi_i^0 | \left(\frac{\partial H}{\partial \theta_k}\right)^0 | \psi_i^0 \rangle \quad ,$$

where H is the radial Hamiltonian for internuclear motion. If the kinetic energy is independent of potential parameters, then we can further simplify by:

$$\left(\frac{\partial H}{\partial \theta_k}\right)^0 = \left(\frac{\partial V}{\partial \theta_k}\right)^0 \quad .$$

The Hellmann-Feynman Theorem is very important in reducing the amount of computer time needed; the alternative is to evaluate the derivatives numerically. For N parameters, we can replace N energy evaluations with N integral summations. This is an important savings since the integrals are a one-shot evaluation, whereas the Numerov-Cooley solution of the radial equation (Appendix II) is an iterative one. Also, the energies need not be evaluated as precisely in order to produce a reliable numerical derivative, so the number of Numerov-Cooley iterations might be reduced. We say "might be" since we have not examined the relationship between the tolerances of the wave function necessary for the integral and the tolerances of the energy[80].

There are several advantages to this method. The first is that one obtains an analytical potential function that can reproduce the experimental energy levels. This method is applicable to any analytical potential function, although the desirability of a flexible series potential is apparent. All rotational information is employed directly rather than through derived parameters. The ground state dissociation energy can be employed more directly, as could have been done with NaAr. Moreover, the Dunham method tends to prejudice the potential toward the bottom of the well, whereas here the energy levels near the top are put on a more equal footing. Finally, one need not worry about the "second order WKB effects" since the Numerov-Cooley solution is a quantum mechanical, not semi-classical, one.

Certain disadvantages are obvious, too. Since the procedure is iterative and all the rotational energy levels must be evaluated, a lot of computer time is required. This clearly restricts the method to systems of limited amount of data such as the van der Waals molecules we have studied. It may also be possible to evaluate only a few of the rotational levels at well-selected intervals. If the potential function has a tendency to misbehave, as we have seen for the Thakkar and Huffaker functions, then the iterative improvement must be monitored to assure that nonphysical singularities do not interfere with the energy and wave function evaluation. A reasonable starting set of potential parameters is necessary for rapid convergence, but our Dunham procedure can probably provide that for the series potentials.

Perhaps the biggest disadvantage is that the method is untested, and hence we have no knowledge of the convergence properties. We feel

that this merits study and hope to do so in the future. If it can be shown that this algorithm converges for a model system, then we can perhaps have the final word on the suitability of the Thakkar function for certain weakly-bound molecules. If it is not, then we still have a direct method for testing other, possibly more suitable, forms without repeating the algebraic drudgery of relating their coefficients to those of the Dunham potential.

We close noting that the Thakkar function has an edge over the Huffaker function using this algorithm. Since the initial Thakkar from our routine procedure tends to overestimate the true dissociation energy some, it possesses all the observed bound levels and then some. Thus the initial Y_{ij} estimate can be used as the initial guess. Not all of the observed levels are bound in the Huffaker estimate as we have seen in this chapter, so the algorithm would have to be tailored to add experimental data after consecutive iterative improvements.

H. Conclusion

We have investigated the suitability of the Thakkar and Huffaker series functions towards describing the potentials of weakly bound diatomic molecules. We have found the Huffaker series to be a rather poor function for modelling these potentials as it badly underestimates the dissociation energy. We ascribe this deficiency to the Morse potential nature of the Huffaker series, which approaches its asymptotic form much too rapidly to accommodate the long-range r^{-n} attraction which influences a large percentage of the potential well.

Thus it is the r^{-p} nature of the Thakkar series that is responsible for its success in describing the molecular ions and rare gas containing dimers discussed in this chapter. When spectroscopic data are sufficient in quantity and accuracy, the Thakkar function can give results as reliable as an RKR curve. When accuracy or quantity of the spectroscopic data is not available, as with Ar_2 and the $X\ ^2\Sigma^+$ state of NaAr, other sources of experimental information can be employed to bring the Thakkar function into line.

The advantages of the Thakkar series are many. Since it is analytic throughout the region of interest, it is suitable for use in studies involving first or higher derivatives, such as the Virial Theorem. This property has been realized and put to good use in describing the nature of van der Waals bonding in comparison to the chemical forces[81]. The potential parameters can provide a means of comparing bonding trends, sometimes subtle as with the alkaline earth dimers, among diatomic molecules of disparate bond energies and bond lengths[65]. From the form of the Thakkar function, the trends concerning the value of p,

and the Thakkar tendency to overestimate the dissociation energy as we have seen in this chapter can suggest methods of approximating molecular properties, as we have done elsewhere for the dissociation energy[82].

Finally, we have presented a method other than our usual Dunham fitting procedure for determining potential parameters directly from the spectroscopic data. Although the algorithm is useful for any analytical potential in general, the Thakkar series enjoys certain initial advantages. This procedure certainly merits study in the near future.

One question we have not resolved here is final choice between integral and nonintegral p. Although we have employed the nonintegral p result in examining the bonding nature in the alkaline earths, the $p \equiv n$ restriction for an r^{-n} attraction enjoys some advantages, such as a somewhat better representation of the A $^2\Pi_{3/2}$ state of NaNe and the Y_{ij}-fit X $^2\Sigma^+$ state of NaAr. It also apparently lacks the annoying tendency of turning over at $r<r_e$. One other advantage is that it will probably appeal to the Chemistry Community in general since it has the r^{-n} behavior built in, even if the <u>pure</u> long-range attraction is not in effect in the region of experimental interest.

REFERENCES

1. J. O. Hirschfelder, C. F. Curtiss, and R. M. Bird, Molecular Theory of Gases and Liquids (Wiley, New York, 1954), Chapter 13.

2. H. Pauly, in Atom-Molecule Collision Theory, edited by R. B. Bernstein (Plenum, New York, 1979) pp. 11-199.

3. R. B. Gerber, M. Shapiro, U. Buck, and J. Schleusener, Phys. Rev. Lett. 41, 236 (1978).

4. Excimer Lasers, edited by Ch. K. Rhodes (Springer-Verlag, Berlin, New York, 1979).

5. J. L. Kinsey, Ann. Rev. Phys. Chem. 28, 349 (1977).

6. D. L. Levy, Ann. Rev. Phys. Chem. 31, 197 (1980).

7. Dennis C. Hartman, Ph. D. Dissertation, University of California, 1979.

8. D. C. Hartman and J. S. Winn, J. Chem. Phys. 74, 4320 (1981).

9. K. V. Subbaram, J. A. Coxon, and W. E. Jones, Can. J. Phys. 53, 2016 (1975).

10. K. V. Subbaram, J. A. Coxon, and W. E. Jones, Can. J. Chem. 54, 1535 (1976).

11. J. A. Coxon, W. E. Jones, and K. V. Subbaram, Can. J. Chem. 55, 254 (1977).

12. R. J. LeRoy and W.-H. Lam, Chem. Phys. Lett. 71, 544 (1980).

13. J. W. Cooley, Math. Computation 15, 363 (1961); J. K. Cashion, J. Chem. Phys. 39, 1872 (1963).

14. J. Tellinghuisen, J. Quant. Spec. Radiat. Transfer 19, 149 (1976).

15. C. E. Moore, Natl. Stand. Ref. Data Ser. Natl. Bur. Stand. 35 (1971).

16. J. H. Goble, D. C. Hartman, and J. S. Winn, J. Chem. Phys. 67, 4206 (1977).

17. J. A. Coxon, W. E. Jones, and K. V. Subbaram, Can. J. Chem. 53, 2321 (1975).

18. C. Zener, Phys. Rev. 37, 556 (1931).

19. R. E. Olson and B. Liu, Chem. Phys. Lett. 56, 537 (1978).

20. I. Dabrowski and G. Herzberg, J. Mol. Spectrosc. 73, 183 (1978).

21. A. Gallagher in ref. 4, pp. 135-174.

22. R. Ahmad-Bitar, W. P. Lapatovich, D. E. Pritchard, and I. Renhorn, Phys. Rev. Lett. 39, 1657 (1977).

23. R. E. Smalley, D. A. Auerbach, P. S. H. Fitch, D. H. Levy, and L. Wharton, J. Chem. Phys. 66, 3778 (1977).

24. R. Compargue, Rev. Sci. Instrum. 35, 111 (1964); R. Compargue, J. Chem. Phys. 52, 1795 (1970); R. Compargue and A. Lebehot, in Rarefied Gas Dynamics, Proc. Int. Symp. 2, C11-1 (1974).

25. J. H. Goble and J. S. Winn, J. Chem. Phys. 70, 2051 (1979).

26. W. P. Lapatovich, R. Ahmad-Bitar, P. E. Moskowitz, I. Renhorn, R. A. Gottscho, and D. E.Pritchard, J. Chem. Phys. 73, 5419 (1980).

27. R. A. Gottscho, R. Ahmad-Bitar, W. P. Lapatovich, I. Renhorn, and D. E. Pritchard, J. Chem. Phys. 75, 2546 (1981).

28. A. Dalgarno and W. D. Davidson, Adv. At. Mol. Phys. 2, 1 (1966); A. Dalgarno, Intermolecular Forces, edited by J. O. Hirshfelder (Interscience, New York, 1967) pp. 143-166 (Vol. XII of Advances in Chemical Physics series).

29. J. Tellinghuisen, A. Ragone, M. S. Kim, D. J. Auerbach, R. E. Smalley, L. Wharton, and D. H. Levy, J. Chem. Phys. 71, 1283 (1979).

30. G. York, R. Scheps, and A. Gallagher, J. Chem. Phys. 63, 1052 (1975).

31. R. D. Saxon, R. E. Olson, and B. Liu, J. Chem. Phys. 67, 2692 (1977).

32. SAFLW estimated the separation of the B-state and the observed vibrational levels of the A $^2\Pi_{1/2}$ state to vary between 80 and 500 cm^{-1}, to be compared with the 17-46 cm^{-1} for NaNe. We therefore expect the B-state interaction/interference to be less for NaAr.

33. R. Düren, W. Gröger, E. Hasselbrink, and R. Liedtke, J. Chem. Phys. 74, 6806 (1981).

34. R. Düren and W. Gröger, Chem. Phys. Lett. 56, 67 (1978).

35. We should point out that our statement in ref. 25 that $\alpha_e = 0.005588\ cm^{-1}$ for the $p \equiv 6$ Thakkar (T II) was in error; the experimental α_e of SAFLW must be used in order to generate the T II potential. We also note a calculation error in the vibrational energies of the T I potential in Table IX of ref. 25. The correct values are given in Table XVIII.

36. See ref. 1, pp. 204-205, pp. 589-596 and references therein. See also refs. 40 and 41 below.

37. J. H. Dymond and B. J. Alder, J. Chem. Phys. 51, 309 (1969).

38. E. A. Colbourn and A. E. Douglas, J. Chem. Phys. 65, 1741 (1976).

39. J. M. Parson, P. E. Siska, and Y. T. Lee, J. Chem. Phys. 56, 1511 (1972).

40. R. A. Aziz and H. H. Chen, J. Chem. Phys. 67, 5719 (1977).

41. A. Koide, W. J. Meath, and A. R. Allnatt, Mol. Phys. 39, 895 (1980).

42. J. A. Barker, R. A. Fisher, and R. O. Watts, Mol. Phys. 21, 657 (1971).

43. For a review, see E. B. Smith, Ann. Reports 63, 13 (1966); G. C. Maitland and E. B. Smith, Chem. Soc. Reviews 2, 181 (1973).

44. For a discussion of standard deviations in a least-squares fit see D. L. Albritton, A. L. Schmeltekopf, and R. N. Zare, Molecular Spectroscopy: Modern Research, Vol. II, K. Narahari Rao, Ed. (Academic Press, N.Y., 1976) pp. 1-67 or A. A. Clifford, Multivariate Error Analysis (Applied Science Publishers LTD, London, 1973).

45. R. W. Bickes, Jr., and R. B. Bernstein, Chem. Phys. Lett. 26, 457 (1974); J. Chem. Phys. 66, 2408 (1977).

46. D. A. McQuarrie, Statistical Mechanics (Harper and Row, N.Y., 1976), p. 242.

47. J. M. H. Levelt Sengers, M. Klein, and J. S. Gallagher, AIP Handbook (McGraw-Hill, N.Y., 1972).

48. Not shown is the nominal Huffaker potential. Although its failure here is not as catastrophic as with previous weakly bound molecules (D_e = 91.3±11.4 cm^{-1}), we do not expect much more improvement in this potential due to its long-range behavior, or rather lack thereof. Its plot can be reviewed and compared with the nominal Thakkar on the microfiche.

49. S. D. Colgate, J. E. Jordan, I. Amdur, and E. A. Mason, J. Chem. Phys. 51, 968 (1969).

50. K. K. Docken and T. P. Schafer, J. Mol. Spectrosc. 46, 454 (1973).

51. This seems to cast further aspersions on the Y_{i1} expansion, but generating a new set of Y_{i1}'s with the new B_5 does not markedly change the nominal Thakkar.

52. a) Karl A. Gingerich, Faraday Symposia #14, Diatomic Metals and Metallic Clusters, (Royal Society of Chemistry, London, 1980), pp. 109-125; b) L. Brewer and J. S. Winn, ibid., pp. 126-134; c) A. R. Miedema ibid., pp. 135-148.

53. C. Kittel, Introduction to Solid State Physics, 5th edition (Wiley, New York, 1976) pp. 30-38.

54. F. A. Cotton and G. Wilkerson, F. R. S., Advanced Inorganic Chemistry, 3rd edition (Interscience, New York, 1972) p.206.

55. W. J. Balfour and A. E. Douglas, Can. J. Phys. 48, 901 (1970).

56. K. C. Li and W. C. Stwalley, J. Chem. Phys. 59, 4423 (1973).

57. H. Scheingraber and C. R. Vidal, J. Chem. Phys. 66, 3694 (1977).

58. C. R. Vidal and H. Scheingraber, J. Mol. Spectrosc. 65, 46 (1977).

59. J. Wyss, Ph.D. dissertation, University of California at Santa Barbara, 1978; J. Chem. Phys. 71, 2949 (1979).

60. C. R. Vidal, J. Chem. Phys. 72, 1864 (1980).

61. K. Sakurai and H. P. Broida, J. Chem. Phys. 65, 1138 (1976).

62. P. F. Liao, private communication, 1977.

63. What remains to be determined is the identity of the carrier of Wyss' red system. His determined molecular constants (D_0 = 2075 cm^{-1} and ω_e = 73 cm^{-1}) do not correspond to any any chemically bound calcium impurity. This appears to be due to a weakly bound system and warrants further study.

64. A. Thakkar, J. Chem. Phys. 62, 1693 (1975).

65. J. S. Winn, Acc. Chem. Res. 14, 341 (1981).

66. T. Bergeman and P. F. Liao, J. Chem. Phys. 72, 886 (1980).

67. R. O. Jones, J. Chem. Phys. 71, 1300 (1979).

68. A. Miedema and J. W. F. Dorleijn, Phil. Mag. B. 43, 251 (1981).

69. R. A. Chiles and C. E. Dykstra, J. Chem. Phys. 74, 4544 (1981).

70. B. Liu and A. D. McLean, J. Chem. Phys. 72, 3418 (1980).

71. B. Liu, private communication, 1980.

72. L. N. Shabanova, Opt. Spectrosc. 27, 205 (1969). Employing the "American" oscillator strengths of W. L. Wiese, M. W. Smith, and B. M. Miles, Natl. Bur. Stand. U.S. Circ. 22 (1969), we obtain a C_6 of 0.925 10^6 cm^{-1} $Å^6$, so that the theoretical value is well within the "error bounds".

73. G. Herzberg, Spectra of Diatomic Molecules, 2nd edition (Van Nostrand, New York, 1950) pp. 357-358.

74. Ref. 54, pp. 206-209.

75. J. M. Brom, Jr., W. D. Hewett, Jr., and W. Weltner, Jr., J. Chem. Phys. 62, 3122 (1975).

76. Ref. 73, pp. 175-192.

77. N. Åslund, J. Mol. Spectrosc. 50, 424 (1974).

78. A. A. Clifford, ref. 44.

79. H. Hellmann, Einführung in die Quantenchemie (Deuticke, Leipzig, 1937) p. 285; R. P. Feynman, Phys. Rev. 56, 340 (1939); see also I. N. Levine, Quantum Chemistry, 2nd edition (Allyn and Bacon, Boston, 1974) pp. 371-374.

80. We have investigated the error of the energy in terms of the theoretical Numerov error at the "matchpoint" (see Appendix II) and found that the iteration uncertainty in the energy is due to the accumulation of the error in the computed wave function. Since the signs of the error change at different points along the potential, the accumulated error may cancel. Generally, we find the actual error of integrated quantities such as B_v to depend more on the number of grid points.

81. J. S. Winn, J. Chem. Phys. 74, 608 (1981).

82. J. H. Goble and J. S. Winn, J. Chem. Phys. 70, 2058 (1979).

Table I. Molecular constants[a] for $BeAr^+$

	$X^2\Sigma^+$	$A^2\Pi_r$
T_e	0	24576.5
ω_e	362.7	583.2[b]
$\omega_e x_e$	8.92	6.70[b]
$\omega_e y_e$	0.033	-
A_e	-	42.68
B_e	0.5271	0.6124
α_e	0.0145	0.0089
$10^5\gamma_e$	6.5	-
r_e(Å)	2.0855	1.9348

[a]Values in wave numbers (cm^{-1}), Ref. 10.

[b]Value corrected from a calculation error in Ref. 10.

Table II. Dunham coefficients[a] for $X^2\Sigma^+$ $BeAr^+$.

a_0	62445. cm^{-1}(18)
a_1	-4.156 (22)
a_2	10.31 (22)
a_3	-14.2 (16)
a_4	-39. (18)

[a]Numbers in parenthesis are one standard deviation corresponding to the last digits of each coefficient.

Table III. Huffaker, SPF, Thakkar, and PA coefficients[a] for $X^2\Sigma^+$ $BeAr^+$

Huffaker	SPF	Thakkar	PA [3,3]
ρ = 4.156(22)	b_0 = 62445.(18)	p = 3.156(22)	f_1 = 62445.
c_0= 3615.(38)	b_1 = -2.156(22)	e_0= 6267.5(864)	f_2 = -97.70
σ = 19.92(15)	b_2 = 0.843(162)	e_1 = 0	g_1 = -93.5
c_2= 0.013(7)	b_3 = 6.11(92)	e_2 = -0.115(13)	g_2 = -399.
c_3 = 0.079(9)	b_4 = -43.4(6.5)	e_3 = 0.0661(215)	g_3 = -680.
c_4 = -0.047(10)		e_4 = -0.227(29)	

[a]Numbers in parenthesis are one standard deviation corresponding to the last digits of each coefficient. c_o, b_o, e_o, and f_1 are in wave numbers.

Table IV. Potential function eigenvalues (cm^{-1}) as $E_{calc}-E_{obs}$ for the lowest vibrational states of $X^2\Sigma^+$ $BeAr^+$

v	0	1	2	3	4
E_{obs}	179.19	524.17	851.61	1161.67	1454.58
Thakkar	-0.02	-0.03	-0.02	0.08	0.31
nuffaker	-0.02	-0.03	-0.10	-0.29	-0.76
Exp[-4]	-0.22	-1.94	-5.31	-10.22	-16.58
SPF(4,0)[a]	-0.03	-0.26	-1.65	-6.44	-18.65
SPF(3,1)	0.09	0.78	2.97	7.89	16.74
SPF(4,1)	-0.03	-0.19	-1.18	-4.50	-13.12
SPF(3,2)	0.08	0.67	2.52	6.58	13.76
SPF(4,2)	-0.03	-0.14	-0.82	-3.07	-8.74
SPF(3,3)	0.07	0.58	2.17	5.60	11.56
SPF(r,e)	-0.02	-0.10	-0.56	-2.04	-5.67
SPF(3,4)	0.06	0.51	1.89	4.83	9.87
SPF(4,4)	-0.02	-0.07	-0.37	-1.29	-3.51

[a]SPF(n,m) means terms through b_n (Table III) plus m constraints were used.

Table V. Theoretical and fitted β parameters for $BeAr^+$ and $BeKr^+$.

	Zener Formula[a]	Fitted from Spectroscopic Constants
$BeAr^+$ X $^2\Sigma^+$	4.220	4.186
$A^2\Pi$	3.968	4.069
$BeKr^+$ X $^2\Sigma^+$	4.103	4.083
$A^2\Pi$	3.851	3.795

[a]Ionization potentials used taken from James E. Huheey, Inorganic Chemistry: Principles of Structure and Reactivity. (Harper and Row, New York, 1972), p. 46.

Table VI. Fundamental potential constants of $BeRg^+$ (Rg = Rare gas).[a]

State	Molecule	r_e	D_e	ω_e	T_e	Ref.
$X\ ^2\Sigma^+$	$BeAr^+$	2.0855	4537	362.7	0	b
	$BeKr^+$	2.2201	(5511)	367.14	0	c
	$BeXe^+$	(2.4578)	(6308)	367	0	d
$A\ ^2\Pi$	$BeAr^+$	1.9348	11888	583.27	24576.5	b
	$BeKr^+$	2.0674	(13656)	554.47	23782.14	c
	$BeXe^+$	(2.3478)	(14870)	545	22096	d

[a]Quantities in parenthesis calculated from model potential.

[b]K. V. Subbaram, J. A. Coxon, and W. E. Jones, Can. J. Physics, 54, 1535 (1976).

[c]J. S. Coxon, W. E. Jones, and K. V. Subbaram, Can. J. Physics, 55, 254 (1977).

[d]J. A. Coxon, W. E. Jones, and K. V. Subbaram, Can. J. Physics, 53, 2321 (1975).

Table VII. Z-values of the model potential for ion molecules involving rare gases.

Molecule	State	r_e	D_e	ω_e	Z	Reference
$BeAr^+$	$X\ ^2\Sigma^+$	2.086	4537	363	1.289	1
$BeAr^+$	$A\ ^2\Pi_r$	1.935	11889	583	1.884	1
$HeAr^+$	$X\ ^2\Sigma^+$	2.492	443	1546	1.201	2
$HeAr^+$	$A\ ^2\Pi$	2.990	106	~83[a]	0.952	2
$HeNe^+$	$X\ ^2\Sigma^+$	1.300	6216	1308	1.469	3
$HeNe^+$	$A\ ^2\Pi_r$	2.319	347	~184[b]	1.081	3
$HeNe^+$	$B\ ^2\Sigma^+$	2.648	364	153	1.069	3
HHe^+	$X\ ^2\Sigma^+$	0.774	16455	3228	1.299	4
HNe^+	$X\ ^2\Sigma^+$	0.996	18390	2896	1.512	5
HAr^+	$X\ ^2\Sigma^+$	1.286	32720	2723	1.716	6
HKr^+	$X\ ^2\Sigma^+$	1.419	38770	2561	1.886	5
He_2^+	$X\ ^2\Sigma_u^+$	1.081	19914	1699	2.727	7
Ne_2^+	$X\ ^2\Sigma_u^+$	1.75	10740	510	3.051	8

[a]Estimated from the Kratzer formula, $\omega_e^2=4B_e^3/\mathcal{D}_e$, using the centrifugal distortion constant, $\mathcal{D}_0$, of reference 2.

[b]Estimated from $\Delta G(1/2)$ for $^3HeNe^+$ of reference 3 and employing isotopic relations for $\Delta G(1/2) = \omega_e - 2\omega_e x_e$.

References:

1. This work.
2. R. E. Olson and B. Liu, Chem. Phys. Lett. 56, 537 (1978).
3. I. Dabrowski and G. Herzberg, J. Mol. Spectrosc. 73, 183 (1978).

Table VII. (continued)

4. K. P. Huber and G. Herzberg, Constants of Diatomic Molecules, (Van Nostrand, NY, 1979) pp. 300-301.

5. P. Rosmus, E.-A. Reinsch, Z. Naturforsch. 35a, 1066 (1980).

6. P. Rosmus, Theor. Chim. Acta (Berlin) 51, 359 (1979).

7. K. P. Huber and G. Herzberg, ibid., p. 298.

8. K. P. Huber and G. Herzberg, ibid., pp. 451-453.

Table VIII. Dunham and Thakkar expansion coefficients for the X and B states of $^4HeNe^+$[a]

i	Dunham a_i		Thakkar e_i
	X State		
0	14262.05 cm^{-1}		6608.82 cm^{-1}
1	-5.645	p =	4.6455
2	20.945		0.0219
3	-70.565		-0.0602
4	293.907		0.0568
	B State		
0	8101.96 cm^{-1}		417.36 cm^{-1}
1	-5.406	p =	4.4060
2	16.431		-0.1246
3	-25.378		0.0122
4	-50.600		-0.0042

[a]Vibrational and rotational Y_{ij}'s from Dabrowski and Herzberg, Ref. 20.

Table IX. Vibrational intervals and rotational constants[a] of $^4HeNe^+$ and differences calculated from the Thakkar potential

v	ΔG(v+1/2) (cm^{-1})	δ(Thakkar) (cm^{-1})	B_v (cm^{-1})	δ(Thakkar) (cm^{-1})
		X State		
6	341.59	43.79	1.58983	0.10341
7	233.42	66.95	1.35755	0.13629
8	146.27	80.62	1.09037	0.20589
9			0.8431	0.2584
		B State		
0	112.46	2.08	0.67529	0.08183
1	78.09	0.65	0.57898	0.00182
2	49.72	1.47	0.47463	0.00360
3	28.64	1.93	0.3644	0.0107
			0.2614	0.0123

[a]Observed values from I. Dabrowski and G. Herzberg, Ref. 20.

Table X

v	$\Delta G(v+1/2)$[a] (cm^{-1})	δ(Thakkar)[b]	B_v[a] (cm^{-1})	δ(Thakkar)
3	15.33	0.11	0.13068	-0.00032
4	10.25	0.13	0.10480	0.00144
5	6.37	0.10	0.08230	0.00065
			0.05826	0.00281

[a]Observed values from ALPR, Ref. 22.

[b]δ(Thakkar) same as defined in Chapter II.

Table XI. NaNe $A^2\Pi_{3/2}$ mechanical constants, Thakkar potential parameters, and RKR potential. Energies are in cm^{-1}; distances are in Å.

	This work	Ref. 27
B_e = 0.216308	e_0 = 150.07	118.8
α_e = 0.02464	p = 4.184	4.532
γ_e = 5×10^{-5}	e_1 = 0.	0.127
ω_e = 47.6	e_2 = 2.1314×10^{-3}	2.80900×10^{-3}
$\omega_e x_e$ = 5.24	e_3 = 1.442×10^{-2}	-2.40327×10^{-4}
$\omega_e y_e$ = 0.2	e_4 = -1.904×10^{-2}	8.465427×10^{-2}
R_e = 2.6955	D_e = 149.70	144.4

v	R_-	R_+	E
0	2.49517	3.03620	22.655
1	2.39854	3.43327	60.425
2	2.35025	3.84439	89.515
3	2.31986	4.32583	111.125
4	2.29981	4.92757	126.455
5	2.28938	5.72353	136.705
6	2.29623	6.83467	143.075

Table XII. Mechanical constants of the NaAr $A^2\Pi$ states.[a] Energies are in cm^{-1}; distances are in Å.

	$A^2\Pi_{1/2}$	$A^2\Pi_{3/2}$
B_e	0.136656	0.136656
α_e	0.006721	0.006721
ω_e	80.897	80.720
$\omega_e x_e$	3.661	3.859
$\omega_e y_e$	0.0365	0.0606
$\omega_e z_e$	8.75×10^{-4}	-
R_e	2.9074	2.9074

[a]Ref. 29.

Table XIII. Thakkar potential constants for the NaAr $A^2\Pi$ states.

	$A^2\Pi_{1/2}$	$A^2\Pi_{3/2}$
$e_0(cm^{-1})$	510.481	508.794
p	4.841	4.839
e_2	0.12587	8.3948×10^{-2}
e_3	-3.380×10^{-2}	-8.7053×10^{-2}
e_4	3.500×10^{-2}	2.3971×10^{-2}
e_5	-1.797×10^{-2}	-
e_6	1.175×10^{-2}	-

Table XIV. Experimental[a] $\Delta G(v+1/2)$'s for the NaAr $A^2\Pi$ states and calculation differences. δ = calculated-experimental. Values in cm^{-1}.

	$A^2\Pi_{1/2}$		$A^2\Pi_{3/2}$	
v	$\Delta G(v+1/2)$	δ	$\Delta G(v+1/2)$	δ
7	31.130(19)[b]	0.204	30.635(25)	-0.177
8	26.429(19)	0.231	26.006(13)	-0.184
9	22.136(12)	0.227	21.747(20)	-0.263
10	18.272(16)	0.178	-	-

[a]Values from Ref. 23

[b]Numbers in parenthesis refer to experimental uncertainty in last two digits.

Table XV. Experimental[a] B_v's for the NaAr $A^2\Pi$ states and calculated differences. Values in cm^{-1}.

	$A^2\Pi_{1/2}$		$A^2\Pi_{3/2}$	
v	B_v	$\delta \cdot 10^4$	B_v	$\delta \cdot 10^4$
7	0.086019(39)	3.0	0.086511(45)	-4.2
8	0.079287(35)	5.2	0.079759(30)	-4.8
9	0.072579(23)	c	0.072921(26)	-4.8
10	0.065942(24)	c	0.06630(37)	-7.0
11	0.059253(83)	c	-	-

[a,b]References and notes as in Table XIV.

[c]Values not calculated.

Table XVI. Spectroscopic constants (in cm^{-1}) for the $X^2\Sigma^+$ state of NaAr[a]

ω_e	=	13.557	B_e	= 0.046372
$\omega_e x_e$	=	1.155	α_e	= 0.003856

[a]Ref. 29.

Table XVII. Comparison of experimental B_v's and $G_0(v)$'s (in cm^{-1}) with those calculated from several model potentials.

	Thakkar p=6	TRKASWL[a]	DG[b]	Experimental[c]
		B_v		
0	0.044284	0.044522	0.042761	0.044442(18)
1	0.39797	0.040518	0.038473	0.040585(64)
2	0.034768	0.036017	0.034366	
3	0.029185	0.030798	0.029326	
4	0.023005	0.024374	0.024027	
		$G_0(v) = G_v - G_0$		
1	11.189	11.[illegible]88	11.013	11.183(147)
2	19.894	20.149	20.264	20.329(315)
3	26.190	26.889	27.339	26.740(623)
4	30.296	31.404	32.169	31.400(794)

[a]From the Morse potential of ref. 29.

[b]From the potential of ref. 34.

[c]Numbers in parenthesis correspond to the uncertainty of the last digits.

Table XVIII. Thakkar constants for potentials fitted to D_0 and D_1.

	TI	TII	TIII	TIV
$e_0(cm^{-1})$	60.358	28.744	60.358	31.399
p	4.3131	6	4.3264	6
e_1	0	0.30991	0	0.27875
e_2	-0.30868	0.13424	-0.32445	0.01992

Table XIX. Spectroscopic constants (in cm^{-1}) derived from the four Thakkar functions fit to D_0 and D_1.

Quantity	Experimental	TI	TII	TIII	TIV
B_0	0.04444[a]	0.04449	0.04429	0.04455	0.04442
B_1	0.04059[a]	0.04082	0.03985	0.03995	0.04005
ΔG	11.261[a]	11.239	11.452	11.441	11.580
	11.247[b]				
D_0	33.941[b]	34.991	34.841	34.045	33.948
D_1	22.694[b]	23.752	23.389	22.604	22.368
D_e	40.430[b]	41.727	41.511	40.775	40.776

[a]From SAFLW, ref. 23.

[b]From TRKASWL, ref. 29.

Table XX. Nominal Thakkar potential constants for Ar_2. The uncertainties relate to the final digits of the respective constants.

R_e =	3.7576(50) Å
B_e =	0.0597676 cm^{-1}
ω_e =	31.22802 cm^{-1}
e_0 =	134.12(10.90) cm^{-1}
p =	5.515(152)
e_2 =	-0.2045(555)
e_3 =	-0.0888(156)
e_4	0.1059(303)
D_e =	108.99(19.72) cm^{-1}

Table XXI. Refined Thakkar potential constants for Ar_2.

R_e =	3.758 Å
e_0 =	140.38 cm^{-1}
p =	5.62
e_2 =	-0.235
e_3 =	-0.07
e_4 =	0.02
D_e =	100.37 cm^{-1}

Table XXII. Vibrational energy levels, G_v, and rotational constants, B_v, for various Ar_2 potentials. All values are in cm^{-1}.

v	Nominal Thakkar	Refined Thakkar	CD[a]	MSVIII[b]
		G_v		
0	14.87	15.41	14.80	14.58
1	40.58	41.92	40.53	40.07
2	61.09	62.58	60.94	60.21
3	76.93	77.82	76.55	75.28
4	88.74	88.27	87.46	85.91
5	97.16	94.79	94.24	92.59
6	102.81	98.35	97.85	96.14
7	106.26	99.91	99.28	97.55
8	108.09	100.35	c	c
		B_v		
0	0.057778	0.057795	0.057777	0.057758
1	0.053379	0.053439	0.053359	0.053491
2	0.048507	0.048351	0.048467	0.048329
3	0.043279	0.042486	0.042841	0.042718
4	0.037779	0.035872	0.036400	0.036267
5	0.032053	0.028623	0.028904	0.028870
6	0.026127	0.020919	0.020740	0.020706
7	0.020025	0.012935	0.011789	0.011709
8	0.013795	0.004812	0.001370	0.001225

a) Colbourn and Douglas potential of Ref. 38. b) Scattering potential of Ref. 39. See also Docken and Schafer, Ref. 50. c) v=8 is bound by less than 0.001 cm^{-1}.

Table XXIII. Thakkar and Huffaker potential constants for Mg_2 $X^1\Sigma_g^+$. Standard deviations in parenthesis refer to last two digits.

Thakkar	Huffaker
e_0 = 545.6(2.9) cm^{-1}	c_0 = 333.7(1.4) cm^{-1}
p = 3.5897(95)	p = 4.5897(95)
e_2 = 0.0620(48)	c_2 = 0.1106(29)
e_3 = 0.0777(92)	c_3 = 0.0837(44)
e_4 = -0.119(13)	c_4 = -0.0039(50)
e_5 = -0.104(20)	c_5 = 0.0076(65)
e_6 = 0.052(25)	c_6 = 0.0320(59)
D_e = 528.7(42.2) cm^{-1}	D_e = 410.5(9.9) cm^{-1}

Experimental values[a]: D_e = 430±1 cm^{-1}, r_e = 3.88941(15)Å .

[a]From ref. 58.

Table XXIV. Thakkar and Huffaker potential constants for Ca_2 $X^1\Sigma_g^+$. Standard deviations the same as Table XXIII.

Thakkar	Huffaker
e_0 = 1812.74(.52) cm^{-1}	c_0 = 1104.43(.25)
p = 3.55688(51)	ρ = 4.55688(51)
e_2 = -0.25518(31)	c_2 = -0.0823(17)
e_3 = -0.39506(33)	c_3 = -0.14104(15)
e_4 = 0.43595(45)	c_4 = 0.17448(15)
e_5 = 1.0613(75)	c_5 = 0.2864(22)
e_6 = -1.14370(96)	c_6 = -0.2343(22)
D_e = 1274.9(33.3) cm^{-1}	D_e = 1108.0(5.6)

Experimental values[a]: D_e = 1095±0.5 cm^{-1}. r_e = 4.2785227(46)Å.

[a]From ref. 60.

XXV. Vibrational levels and rotational constants derived from Liu and McLean's Be_2 potential.

v	$G_v(cm^{-1})$	$B_v(cm^{-1})$
0	116.690	0.58280
1	318.931	0.53413
2	471.892	0.46928
3	573.119	0.39008
4	638.876	0.32999
5	689.913	0.28901
6	732.182	0.25333
7	765.752	0.21453
8	790.312	0.17241
9	805.787	0.12321
10	812.567	0.06611

FIGURE CAPTIONS

Fig. 1. Thakkar, Huffaker, SPF, and Dunham potentials for $BeAr^+$. Tie lines connect the RKR turning points of the first five vibrational levels. The heavy solid line indicates those regions where two or more potentials are superposed.

Fig. 2. Log - log plot of the long range behavior of the Thakkar and Huffaker potentials of $BeAr^+$. The dashed lines bound the range of the Thakkar potential when varied over the experimental uncertainties of the molecular constants. The straight line labeled "ion-induced dipole" is for the "pure" r^{-4} interaction discussed in the text.

Fig. 3. The $X^2\Sigma^+$ state of $HeNe^+$. Solid line is the Thakkar function, dashed is that of Huffaker. Horizontal bars are the RKR tie lines.

Fig. 4. The $B^2\Sigma^+$ state of $HeNe^+$. Assignment of lines are the same as in Fig. 3.

Fig. 5. Log - log plot of the long-range potentials of the B state of $HeNe^+$. The upper line is the Thakkar function, the lower line is for a "pure" r^{-4} potential. The heavy dots are the outer turning points of the RKR curve.

Fig. 6. Potential functions and RKR tie lines for the $A^2\Pi_{3/2}$ state of NaAr. The potentials are Thakkar(——), Huffaker(----), Dunahm (— —), and SPF (— . . —). Vibrational levels are the horizontal, RKR tie lines. Note that the Huffaker potential was constructed from data on v' = 7-10, but it does not have these levels bound.

Fig. 7. Some potential functions for the $X^2\Sigma^+$ state of NaAr. The potentials illustrated are the p ≡ 6 Thakkar (—) the TRKASWL's Morse (....), and Duren and Groger's potential (---). The dissociation energy (long horizontal line) as well as the Y_{ij}'s used to calculate the RKR tie lines are from TRKASWL. Note that even the standard RKR procedure does not produce a reliable potential towards the top of the well.

Fig. 8. Calculated elastic differential cross sections for Ar compared to the measurement of Ref. 39. Curve (a) is calculated using the MSV III potential; curve (b), the nominal Thakkar potential; curve (c), the refined Thakkar potential.

Fig. 9. Deviations of calculated second virial coefficients for Ar from the measurements of Ref. 47. Curves are for the CD

potential (——), the MSV III (···), the nominal (---) and refined (-·-) Thakkar potentials.

Fig. 10. Comparison of the CD potential (——), the MSV III potential (···), the nominal Thakkar potential (---), and the refined Thakkar potential (-·-) for Ar_2. Note the change in the ordinate scale at 10 cm^{-1}.

Fig. 11. Potential functions for Mg_2. The solid line is the RKR potential from Ref. 58. The analytic functions fits are the Thakkar function (--) and the Huffaker-Morse function (— - —).

Fig. 12. Potential functions for Ca_2. The solid line is the RKR potential from Ref. 60. The analytic functions are denoted as in Fig. 11.

Fig. 13. Thakkar (— — ·), Huffaker (---), and the spline-interpolated <u>ab initio</u> potential of ref. 70 (——) for Be_2. Note the abrupt change in convexity of the theoretical potential at 3.5 and 5 Å .

Fig. 14. <u>Ab initio</u> potential points(•) for Be_2 (from Ref. 70) compared to a Thakkar function fit to the well region (solid line) and the long-range tail (dashed line).

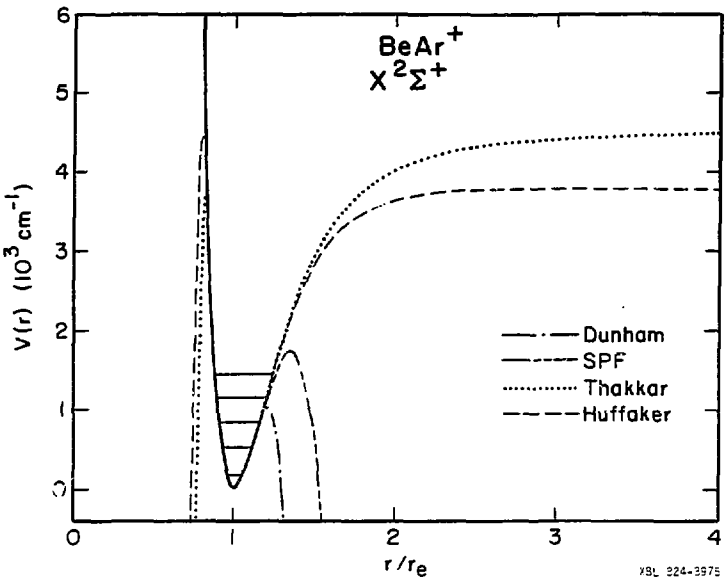
BeAr+
X 2Σ+
V(r) (10^3 cm^-1)
r/re
Dunham
SPF
Thakkar
Huffaker
XBL 824-3975

Figure 1.

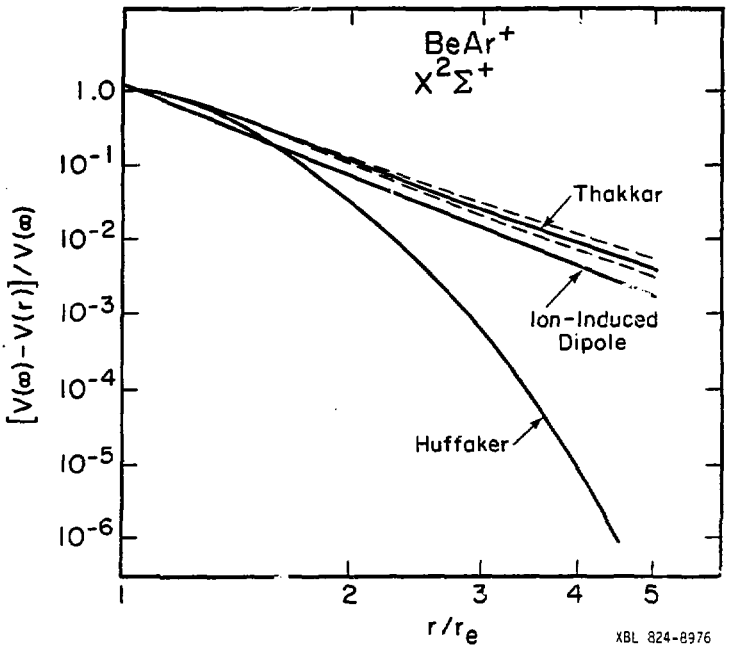
BeAr+
X2Σ+
1.0
10-1
10-2
10-3
10-4
10-5
10-6
[V(∞)-V(r)]/V(∞)
Thakkar
Ion-Induced
Dipole
Huffaker
1
2
3
4
5
r/re
XBL 824-8976

Figure 2

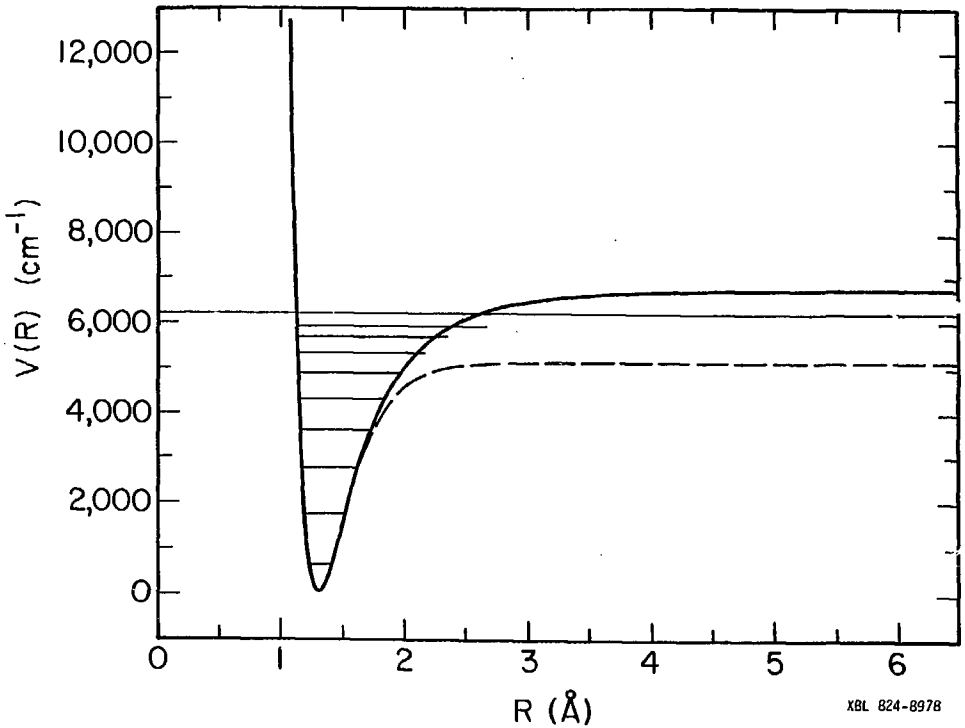
12,000
10,000
8,000
6,000
4,000
2,000
0
V(R) (cm^{-1})
0
1
2
3
4
5
6
R (Å)
XBL 824-8978

Figure 3

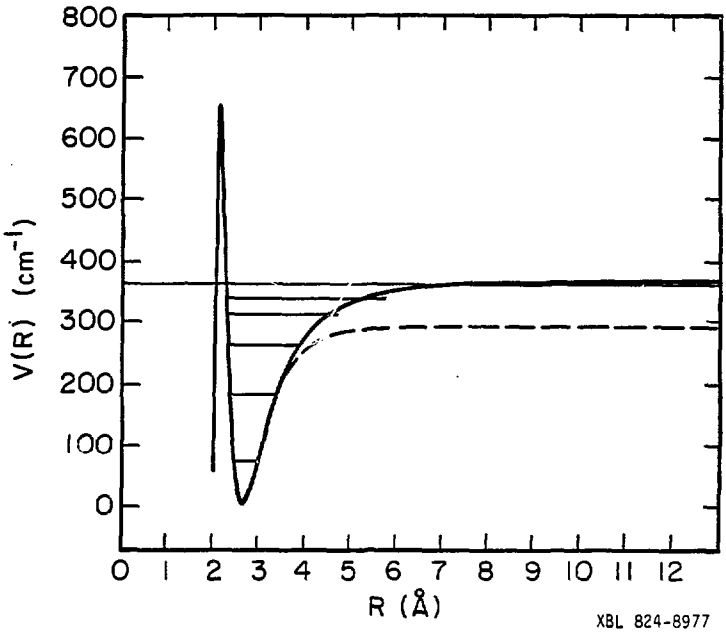
800
700
600
500
400
300
200
100
0
V(R) (cm^{-1})
0 1 2 3 4 5 6 7 8 9 10 11 12
R (Å)
XBL 824-8977

Figure 4

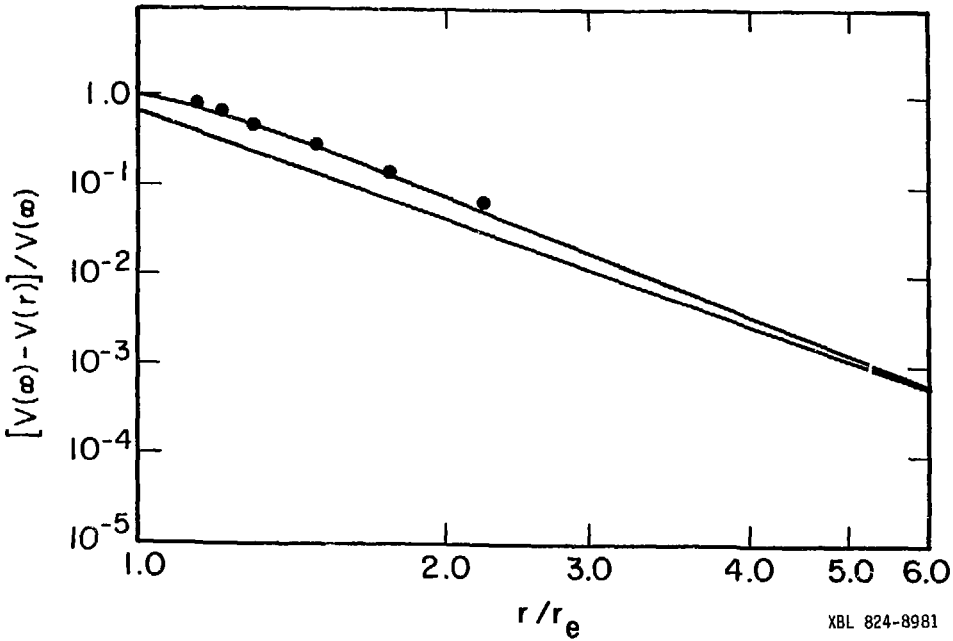
1.0
10^{-1}
10^{-2}
10^{-3}
10^{-4}
10^{-5}
$[V(\infty) - V(r)]/V(\infty)$
1.0
2.0
3.0
4.0
5.0
6.0
r/r_e
XBL 824-8981

Figure 5

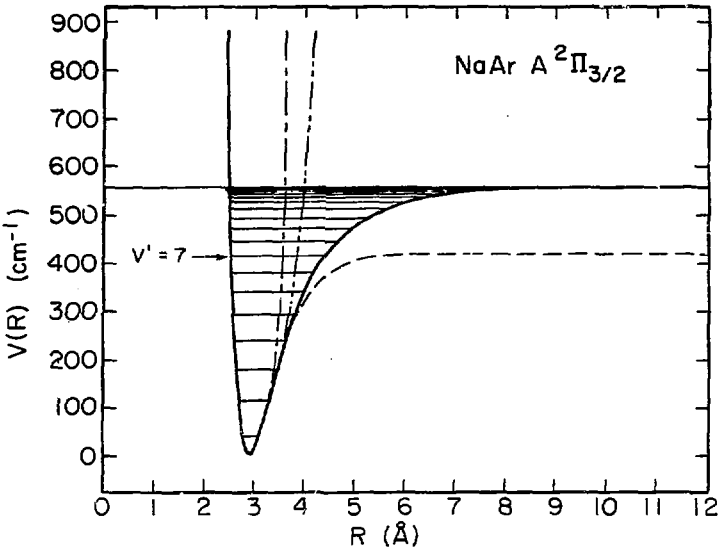

XBL 792-8367

Figure 6

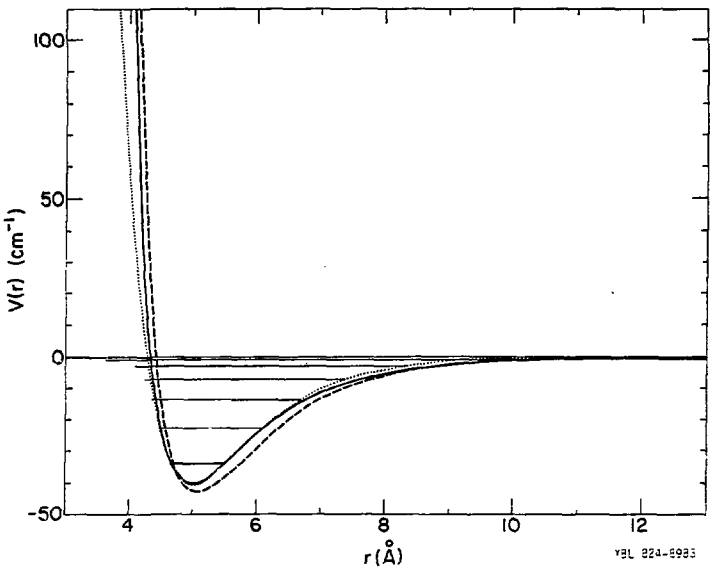

Figure 7

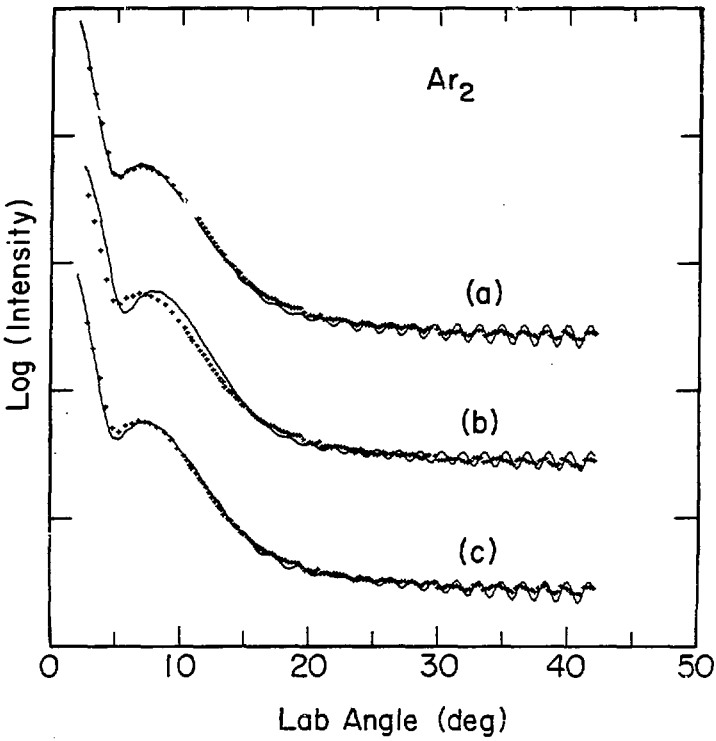

XBL 811-7708

Figure 8

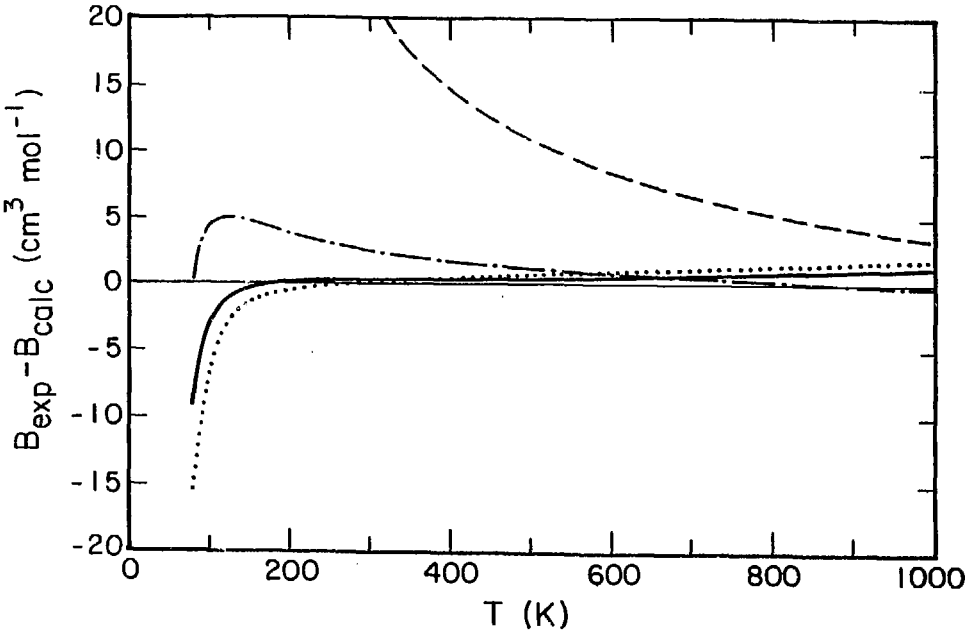

XBL 811-7706

Figure 9

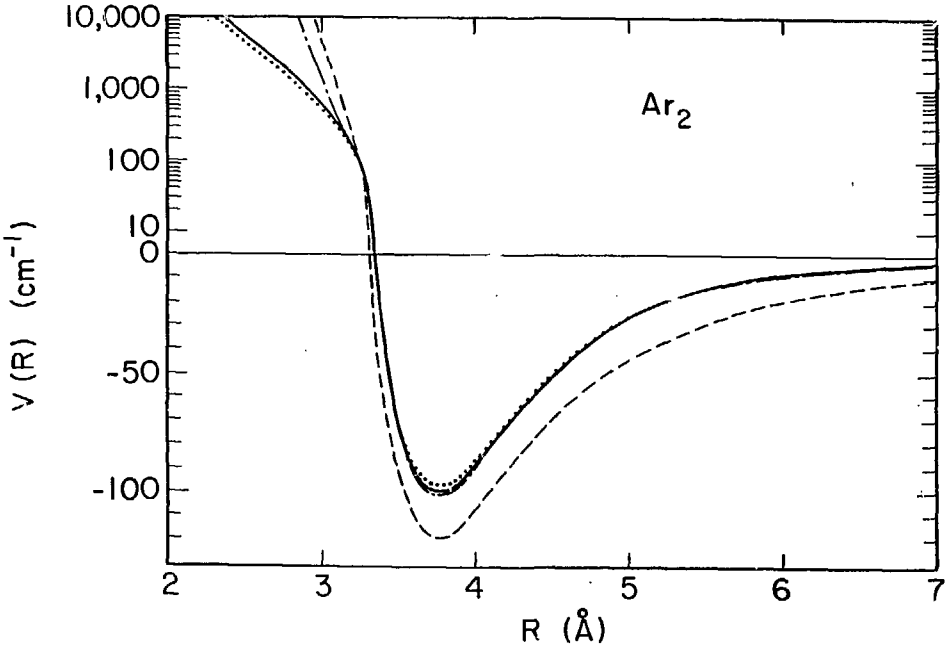

XBL 811-7707

Figure 10

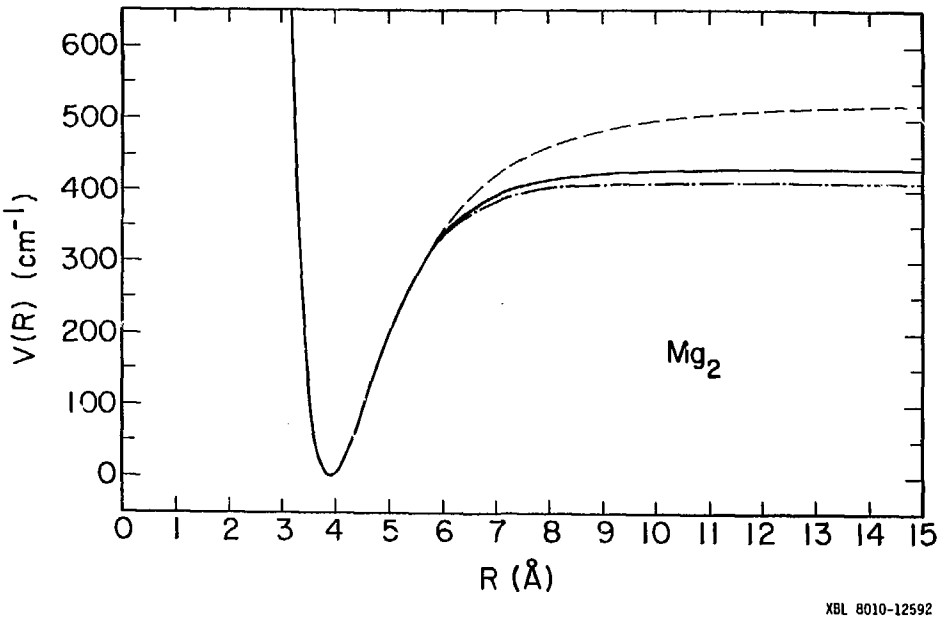
600
500
400
300
200
100
0
V(R) (cm^{-1})
0 1 2 3 4 5 6 7 8 9 10 11 12 13 14 15
R (Å)
Mg_2
XBL 8010-12592

Figure 11

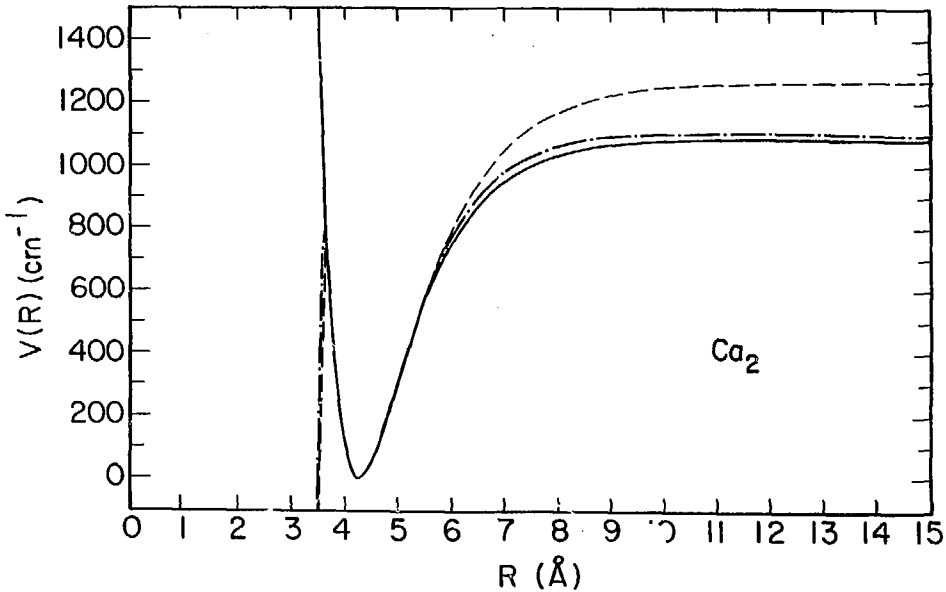

XBL 8010-12591

Figure 12

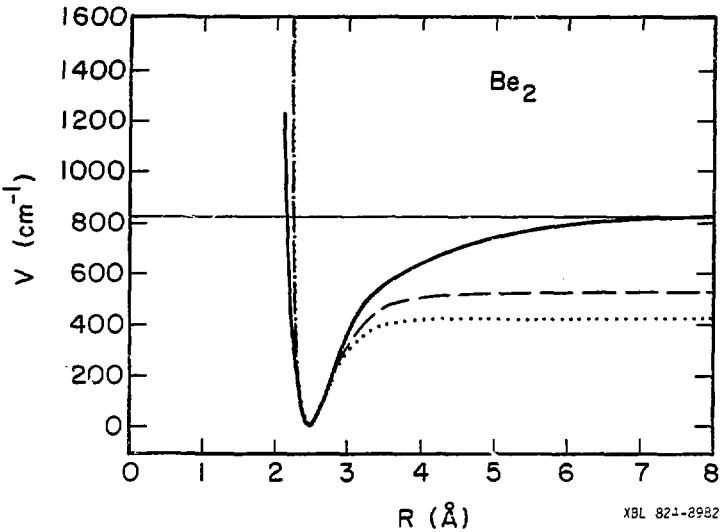
1600
1400
1200
1000
800
600
400
200
0
V (cm^{-1})
Be$_2$
0
1
2
3
4
5
6
7
8
R (Å)
XBL 821-2982

Figure 13

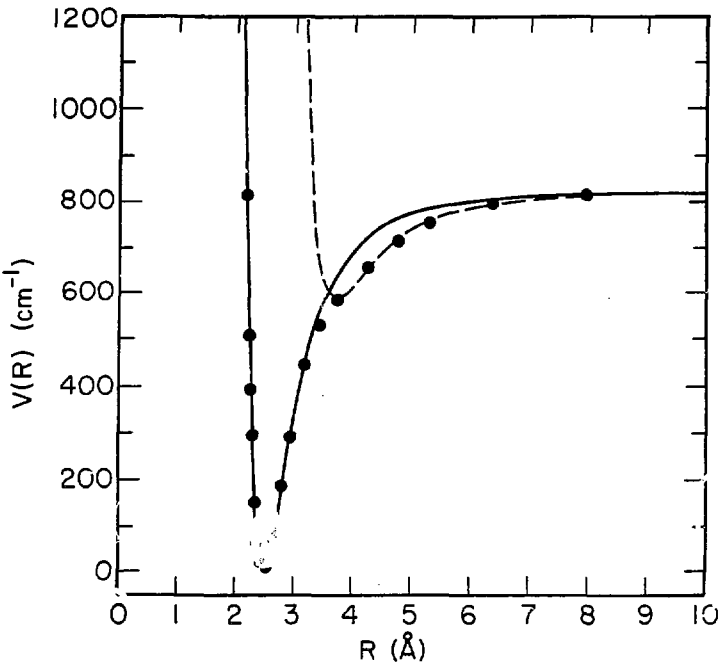

XBL 8010-12590

Figure 14

Chapter IV

Laser Assisted Penning Ionization

A. Introduction

Absorption of light by colliding atomic and/or molecular species is hardly a new phenomena, as it is the source of pressure broadening of resonant absorption and emission lines[1] and collision-induced absorption[2]. What has generated much interest of late is the absorption of light, nonresonant with respect to the reactants, which changes the state of internal excitation of the products.

The simplest of these processes is laser-induced energy transfer as studied by Harris and co-workers[3,4] for the Sr/Ca pair and by Cahuzak and Foschek[5] for Eu/Sr. An example is the system:

$$Sr(5p\,^1P) + Ca + h\nu(4977\ \mathring{A}) \rightarrow Sr + Ca(4p^2\,^1S)$$

where the $4p^2\ ^1S \rightarrow 4s4p\ ^1P$ emission is monitored at 5513 Å. The unique point here is that the photon does not correspond to a resonant absorption of Ca or Sr, but makes up for the energy deficit for the Sr $5p\ ^1P$ excitation and the Ca $4p^2\ ^1S$ level. In effect, the photon is resonant with the transient "collisional complex" of Sr* and Ca, and the absorption is fairly broad (14 cm^{-1} FWHM) due to the short lifetime of the pair as they pass by each other.

Still other related phenomena are the laser-assisted excitive charge transfer between Ca^+ and Sr[4,6], collisional fluorescence between two Ba^* atoms[4,7] and laser-assisted intermolecular energy

transfer between CO in the ground state and another CO in the $v = 5$ level of the $A\ ^1\Pi$ state to yield one CO in the $B\ ^1\Sigma^+$ state[8]. We have already discussed photoassociation of Mg_2^* and Ca_2^* in the previous chapter and should also point out that photoassociation of Hg_2^* has been observed[9].

These absorption phenomena are not strictly limited to particles that are passing in close proximity of each other; absorption and emission of light by a chemical transition state, or activated complex, have been observed. Hering and co-workers[10] note that absorption of the complex for $K + HgBr_2$ opens up a new channel for chemiluminescence of $HgBr^*$. Arrowsmith and colleagues have studied chemiluminescence of the transition state from the $F + Na_2$[11] reaction. Similar effects have also been observed for $Cl + Na_2$[12]. There have been theoretical speculations[13] concerning the modification of other chemical reactions by radiation field effects on the transition state.

The system we will be considering is more along the lines of the atom-atom energy transfer scheme, but a bit more interesting. We refer to the effects of light absorption on a Penning ionization collision. Penning ionization (PgI) corresponds to the transfer of electronic excitation energy from one species to another, leading to ionization of the latter:

$$A^* + B \rightarrow A + B^+ + e^-$$

A similar phenomenon is associative ionization (AI), where the colliding species "stick" to form a molecular ion:

$$A^* + B \rightarrow AB^+ + e^-$$

Niehaus[14] has recently reviewed the PgI phenomena.

To date, Weiner and co-workers[15] have recently observed laser-assisted PgI and AI in collisions of two Li^* and in two Na^* atoms, where the excitation energy is in the 2p and 3p levels, respectively. The two excited atoms together do not possess enough energy to ionize one of their kind, so the energy deficit must be made up by photon absorption during collision. The processes of laser-assisted and -enhanced collisional ionization have generated much theoretical interest and speculation, ranging from the perturbation treatments of Geltman[16], of Weiner[17], and of Nayfeh and Payne[18] to the full-blown second-quantization calculations of George and co-workers[13,19,20]. What we find intriguing is George's prediction that the ionization collisional cross section should be enhanced by the presence of the radiation field.

These reactions may be more than just a theoretical curiosity. Energy transfer and ionization in the presence of a high intensity radiation field are of importance in laser-produced plasmas, such as in welding or annealing processes, or in plasma-produced lasers, such as excimer or ion lasers. The field-enhanced collisional cross sections can be of considerable importance with respect to the ever-increasing energy densities used in inertial confinement

fusion experiments.

We believe we have observed just such an effect in the system we are to discuss. The field-free reaction,

$$Ar(^3P_2) + Ca \rightarrow Ar + Ca^+(4p\ ^2P_J) + e^- \quad ,$$

has been previously studied in this laboratory by Hartman[21,22]. Monitoring the fluorescence intensity of the $^2P_{3/2}$ and $^2P_{1/2}$ lines at 3934 and 3968 Å, respectively, Hartman found a 5:1 propensity for excitive Penning ionization of the J = 3/2 state. This could be rationalized in terms of electronic angular momentum conservation[23]. He also determined absolute reaction rate constants of 1.6×10^{-10} and 3.2×10^{-11} cm^3 $molecule^{-1}$ sec^{-1} for the J = 3/2 and 1/2 ^2P levels, respectively, by comparing the intensities to that of the 7602 Å emission of Kr^* from the known rate of energy transfer from Ar^* to Kr. These rate constants yield thermally averaged cross sections of 28 and 5.5 $Å^2$. Emission from the A $^2\Pi_\Omega$ state of $CaAr^+$ by excitive AI was also observed and estimates of the well depths of the ground and excited states were made.

We report here the first observation of a resonant, field-modified excitive channel in this system. The new channel described here,

$$Ar^*(^3P_2^0) + Ca + h\nu \rightarrow Ar + Ca^+(5p\ ^2P) + e^- \quad ,$$

has been discussed as a likely one for the study of field-modified collisional ionization[24]. In this process, $h\nu$ equals (approximately) the energy difference between Ar^* and the 5p ^2P state of Ca^+, as illustrated in Fig. 1.

The new channel can be viewed as the excitive photoionization of the (autoionizing) quasi molecule $CaAr^*$ from a continuum state to an excited (and also unbound) state of $CaAr^+$ that correlates to $Ca^+(5p\ ^2P) + Ar(^1S)$. This state of Ca^+ has a radiative lifetime[25] of 34 nsec. It decays predominantly (80%) to the 5s level, which subsequently decays to the 4p doublet at 3737 and 3706 Å. These latter emissions determine the number of 5p ^2P ions formed (see Fig. 1).

What we expect from this view of the process is laser-excited fluorescence from the photoionization of $CaAr^*$ to yield $Ca^+(5s\ ^2S)$, whose energy threshold corresponds to a photon wavelength of 12003 Å. As the exciting radiation is scanned through shorter wavelengths, there should be a stepwise increase in fluorescence intensity at 5988 Å and 5960 Å as the thresholds of the 5p $^2P_{1/2}$ and $^2P_{3/2}$ are, respectively, attained. What is in fact observed are resonances at these thresholds. We also estimate the laser-assisted collision cross section to be 250 times that of the field-free reaction.

B. Experimental

Our experiment employs the flowing afterglow apparatus used by Hartman. Argon is passed through a $CaSO_4$ drying tube and then through a liquid nitrogen trap to remove H_2O. It is then passed through a 19 mm pyrex tube which encloses a hollow cathode discharge maintained at 275 V. The ions and excited states of argon recombine and decay to the $(^3P_2;\ 4s[3/2]_2^0)$ state, which is stable with respect to radiative decay. This afterglow contains ca. 10^9-10^{10} cm^{-3} metastables in a one torr bath of argon. The metastables flow down the remaining 35 cm of the pyrex tube and into the interaction region at a measured flow velocity of 7×10^3 cm/sec.

The interaction region is a stainless steel cross, with six two inch diameter side arms, in which the target gas is introduced. In this case the target gas is atomic calcium produced in an oven beneath the cross. The calcium vapor is entrained in a second flow of argon, introduced from beneath the oven, bringing the Ca into the cross at a density of greater than 10^{14} atoms/cm^3 and producing a red-violet, conical flame at the mouth of the pyrex tube. The visible fluorescence is predominantly due to production of neutral $Ca^*(4s4p\ ^1P$ and $^3P)$ by various secondary processes such as ion-electron recombination and excitation of neutral calcium by Penning electrons. After passing through the interaction region the flow proceeds through the foreline port of the cross, in line with the afterglow tube, and on to the 1000 ℓ/min Welch 1375 mechanical pump.

The calcium oven is a stainless steel crucible, 3/4" diameter

and 3" deep, which is radiatively heated by a surrounding foil heater. The heater is 0.010" tantalum foil about 10" long and around 3-1/2" wide, rolled lenghtwise into a cylinder. About 5" of this cylinder is cut lengthwise into six strips of equal width. The strips are bent out and down to form a concentric outer cylinder. The inner and outer cylinders are connected to two water-cooled copper bus lines that carry 400 amps of current at one volt a.c. potential difference. The crucible rests inside the inner tantalum cylinder and can be heated to 800°C. The entire assembly is held in place inside a 3 liter stainless steel chamber which is bolted to the interaction cross. Further details of the apparatus are given by Hartman[21].

The pulsed laser beam passes through the flame perpendicular to the axis of the pyrex tube. The laser entrance port is Brewster angle window on a six inch sidearm, epoxied to a stainless steel flange. The "aperture" in the flange (actually a 1/8" NPT hole originally drilled through for a thermocouple gauge) proved to be a little small for the laser beam, so the beam is brought to a focus at the aperture by a 50 cm focal length lens. This leads to a 6.7 mm beam diameter in the flame region. After crossing the flame, the beam exits through a similar window arrangement and the average power is monitored by a Scientech power meter.

Fluorescence from the flame is collected from the port directly above the flame and oven. The fluorescence first passes through a bandpass filter (Oriel G-774-4000) centered at 4000 Å with a width of 800 Å. The light is then passed through a 0.25 meter Jarrell-Ash

monochromator, centered at 3737 Å, with the slits removed (aperture width of 12 mm). These measures effectively eliminate background radiation of the oven, scattered laser radiation, and most of the fluorescence from neutral calcium excitation.

Since all six ports of the cross are employed, the preceding discussion may still be confusing. A block diagram of the experiment, illustrated in Fig. 2, should help.

The filtered signal is detected by a cooled RCA C31034 photomultiplier, amplified by a fast discriminator (PAR 1120, 30 nsec ECL pulse width), and counted by both a gated Ortec 770 counter and an ungated Intel 8253 counter interfaced to a computer. The gated counter is enabled for 1 μsec after a 10 nsec delay. The ungated counter monitors the background emission ($Ca^+(4p\ ^2P_{3/2}) \rightarrow (4s\ ^2S)$ at 3934 Å) which is responsible for 30% of the gated signal. Signal at each wavelength is accumulated for 1200 laser shots (2 min).

The laser system used for this experiment was on loan from the San Francisco Laser Center. The second harmonic from a pulsed Quanta Ray DCR YAG laser (with amplifier) was used to pump Rhodamine 101 in a Quanta Ray PDL-1 dye laser. This produced tunable radiation in the region of 5975 Å at 12 mJ per pulse with a pulse duration of around 10 nsec and a repetition rate of 10 Hz. There is a 20% attenuation of the beam by reflection losses of all the optics used to channel the beam into the chamber. Including the losses and the estimated beam diameter, we find a power density of 2.8×10^6 W/cm^2 in the flame.

The wavelength of the dye laser grating drive was calibrated to

0.05 Å against atomic neon emission on a 1.5 meter Jobin-Yvon monochromator. For operation without an etalon, Quanta Ray specifies a bandwidth of 0.4 cm^{-1} and we have found it to be less than our instrumental bandwidth of 0.7 cm^{-1}.

C. Signal Treatment and Results

During the course of our two minute data collection interval, there is a very large background of $(2\text{-}5)\times10^6$ counts. With the monochromator set at 3737 Å and an effective slit width of 12 mm, the primary source of this background is the 3734 Å line from field-free excitive ionization. This background proves to be a mixed blessing. On the one hand, it is a monitor of the flame intensity, which varies with Ca concentration due to oven temperature fluctuations. On the other hand, with a gated counter duty cycle of 1×10^{-5}, it also contributes 20-50 events recorded by the Ortec counter.

In order to obtain a corrected signal, S, we must subtract the product of the background, B, and the duty cycle, D, from the number of gated counts, G. Since the signal is proportional to the calcium concentration, we correct for fluctuations by normalizing with respect to the background. The 5975 Å region is on the blue side of the Rhodamine 101 gain curve and we found the power to fall off rapidly. For a single-photon process we expect the signal to be proportional to the intensity, so we also divide the corrected signal by the monitored laser power, P. We finally derive the corrected, normalized signal,

$$S = (G - D\times B)/(B\times P)$$

The uncertainty, $\sigma(S)$, is the standard counting uncertainty, $\sqrt{G}$, normalized with respect to background and laser power.

The results of this data massaging are presented in Fig. 3. The signal level for this experiment is very low; our largest signal at 5958 Å corresponds to 97 event, 1/3 of which is background. The repeated scan in Fig. 3b is an indication of the reproducibility of the signal. Attempts to improve on the red band at 5989 Å proved unsuccessful.

Table I lists the observed resonances and their bandwidths, along with anticipated frequencies based on asymptotic energy differences. Although we list two maxima for the $^2P_{1/2}$ excitation, the statistics of the data do not warrant the resolution of this band into a doublet; we note the average position (16 691±5 cm^{-1}) parenthetically in the Table. The maxima occur very close to the asymptotic predictions, with the $^2P_{3/2}$ signal about 7 cm^{-1} to the blue of its expected location. This shift is not exceptional, compared to the observed 68 cm^{-1} blue shift of laser-assisted charge transfer[6].

We were, of course, careful to ascertain that this signal occurred in the presence of both calcium and metastable argon. When either the discharge or the oven was off, no signal appeared on the gated counter.

Not shown in Fig. 3 is a very large signal at 6001 Å due to two-photon excitation of neutral Ca to the (4s5s ^1S) level. Subsequent cascade to the (4s4p ^1P) level produces a 4227 Å signal which is so strong that, even though the line is outside the monochromator bandpass, scattered light produces signal orders of magnitude larger, even with 250 μ slits in place. We are fortunate that this absorption is out of the region of interest.

One further bugbear is the two-photon absorption of argon metastables to produce argon in the n = 15-20 Rydberg states. If this were to happen, a collisional ionization would produce an excited calcium ion which would ultimately cascade to the 5s level we monitor. These Rydberg levels have not been observed to date, so we have computed the supposed resonances by quantum defect estimations (good to $\pm 1\ cm^{-1}$). We do not find these resonances in Fig. 3 and dismiss this mechanism.

D. Discussion

We have estimated a 10 nsec delay to occur following the end of the laser excitation pulse. This is based upon the conversion of the photodiode pulse to a TTL signal which controls the Ortec counter gate, which should take >20 nsec. The transit time of the photomultiplier tube and the response time of the PAR ECL discriminator should be on the order of 10-15 nsec, giving a net delay difference of 5-10 nsec. This assignment of delay is critical because it is conceivable that $Ca^+(5s\ ^2S)$ could be formed directly, with the excess energy of the photon going into Penning electron kinetic energy. Since the lifetime of this state is 5 nsec, any formed directly would have completely decayed before gated counting began. Similar lifetime arguments hold for laser enhancement of the 4p level. Emissions from 4d ^2D levels occur outside the bandpass of our filter-monochromator. Thus our experiment would be sensitive to the 5p ^2P cascade exclusively.

The most remarkable feature of Fig. 3 is the apparent resonance behavior. This feature is worth some consideration. We should first point out that our experiment is sensitive only to the probability of ionization that leads to a 5p ^2P_J excitation. Thus it is possible that the total laser-assisted ionization may be constant, for example, and we are only seeing a resonance in the branching ratio.

Assuming that we are, in fact, seeing all of the laser-assisted processes through fluorescence detection, we note that the bandwidths of 11-14 cm^{-1} are characteristic of Harris' fly-by time[3c], or the duration of the collision. The fact that the resonances occur in very

close proximity to the expected wavelengths for the $^2P_{1/2}$ and $^2P_{3/2}$ channels supports our premise that we are observing a collision complex absorption.

Another possibility which could explain the resonance effect is laser-assisted collisional energy transfer to an autoionizing state of atomic calcium, which spontaneously ionizes to form 5p ^2P Ca^+. Although autoionizing states of calcium have been studied through photoionization of ground state Ca^{26}, the region of interest to us (910 Å for photoionization of the ground state) is yet to be studied. Thus the presence of these hypothetical autoionization states can neither be confirmed nor denied. The wavelengths of these resonances seem very fortuitous unless the autoionizing states are of the form 5pnl, where nl corresponds to a Rydberg level. Cooke and Gallagher[27] have studied the 6p20s states of barium, and we note that the observed autoionizing linewidths of 3-11 cm^{-1} could contribute to the broadening we see in our lines.

We can take advantage of the fact that we are monitoring the field-free ion production in order to estimate a collisional cross section. Since our background is primarily due to the 3934 Å line from field-free $Ca^+(4p\ ^2P_{3/2})$ production, the ratio of the number of field-assisted events per laser shot to the average number of field-free events per shot is proportional to the ratio of the field-assisted cross section to the field free cross section (known to be 28 $Å^2$). The average number of field-free collisions is found by multiplying the average background count rate by the 10 nsec duration

of the laser pulse. In this ratio we are neglecting a proportionality constant that accounts for a geometrical correction of the laser beam-flame intersection fraction and the efficiency of 3934 Å transmission by the filter/monochromator arrangement. These two effects cancel one another, and we assume this factor to be close to unity. The ratio itself is 225±93, implying a field-assisted cross section of (6.3 ±2.6)×10^3 $Å^2$ at a power density of 10^6 W/cm^2, where the uncertainty is the standard deviation of four separate measurements.

Although we are confident of the qualitative result that the field-assisted rate exceeds the field-free rates by a significant amount, we should be more circumspect of the exact magnitude. George and co-workers[13,20] have indicated that long range radiative coupling between the two atoms should increase the PI cross section. Cross sections of 10^3 $Å^2$ have been reported for collisional energy transfer[3b,4] at hundreds of times higher power densities. At powers similar to ours, however, Weiner and co-workers[15,17] find a PI cross section 0.1 $Å^2$. The resonance structure is most likely the key to these very large cross sections.

If the postulate for energy transfer to an autoionizing state of calcium is born out, we may have the necessary rationalization for our estimated cross section. The photon does not ionize the complex directly but rather excites it to a state that correlates to a relatively large, doubly excited calcium atom. Such a mechanism would put this system on the same footing as those studied by Harris and co-workers.

We present one other alternate interpretation which we would like to ignore, but as scientists must consider. Because of the numerous secondary processes occuring, such as ion-electron recombination, there will be a small concentration of neutral calcium atoms in excited Rydberg levels. These levels can be excited to the autoionization states mentioned in the previous paragraph through a two or three photon process. If this is the case, then our observations are not of a collisional photon absorption at all. This possibility can be tested by carefully monitoring our signal as a function of laser power. We have observed the 5958 Å peak at two different power levels, and there appears to be very little power dependence in the net signal. Since ion-electron recombination is second order in metastable concentration, we can determine the dependence of the signal on $[Ar^*]$ by varying the current to the hollow cathode discharge. Resolution of this question must await further experiments.

E. Theoretical Considerations

Since part of the motivation of this experiment is inspired by theoretical speculations, it behooves us to at least outline the theory behind Penning ionization and consider the effects of the radiation field. We start with Miller's classical expression[29] for the probability of ionization, or "opacity", P_b:

$$P_b = 1 - \exp\{-2 \int_{r_0}^{\infty} dr\, \Gamma(r)(\hbar v_b(r))^{-1}\} \qquad (1)$$

In this expression b is the classical impact parameter, $\Gamma(r)$ is the autoionization width, and v_b is the classical velocity between the two approaching atoms with initial kinetic energy, E

$$v_b = \sqrt{2\mu E(1-V_*(r)/E-(b/r)^2)} \qquad (2),$$

where $V_*(r)$ is the potential between the two atoms before Penning ionization, and r_0 corresponds to the classical turning point, $v_b(r_0) = 0$.

The total ionization cross section, σ_{TOTAL}, can be found by integrating P_b with respect to the area element, $2\pi b db$. The equivalent quantum mechanical evaluation can be made by substituting the relation

$$b = (\ell+1/2)/k_0 \qquad (3)$$

and

$$k_0 = h/(2uE)^{1/2} \qquad (4)$$

to obtain the sum

$$\sigma_{TOTAL} = (\pi/k_0^2) \sum_{\ell=0}^{\infty} (2\ell+1)P_\ell \qquad (5).$$

Since we are examining a system with more than one ionization channel, the above formulas must be modified. The autoionization width must be resolved[14] into the individual channels

$$\Gamma(r) = \Sigma_i \Gamma_i(r) \qquad (6).$$

The expression for $\Gamma_i(r)$ can be obtained from the "Golden Rule" formula[30]:

$$\Gamma_i(r) = 2\pi\rho_i |\langle\phi|H-E|X_i\rangle|^2 \qquad (7),$$

where X_i is shorthand for the product of the wave functions of the unbound Penning electron and the discrete electronic states of the ion and ground state rare gas. H is the electronic Hamiltonian, and E is the total electronic energy of the atoms in state φ before the collision. If the wave function of the departing electron is normalized as that of a spherical Bessel function (i.e., has units of reciprocal length), then the density of states, $\rho_i = (8m_e/h^2\varepsilon_i)^{1/2}$, where m_e and ε_i are the mass and kinetic energy of the electron, respectively.

In order to find the probability of producing channel i, we must use the expression[29]:

$$P_b^i(r) = (2\Gamma_i(r)/\mu v_b(r))\exp\{-\int_{r_0}^{\infty} dr'(\Gamma(r')/hv_b(r'))\} \times$$

$$\cosh\{\int_{r_0}^{r} dr''(\Gamma(r'')/hv_b(r''))\} \qquad (8).$$

Integration of <u>this</u> expression with respect to r from r_0 to infinity does not give the simple closed form of Eq. (1) since the argument of the hyperbolic cosine (the latter being called the "survival function" in the literature) is the total ionization width, whereas the factor is the width of the individual channel. Following the radial integration, the resultant P_b^i is treated as before to obtain the cross section of this individual channel, σ_i.

Niehaus[14] has discussed the problems of determining branching ratios, $\Gamma_i(r)/\Gamma(r)$, from cross section ratios, concluding that doing so is not a good idea unless (1) the ratios do not vary significantly with r and (2) the opacity function is much less than one. Moreover, we measure rate constants, or velocity averaged cross sections, and these latter quantities can show very strong velocity dependences[14,31]. Because of the convolutions and assumptions involved (assumption (2) is probably not valid in our case), we hesitate to determine dynamic, microscopic branching ratios from our measurements.

Up to this point, we have only discussed field-free Penning ionization. For field-modified processes there are two elements in the Hamiltonian that couple the discrete electronic states of the colliding atoms to the ionization continuum of the products. The first is the electronic Hamiltonian itself, or the Coulombic coupling, which

is responsible for the field-free ionization as expressed in the ionization width of Eq. (7). The second interaction term is that of the atoms with the radiation field. This interaction is usually represented in the dipole approximation as $-\vec{\mu}\cdot\vec{E}$, where $\vec{E}$ is the oscillatory electric field and $\vec{\mu}$ is the dipole moment of the electrons and nuclei A and B: $-e\Sigma_i\vec{r}_i+Z_Ae\vec{r}_A+Ze_B\vec{r}_B$.

The treatment of this process follows two schemes. The first is perturbation theory, and we will concentrate on John Weiner's work[17] as an example. The other is the more elegant treatment by Bellum and George[13,19], which uses second-quantization treatment for the radiation field and a set of coupled-channel equations for the actual collision dynamics (as opposed to the classical treatment presented here earlier). Since these methods are a bit sophisticated, we will only qualitatively discuss their results.

Weiner considers laser-assisted collisional ionization relevant to his experiments (where field-free ionization does not occur) in terms of second order perturbation theory. The first order corresponds to laser excitation of the diatomic system from state 1 to state 2. It is important to note that state 2 is a discrete excited state, so that this process is a resonant transition. The second order perturbation is the coupling of state 2 to ionization continuum, i.e. Penning ionization. Using Miller's theory and the small opacity approximation, he obtains the expression for the cross section. It is:

$$\sigma = 4\pi(\mu_{12}E/2\hbar\Delta\omega)^2AB^3\exp(-b_0/B)(b_0/B+1)/hv \qquad (9),$$

where $h\Delta\omega$ is the energy difference between state 2 and the molecular-ion potential, v is an average velocity, and the autoionization width is

$$\Gamma(r) = A \exp(-r/B) \qquad (10),$$

which has been shown[14] to be a reasonable functional form. He chooses a value of 2 Å for b_0, which is a minimum impact parameter. Using 3 Debye for the transition moment, μ_{12}, and the PgI parameters for the H/He(^{3}S) system, he finds a cross section of 0.10 Å^2 for a laser power of 10^6 W/cm^2.

Bellum and George consider field-modified processes (i.e. where the system also ionizes under field-free conditions) as well as the field-assisted processes above (although resonance excitation is not necessary). They argue that the dipole coupling element,

$$\vec{\mu}(r) = \langle\phi|\vec{\mu}|\chi\rangle \qquad (11),$$

should die off more slowly with increasing r than the field-free Coulombic matrix element. Their rationale is that the Coulombic term only becomes appreciable when the electron clouds of the two atoms start to overlap at close distances, whereas the above function may still be appreciable at larger separations. Although their arguments may be plausible, an <u>ab initio</u> calculation of Eq. (11) would be far more compelling. They report a numerical calculation of field-modified PgI of Ar by He(^{3}S)[32], but Eq. (11) is purposely parameterized as a

function of r to support their qualitative conclusions. Moreover, the calculated field-modified cross sections are at best only comparable to the field-free processes, even for laser intensities of 10^9 W/cm^2. The cross sections (or rather differential cross sections as a function of emitted electron energy) appear in Fig. 4 of ref. 32. We estimate from this figure field-modified cross section of ≤ 1 Å^2.

It would seem that theory does not bear out the amount of enhancement seen in our experiment. This makes our alternate proposal of laser-assisted energy transfer to a discrete, autoionizing state of calcium seem somewhat more desirable. Harris and colleagues observe[3,4] collision cross sections comparable to the one we estimate, but theirs are for power densities of 10^{11}W/cm^2. Due to our ignorance of the autoionization states in this energy regime, this particular interpretation must remain only speculation.

F. Future Considerations

There are several experimental improvements that could enhance the signal and make more reproducible and refined measurements possible. One would be a collection lens that would focus the fluorescence onto the monochromator slit. Care should he taken in the choice of the lens so that the magnification factor places the flame image within the slit size and that the angle of divergence following the slit matches the throughput, or f#, of the monochromator. This would permit better dispersion. Since the region being monitored lies in the ultraviolet, an RCA 8850 photomultiplier would be more appropriate, and less sensitive to oven background and scattered laser light, than the red-sensitive 31034. The effective lifetime of the 5p ^2P cascade is less that 100 nsec, so that either a faster discriminator or a gated integrated would be in order. The gate trigger used in this experiment had a minimum enable time of 1 μsec. Clearly, a shorter gate time would significantly reduce the background.

Some of these modifications were employed in later attempts to reproduce the signal. These efforts were hampered by breakdown of the laser, oven, and photomultiplier tube (occurring consecutively in order to maximize frustration). To date, our best data are from our initial measurements.

There are at least two other systems which lend themselves to study. Excitation at 5634 Å of Sr in collision with Ar^* would lead to production of the 7s ^2S ion state. This cascade is best observed

by monitoring the 6s $^2S \rightarrow 6p\ ^2P_{3/2}$ line at 4305 Å, which is also present in the field-free flame. Absolute rate constants have not been measured for this system, but relative rate constants for the field-assisted reaction would be instructive. Another scheme involves excitation of the 3p ^2P_J levels of Mg^+ at 5759 Å and 5729 Å during the collision of Mg with $Kr(^3P_2)$. Since Kr^* produces no excitive ionization of Mg, the appearance of the resonance lines at 2796 and 2803 Å would present a clear-cut demonstration of the laser assisted process. The 3.7 nsec radiative lifetimes prohibit a counting system since a discriminator would only record one event per laser shot.

In light of the results reported here, it would also be worthwhile considering energy transfer to <u>known</u> autoionizing states of the alkaline earths.

G. Conclusion

We have observed the opening of a new excitive Penning ionizaion channel by laser excitation of the nascent ionization complex of Ca and Ar^*. Cascade fluorescence from the 5p ^2P_J states, unexcited in the field-free case, is monitored as a function of laser excitation wavelength. The excitation signal showed resonances at wavelengths corresponding to the excitation of the $^2P_{1/2}$ and $^2P_{3/2}$ levels with a small blue-shifting of the $^2P_{3/2}$ resonance.

A laser-assisted cross section of 6.7×10^3 $\mathring{A}^2$ has been estimated from this work. While the magnitude of this cross section should be confirmed or adjusted through further work, there can be no question that the field-assisted reaction proceeds at a faster rate than the field-free production of $Ca^+(4p\ ^2P_J)$.

REFERENCES

1. A. C. G. Mitchell and M. W. Zemansky, Resonance Radiation and Excited Atoms (Cambridge University Press, Cambridge, 1961).

2. D. R. Bosomworth and H. P. Gush, Can. J. Phys. 43, 751 (1965).

3. a) R. W. Falcone, W. R. Green, J. C. White, J. F. Young, and S. E. Harris, Phys. Rev. A 15, 1333 (1977); b) W. R. Green, J. Lukasik, J. R. Willison, M. D. Wright, J. F. Young, and S. E. Harris, Phys. Rev. Lett. 42, 970 (1979); c) S. E. Harris, R. W. Falcone, W. R. Green, D. B. Lidow, J. C. White, and J. F. Young, in Tunable Lasers and Applications, edited by A. Mooradian, T. Jaeger, and P. Stokseth (Springer, Berlin, 1976) p. 193.

4. S. E. Harris, J. F. Young, W. R. Green, R. W. Falcone, J. Lukasik, J. C. White, J. R. Willison, M. D. Wright, and G. A. Zdasiuk, in Laser Spectroscopy, edited H. Walther and K. W. Rothe (Springer, Berlin, 1979) p. 349.

5. Ph. Cahuzak and P. E. Toschek, in Laser Spectroscopy, edited by J. L. Hall and J. L. Carlsten (Springer, Berlin, 1977) p. 431; Ph. Cahuzak and P. E. Toschek, Phys. Rev. Lett. 40, 1087 (1978).

6. W. R. Green, M. D. Wright, J. F. Young, and S. E. Harris, Phys. Rev. Lett. 43, 120 (1979).

7. J. C. White, G. A. Zdasiuk, J. F. Young and S. E. Harris, Phys. Rev. Lett. 41, 1709 (1978).

8. J. Kukasik and S. C. Wallace, Phys. Rev. Lett. 47, 240 (1981).

9. D. J. Ehrlicka and R. M. Osgood, Jr., Phys. Rev. Lett. 41, 547 (1978).

10. P. Hering, P. R. Brooks, R. F. Curl, Jr., R. S. Judson, and R. S. Lowe, Phys. Rev. Lett. 44, 687 (1980).

11. P. Arrowsmith, F. E. Bartoszek, S. H. P. Bly, T. Carrington, Jr., P. E. Charters, and J. C. Polanyi, J. Chem. Phys. 73, 5895 (1980).

12. P. Arrowsmith, S. H. P. Bly, T. Carrington, P. E. Charters, J. C. Polanyi, and R. J. Wolf, J. Photochem. 17, 172 (1981). (Abstract from the Xth International Conference of Photochemistry, Iraklion, Crete, Greece, 1981).

13. T. F. George, I. H. Zimmerman, P. L. De Vries, J. M. Yuan, K. S. Lam, J. C. Bellum, H. W. Lee, M. A. Slutsky, and J. T. Lin in Chemical and Biochemical Application of Lasers, edited by C. B. Moore (Academic, New York, 1979) p. 253 and references cited therein.

14. A. Niehaus, Advances in Chemical Physics, vol. 45, edited by J. Wm. McGowan (Wiley, New York, 1981) pp. 395-486.

15. A. v. Hellfeld, J. Caddick, and J. Weiner, Phys. Rev. Lett. 40, 1389 (1978); P. Polak-Dingels, J. -F. Delpech, and J. Weiner, Phys. Rev. Lett. 44, 1663 (1980).

16. S. Geltman, J. Phys. B 10, 3057 (1977).

17. J. Weiner, J. Chem. Phys. 72, 2856 (1980).

18. M. H. Nahfeh and M. G. Payne, Phys. Rev. A 17, 1695 (1978).

19. J. C. Bellum and T. F. George, J. Chem. Phys. 68, 134 (1978).

20. J. C. Bellum, K. -S. Lam, and T. F. George, J. Chem. Phys. 69, 1781 (1978).

21. D. C. Hartman, Ph.D. dissertation, University of California, Berkeley (1979).

22. D. C. Hartman and J. S. Winn, J. Chem. Phys. 74, 4320 (1981).

23. A similar J = 3/2 propensity has recently been reported for Cd ionization by Ne metastables (S. Inaba, T. Goto, and S. Hattori, J. Chem. Phys. 75, 5209 (1981)).

24. J. S. Winn, in Advances in Laser Chemistry, edited by A. M. Zewail (Springer, Berlin, 1978) p. 426.

25. W. L. Wiese, M. W. Smith, and B. M. Miles, Natl. Bur. Stand. U.S. Circ. 22 (1969).

26. R. W. Ditchburn and R. D. Hudson, Proc. R. Soc. (London) A256, 53 (1960); W. R. S. Garton and K. Codling, Proc. Phys. Soc. 86, 1067 (1965); G. H. Newsom, Proc. Phys. Soc. 87, 975 (1966); M. W. D. Mansfield and G. H. Newsom, Proc. R. Soc. A357, 77 (1977); C. M. Brown, S. G. Tilford, and M. L. Ginter, J. Opt. Soc. Am. 63, 1454 (1973); C. M.Brown and M. L. Ginter, J. Opt. Soc. Am. 70, 87 (1980).

27. W. E. Cooke and T. F. Gallagher, Phys. Rev. Lett. 41, 1648 (1978).

28. C. E. Moore, Natl. Stand. Ref. Data Ser., Natl. Bur. Stand. 35 (1971); J. Sugar and C. Corliss, J. Phys. Chem. Ref. Data, 8, 865 (1979).

29. W. H. Miller, J. Chem. Phys. 52, 3563 (1970).

30. W. H. Miller, Chem. Phys. Lett. 4, 627 (1970).

31. H. Haberland, Y. T. Lee, and P. E. Siska, Advances in Chemical Physics, vol. 45, edited by J. Wm. McGowan (Wiley, New York, 1981) pp. 487-585.

32. J. C. Bellum and T. F. George, J. Chem. Phys. 70, 5059 (1979).

Table I. Expected and observed transitions for laser-assisted excitative Penning ionization of calcium by metastable argon. (FWHM is full width at half maximum.)

Ca state	γ observed (Å)	ν observed (cm^{-1})	ν expected (cm^{-1})	FWHM (cm^{-1})
5p $^2P_{1/2}$	5991,5988	16 687,16 695	16 695.19	5.6, 1.39
		(16 691±5)		
5p $^2P_{3/2}$	5958	16 780	16 773.44	11.3

FIGURE CAPTIONS

Fig. 1. Energy level diagram for Ca^+ + Ar relative to $Ca(4s^2\ ^1S)$ + $Ar(^1S)$. The dashed line locates the energy of $Ar^*(^3P_2^0)$. Wavelengths (in Å) of the transitions are: (a) 5958, 5988; (b) 11 836, 11 947; (c) 3706, 3737; (d) 3934, 3968; (e) 3159, 3179, 3181. Energy level values are from Ref. 28.

Fig. 2. Block diagram of flowing afterglow/laser excitation apparatus. A-argon flow, B-hollow cathode D.C. discharge, C-calcium crucible (tantalum oven assembly not shown), D-exhaust to 1000 ℓ/min pump, E-dye laser beam, F-power meter, G-fluorescence, H-bandpass filter, I-0.25 meter monochromator, J-cooled PMT, K-to counting instruments.

Fig. 3. Laser excitation spectrum of $Ca^+(5p\ ^2P)$ fluorescence resulting from Ca + Ar^* + hν collisions. (a) Complete excitation spectrum. (b) Second scan of blue portion of spectrum to illustrate the degree of reproducibility. Error bars represent ± one standard deviation due to counting statistics.

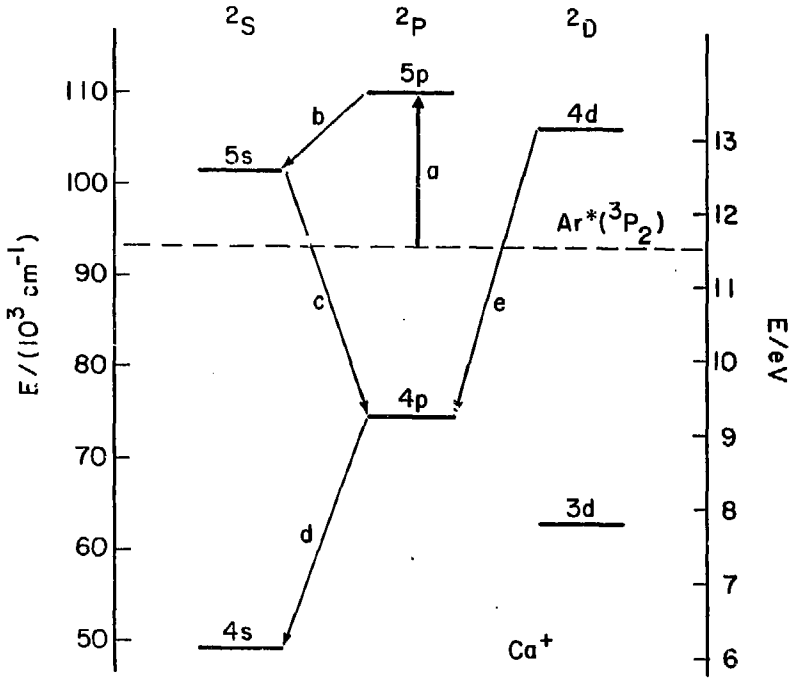

XBL 818-11152

Figure 1

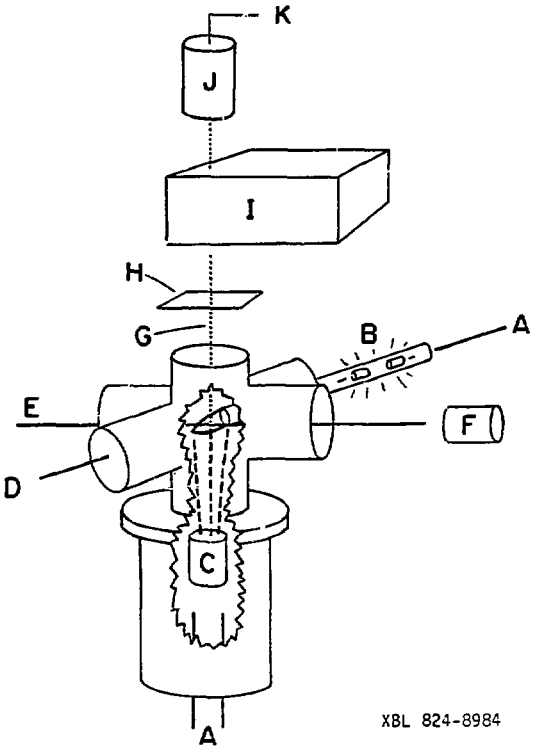

Figure 2

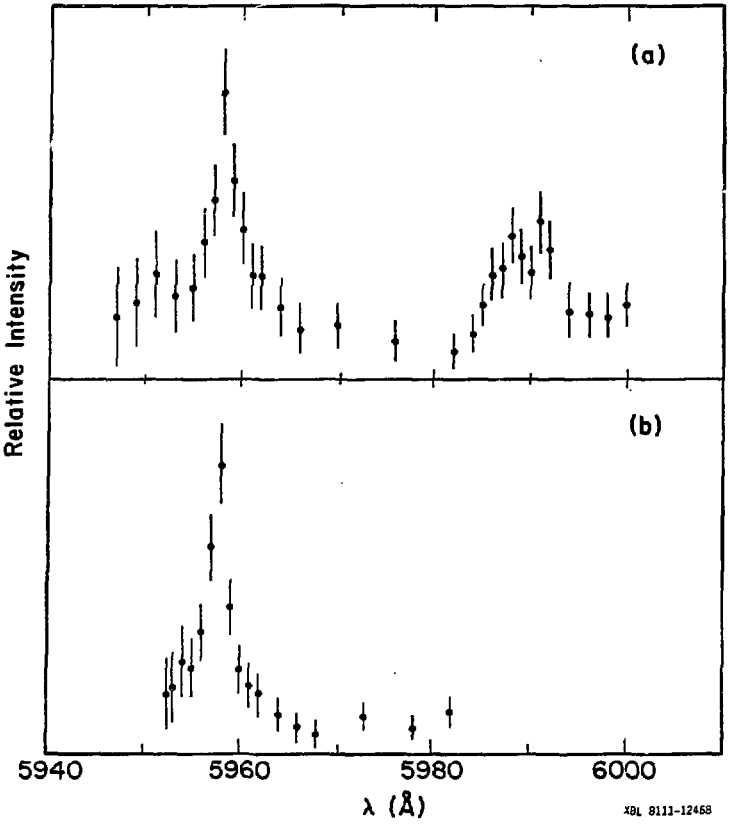

Figure 3

APPENDIX I.

This appendix provides "black box" directions for using the program DUNPOT to calculate the series potential coefficients. A sample set of control cards for use on the Lawrence Berkeley Laboratory's CDC 7600 computer is given, as well as a sample input deck. A listing of the program is also provided.

Since the program was never annotated with any comment cards, the listing is pretty cryptic. The brief subroutine-by-subroutine descriptions that follow are in order.

I. Main Program:

DUNPOT (INPUT,OUTPUT,COFOUT,FILM,TAPE9,TAPE10)

This is the controlling program and reads all the input data. Except for the RKR results, it is also the source of all the data on the output and COFOUT files. COFOUT is a file of all the series potential parameters to be viewed as an abbreviated output of this program or to be used as an input file for other programs. FILM is the output file containing plotting information to be disposed to the appropriate plotting hardware. TAPE9 and TAPE10 are scratch files used by the BKY plotting software.

The ordering of the Y_{ij}'s in the array, YIJ(I) is in the manner outlined in Chapter II, i.e. YIJ(1)=B_e, YIJ(2)=ω_e, YIJ(3)=$-\omega_e x_e$, etc. There are also two arrays, YN0(I) and YN1(I) containing the G_v and B_v expansions, respectively, that are used later by the RKR section. The arrays X(I),Y(I), and Z(I) contain Dunham's resolution of the Y_{ij}'s into first order terms and higher order corrections. Z(I) is not used

by the program but is included in anticipation of future expansion. YTMP(I), XT(I), etc., are temporary arrays used in the error analysis.

The Dunham coefficients are contained in the A(I) array, where $A(1)=a_0$, $A(2)=r_e$, $A(3)=a_1$, etc. B(I), E(I), and C(I) refer to the SPF, Thakkar, and Huffaker potentials, respectively. The arrays in common block /ERRSTUF/ contain the Jacobians, variance matrices, and scratch arrays of differentials used in the error analysis. The minimum number of a_n's to be calculated is up to a_2 (there is no point in using the program for any fewer). The maximum number of a_n's is up to a_6. "Extra" Y_{ij}'s, up to $Y_{10,0}$ and $Y_{9,1}$, can be read in and used by the RKR section.

The outputting of the potential coefficients is done by one of two sections, depending upon whether an error analysis was performed. The next two sections call the option RKR and plotting routine packages. The last section writes out the potential parameters and RKR turning points, if calculated to the file COFOUT.

II. The a_n algorithm:

SUBROUTINE KALKAN

This is the workhorse of the program, iteratively calculating the a_n's from the Y_{ij}'s. The maximum number of iterations is 30, fewer if the sum of the relative changes of all the a_n's is less than 2^{-47}. The b_n's and e_n's are calculated from a_n's. The c_n's are determined directly from the second-order-corrected Y_{ij}'s using Huffaker's published relations (J. N. Huffaker, J. Chem. Phys. 64, 3175 (1976)).

III. Error Analysis:

SUBROUTINE ERRANS

This routine calculates the deivatives, a_n / Y_{ij}'s, in order to form the Jacobian, AJ(I,J). The numerical differentiation is performed by adjusting the relative value of each Y_{ij} by 1×10^{-8}. The a_n variance matrix, AV(I,J), is calculated from the Y_{ij} variance matrix by SUBROUTINE JVJ. AV(I,J) is then rescaled so that the a_n standard deviations lie on the diagonal and off-diagonal elements correspond to the correlation coefficients (See A. A. Clifford, ref. 44 of Chapter III, for definitions of the terms used here).

IV. RKR Package:

SUBROUTINE RKMSKR

This set of routines uses the RKR algorithm suggested by M. E. Kaminsky, J. Chem. Phys. 66, 4951 (1977). The above subroutine prints out a table heading and coordinates the other routines. WMFIG determines v such that $G_v=0$. ABNK calculates some intermediate coefficients and KMNSKI evaluates the f_v and g_v integrals and prints out the results. BLOCK DATA RKRQD contains the set of 50 Gaussian quadrature point pairs, in octal, used in the integral evaluation. Most likely the number of points used is a factor of 2-10 larger than necessary.

V. Plotting Package:

SUBROUTINE PLOTPOT:

The above routine calculates an array of points to be plotted for each of the series potentials and the RKR turning points. It employs FUNCTION VOFR to evaluate the potential for each value of r. The ordinate is scaled from $-\frac{1}{5} D_e$ to $2\frac{1}{5} D_e$ and the abscissa for 0 to 5 r_e, where D_e is supplied from the input deck and r_e is determined by the program. The appropriate increments by which the abscissa and ordinate should be labelled are determined by SUBROUTINE TICKGEN.

The actual plotting instructions are made by a series of calls to the BKY IDDS package, making this part of the program "site dependent". The program exploits one of the BKY features by determining whether the plots are being made on a Tektronix interactive terminal and, if so, requesting interactive instructions from the terminal to determine the time of viewing.

A sample control card sequence for running on the CDC 7600 and plotting on the Calcomp pen plotter would be as follows:

```
(jobcard)
$ID=password
FETCHPS(JSWB,DUNPLOT,DUNPLT7)
FETCHPS(GPACBN7,GPAC,CCBN)
FETCHPS(IDDS,ULIB,ULIBX)
LINK,X,F=DUNPLOT,F=GPAC,P=ULIB.
RETURN,DUNPLOT,GPAC,ULIB,FTN4LIB.
DISPOSE,FILM=PL.
FETCHPS(JHG,COFISH,COFISH)
COPY(COFISH,OF,NULL)
COPY(COFOUT/RB,OR,COFISH)
LIBRITE(JSW,COFISH/RB,COFISH,395,W=[GOBLE])
EXIT.
DUMP(0)
FIN.
END.
(7/8/9 card)
(datadeck)
(6/7/8/9 card)
```

The following is a description of the input structure and a sample input deck.

(TITLE(K),K=1,8)
FORMAT(8A10)

One card, or 80 characters, giving a label for the data set.

(LITCHER(K),K=1,8)
FORMAT(8A10)

Another card of alphanumeric characters giving reference source for the Y_{ij} data. The form is: First Author/Journal and Volume/Pg.No./Year/Y_{ij} Status. Further details are given in Chapter II.

RM1,RM2,Z1,Z2,DSUBE
(Free format)

The first two values are the atomic masses (in amu's), the atomic numbers, and the estimated dissociation energy in cm^{-1} (for scaling the plot).

(IFL(J),J=1,16)
FORMAT(16I5)

Various integers and flags for controlling the program. The purposes are:

IFL(1) : Number of Dunham corrections calculated. Minimum is 2, maximum is 6.

IFL(2) : Option flag for an error analysis. If IFL(2)=0, the Y_{ij}'s uncertainties are read and an error analysis performed.

IFL(2) Also controls printing options, which are:

IFL(2) = 1: Only a_n's standard deviations are printed.

= 2: The a_n's correlation matrix is also printed.

= 3: Correlation and Jacobian matrices are printed.

IFL(3): Determines whether RKR turning points are computed or read in.

IFL(3) < 0: Read in G_v and the turning points for |IFL(3)| number of energies.

= 0: No RKR turning points read in or computed.

> 0: Calculate the RKR turning points for IFL(3) energies (maximum is 49).

IFL(4): Number of turning points calculated for each vibrational level, i.e. if IFL(4) = 3, turning points are calculated for each level and for two energies between each level. IFL(4) ignored if IFL(3) $\leq$ 0.

IFL(5): If > 0, a plot is produced.

The remaining 11 integers are not used by the program at this time.

```
I J YIJ(K)
FORMAT(4(2I2,E16.9))
```

No particular ordering of the Y_{ij}'s is necessary. If a set of I,J, and YIJ is blank, the program skips that set and goes on to the next. When the last I,J,YIJ set is read in, the next I,J pair should be "-1-1" in order to terminate the input routine.

I J K L YV(M) (For IFL(2) > 0, only)
FORMAT(4(4I2,E12.5))

Data input needed to construct the Y_{ij} variance matrix. If I=K and J=L, YV should be the standard deviation of Y_{IJ}. Otherwise, YV should be the correlation coefficient between Y_{IJ} and Y_{KL}. As with the Y_{ij}'s, order is not important. Data read-in is terminated by "-1-1-1-1" for I,J,K, and L.

GRKR(K),RKR1(K),RKR2(K) (For IFL(3) < 0, only)
FORMAT(F10.3,2F10.7)

These values are the G_v, inner and outer turning points to be read in. There should be |IFL(3)| levels.

If a new data set is to be processed, repeat the above beginning with the title card. If no new data sets remain, add a card with "STOP" on it, with "S" in the first column.

The following is a sample input deck to DUNPOT:

```
AR2/TO A4/BEST OF NOMINAL REVISITED (ERROR WITH CORRELATION)
COLBOURN, DOUGLAS/JCP 65/1741/76/N
39.9623842 39.9623842 18. 18. 99.545
    4    3    6    0    1
 1 0 31.333584       2 0 -2.8994762       3 0 .058648148     0 0
 0 1 .059773839      1 1 -3.785      E-03 2 1 -3.0535714 E-04-1-1
 1 0 1 0 .1174310    2 0 2 0 .0456292     3 0 3 0 .0050164     1 0 2 0 -.976687
 1 0 3 0 .937665     2 0 3 0 -.989455
 0 1 0 1 1.52616E-04 1 1 1 1 1.19277E-04 2 1 2 1 1.93155E-05 0 1 1 1 -.879247
 0 1 2 1 .769924     1 1 2 1 -.971625   -1-1-1-1
STOP
```

After the preceding input deck is processed, the information below is written on file COFOUT:

```
AR2/TO A4/BEST OF NOMINAL REVISITED (ERROR WITH CORRELATION)
COLBOURN, DOUGLAS/JCP 65/1741/76/N
 99.545 3.757579780737 39.9623842 39.9623842 18. 18.
 31.2280199187 .05976763028925 -.09070218154745
    1    6    7
 4.07908605E+03 3.75757978E+00-6.51476496E+00 2.07110471E+01-2.17597211E+01
-1.26214542E+01 5.97676303E-02
    2    6    8
 4.07908605E+03 3.75757978E+00-4.51476496E+00 4.16675228E+00 2.59958778E+01
 2.55427624E+01 5.97676303E-02 2.12890060E+05
    3    6    8
 1.34124727E+02 3.75757978E+00 5.51476496E+00-2.04469944E-01-8.87692408E-02
 1.05850079E-01 5.97676303E-02 1.08991215E+02
    4    6    9
 9.61092889E+01 3.75757978E+00 6.51476496E+00-9.53504890E-02-1.93977773E-02
 6.49804578E-C2 5.97676303E-02 9.13261402E+01 6.15532391E+00
   10    7
    14.859 3.5660978 4.0476667
    40.584 3.4676561 4.3791809
    61.038 3.4194167 4.7202768
    76.573 3.3915963 5.1252004
    87.540 3.3718093 5.6543510
    94.292 3.3394837 6.4519330
    99.545 0.        18.7878989
STOP
```

```
      PROGRAM CUMPOT(INPUT,OUTPUT,COFOUT,FILM,TAPE9,TAPE10,
     1 TAPE1=INPUT,TAPE2=OUTPUT,TAPE4=COFOUT)
      COMMON/OLNCOF/A(14),B(14),E(14),C(14),NOUN
      COMMON/RKRYIJ/YNC(10),NG,YN1(10),N3,YOC
      COMMON/YIJJ/YIJ(14),X(14),Y(14),Z(14),YTMP(14),XT(14),YT(14),ZT(14)
      COMMON/ERRSTUF/ AJ(14,14),BJ(14,14),EJ(14,14),CJ(14,14),
     1 AV(14,14),BV(14,14),EV(14,14),CV(14,14),YV(14,14),SCRTCH(14,14),
     2 DA(14),CB(14),CE(14),DC(14)
      INTEGER TITLE(8),IBF(4),JBF(4),KBF(4),LBF(4),IFL(16),NNFMT(8,6)
      INTEGER LITCHER(8)
      REAL ME,XBF(4),RKR1(102),RKR2(102),GPKR(102)
      DATA PE/.000548579/
      DATA (NPFMT(1,K),K=1,6)/10HDUNNAM CDE,10HFFICIENTS ,
     1 4*(10H          )/
      DATA (NPFMT(2,K),K=1,6)/10HSIMON-PARR,10H-FINLAN CO,10HEFFICIENTS,
     1 10H AND OSUBE,2*(10H          )/
      DATA (NPFMT(3,K),K=1,6)/10HTMAKKAR CO,10HEFFICIENTS,10H AND OSUBE,
     1 3*(10H          )/
      DATA (NPFMT(4,K),K=1,6)/10HMUFFAKER C,10HOEFFICIENT,10HS. OSUBE A,
     1 10HNC SIGMA  ,2*(10H          )/
      DATA (NPFMT(5,K),K=1,6)/10HDUNNAM CDE,10HFFICIENTS ,10HAND STD DE,
     1 10HVIATION   ,2*(10H          )/
      DATA (NPFMT(6,K),K=1,6)/10HSIMON-PARR,10H-FINLAN CO,10HEFFICIENTS,
     1 10H, OSUBE AN,10HD STD DEVI,10HATIONS     /
      DATA (NPFMT(7,K),K=1,6)/10HTMAKKAR CO,10HEFFICIENTS,10H, OSUBE AN,
     1 10HD STD DEVI,10HATIONS     ,10H          /
      DATA (NPFMT(8,K),K=1,6)/10HMUFFAKER C,10HOEFFICIENT,10HS. OSUBE. ,
     1 10HSIGMA AND ,10HSTD DEVIAT,10HIONS       /
      RSUBE(X) = SQRT(CNVRT/RML/X)
      CNVRT = 662.6176*6.02204E/(8.*(3.141592653589)**2*2.997924580)
1001  FORMAT(8A10)
1005  FORMAT(4HSTOP)
1101  FORMAT(1E15)
1401  FORMAT(4(2I2, E16.9))
1601  FORMAT(4(4I2, E12.5))
2001  FORMAT(1H1,20X,8A10)
2002  FORMAT(21X,8A10)
2202  FORMAT(5(1X,1PE13.6,7X))
2300  FORMAT(//20X,*THE YNG*S*/)
2400  FORMAT(//20X,*THE YN1*S*/)
2403  FORMAT(215,2(2X,1PE20.13))
2500  FORMAT(10(1X,1PE12.5))
2525  FORMAT(//11X*ATOMIC MASSES, ATOMIC NUMBERS, AND ESTIMATED DISSOCIA
     1TION ENERGY*/)
2530  FORMAT(/11X*M1, M2, AND MU (IN AMU*S) CORRECTED FOR ELECTRONS* MAS
     1SES*/)
2550  FORMAT(//20X,*YOC =*,F14.10,/)
2600  FORMAT(13(2X,F6.6))
2701  FORMAT(/1X,*++++++ WARNING: MAXIMUM NUMBER OF DUMMAR PARAMETERS =
     1 10 AT THIS TIME+++++*/1X*+++++ NOUN SET TO 9 ++++++*/)
2702  FORMAT(/1X*+++++ WARNING: MAXIMUM NUMBER OF YNG*S = 10 ++++++*/1X
     1*+++++ EXTRA YNG*S ARE IGNORED ++++++*)
2703  FORMAT(/1X*+++++ WARNING: MAXIMUM NUMBER OF YN1*S = 10 ++++++*/1X
     1*+++++ EXTRA YN1*S ARE IGNORED ++++++*)
3003  FORMAT(///,20X,*LATEST X AND Y=S*,/)
3004  FORMAT(/20X,8A10//,(5(1X,1PE20.13)))
3010  FORMAT(/11X,*YIJ VARIANCE MATRIX*/)
```

```
4000 FORMAT(/11X,*JACOBIAN MATRIX*/)
4001 FORMAT(/11X,*CORRELATION MATRIX*/)
5000 FORMAT(3I5/,(10,5E15.6))
6000 FORMAT(F10.3,2F16.7)
   1 CONTINUE
     DO 10 I=1,10
     X(I) = 0.  $  YIJ(I) = 0.
  10 Y(I) = 0.
     READ 1601, (TITLE(K), K = 1,8)
     IF(TITLE(1).EQ.4HSTOP) STOP
     PRINT 2001, (TITLE(K), K=1,8)
     READ 1001, LITCHER
     PRINT 2002, LITCHER
     READ*, RM1,RM2,Z1,Z2,DSUBE
     PRINT 2525
     PRINT*,RM1,RM2,Z1,Z2,DSUBE
     RN1=RM1-Z1*ME  $ RN2=RM2-Z2*ME
     RMU=RN1*RN2/(RN1+RN2)
     PRINT 2530
     PRINT*, RN1,RN2,RMU
     READ 1101, (IFL(J),J=1,16)
     NOUN=IFL(1)+2
     IF(NOUN.GT.8) NOUN=8
     IF(NOUN.GT.8) PRINT 2701
     IJNC = NE = NB = 0
     IFNB = IFNG = 0
     DO 16 KK=1,8
     READ 1401, ((IBF(K), JBF(K), XBF(K)), K=1,4)
     DO 15 K=1,4
     IJ = 2*IBF(K) + JBF(K)
     IF(IJ) 17,15,11
  11 IF(IJNC.LT.IJ) IJNC = IJ
     IF(JBF(K)) 13,13,12
  12 IB = IBF(K) + 1
     IF(IB.GT.10) IFNB=1
     IF(IB.GT.10) GOTO15
     YN1(IB) = XBF(K)
     IF(IB.GT.NB) NB=IB
     GO TO 14
  13 IG = IBF(K)
     IF(IG.GT.10) IFNG=1
     IF(IG.GT.10) GOTO15
     YN0(IG) = XBF(K)
     IF(IG.GT.NG) NG=IG
  14 YIJ(IJ) = XBF(K)
  15 CONTINUE
  16 CONTINUE
  17 CONTINUE
     PRINT 2300 $ PRINT*, (YN0(K),K=1,NG)
     PRINT 2400 $ PRINT*, (YN1(K),K=1,NB)
     IF(IFNG.EQ.1) PRINT 2702
     IF(IFNB.EQ.1) PRINT 2703
     CALL KALKAN(YIJ,X,Y,Z,A,E,E,C,NOUN,14)
     PRINT 2003
     DO 33 IJ=1,NOUN
     IJ02 = IJ/2   $   I = IJL2
     IJ02T2 = IJ02*2
```

```
      IF(IJ-IJC2T2) 30,30,31
   30 J = 0    $   GO TC 32
   31 J=1
   32 CCNTINUE
      PRINT 2403,I, J, X(IJ), Y(IJ)
   33 CONTINUE
      Y00 = .125*X(1)*(3.*A(4)-1.75*A(3)*A(3))
      PRINT 2550, Y00
      SIGMA = C(2)
      BOE=1.,B(3) $ ECE=COE=1.
      CO 35 I=4,NOUN
      BOE=BOE+B(I) $ ECE=ECE+E(I) $COE=COE+C(I)
   35 CCNTINUE
      BOE=B(1)*BOE $ ECE=E(1)*ECE $ COE=C(1)*COE
      A(2)=B(2)=E(2)=C(2)=RSUBE(X(1))
      IF(IFL(2)) 40,40,50
   40 PRINT3004,(NMFNT(1,K),K=1,6),(A(K),K=1,NOUN)
      PRINT3004,(NMFNT(2,K),K=1,6),(B(K),K=1,NOUN),ECE
      PRINT3004,(NMFNT(3,K),K=1,6),(E(K),K=1,NOUN),ECE
      PRINT3004,(NMFNT(4,K),K=1,6),(C(K),K=1,NOUN),COE,SIGMA
      GO TO 200
   50 CO 52 I=1,NOUN
      CO 52 J=1,NOUN
   52 YY(I,J)=C.
      DO 55 KK=1,250
      NEAC 1601, ((IBF(K),JBF(K),KBF(K),LBF(K),XBF(K)),K=1,4)
      CO 54 K=1,4
      IJ=2*IBF(K)+JBF(K) $ KL=2*KBF(K)+LBF(K)
      IF(IJ) 54,54,53
   53 IF(IJ.GT.IJNO.OR.KL.GT.IJNO) GOTO 54
      YY(IJ,KL)=YY(KL,IJ)=XBF(K)
   54 CCNTINUE
   55 CCNTINUE
   56 CCNTINUE
      NOM1=NOUN-1
      CO 75 I=1,NOM1
      IP1=I+1
      CO 74 J=IP1,NOUN
      YY(I,J)=YY(I,J)*YY(I,I)*YY(J,J)
   74 YY(J,I)=YY(I,J)
   75 YY(I,I)=YY(I,I)*YY(I,I)
      YY(NOUN,NOUN)=YY(NOUN,NOUN)*YY(NOUN,NOUN)
      PRINT 3010
      CO 79 I=1,NOUN
   79 PRINT2500, (YY(I,J),J=1,NOUN)
      CALL ERRANS(CNVRT,NOU,NOUN,14)
      OBOE=(OB(1)*BOE/B(1)**2)**2+OB(3)**2
      CEOE=(CE(1)*EOE/E(1)**2)**2
      CCOE=(CC(1)*COE/C(1)**2)**2
      CO 102 I=4,NOUN
      OBCE=OBOE+(OB(I))**2
      CEOE=OECE+(OE(I))**2
      CCOE=CCCE+(OC(I))**2
  102 CCNTINUE
      OSGM=(.5*OC(1)/C(1))**2+(CC(2)/C(2))**2+(OC(3)/C(3))**2
      OSGM=SIGMA*SQRT(CSGM)
      OBOE=B(1)*SQRT(CEOE)
```

```
      CEDE=E(1)*SQRT(CEDE)
      CCDE=C(1)*SQRT(CCCE)
      PRINT3004, (NMFMT(5,K),K=1,6),(A(K),K=1,NOUN)
      PRINT2202, (DA(K),K=1,NOUN)
      IF(IFL(2)-2) 120,115,111
111   PRINT4000
      DO 112 I=1,NOUN
112   PRINT2500, (AJ(I,J),J=1,ACUN)
115   PRINT4001
      DO 116 I=1,NOUN
116   PRINT2600, (AV(I,J),J=1,I)
120   PRINT3004, (NMFMT(6,K),K=1,6),(B(K),K=1,NOUN),BDE
      PRINT2202, (DB(K),K=1,NOUN),BDDE
      IF(IFL(2)-2) 130,125,121
121   PRINT4000
      DO 122 I=1,NOUN
122   PRINT2500, (BJ(I,J),J=1,NOUN)
125   PRINT4001
      DO 126 I=1,NOUN
126   PRINT2600, (BV(I,J),J=1,I)
130   PRINT3004, (NMFMT(7,K),K=1,6),(E(K),K=1,NOUN),ECE
      PRINT2202, (DF(K),K=1,NOUN),CEDE
      IF(IFL(2)-2) 140,135,131
131   PRINT4000
      DO 132 I=1,NOUN
132   PRINT2500, (EJ(I,J),J=1,ACUN)
135   PRINT4001
      DO 136 I=1,NOUN
136   PRINT2600, (EV(I,J),J=1,I)
140   PRINT3004, (NMFMT(8,K),K=1,6),(C(K),K=1,NOUN),CDE,SIGPA
      PRINT2202, (DC(K),K=1,NOUN),CCDE,DSGM
      IF(IFL(2)-2) 150,145,141
141   PRINT4000
      DO 142 I=1,NOUN
142   PRINT2500, (CJ(I,J),J=1,ACUN)
145   PRINT4001
      DO 146 I=1,NOUN
146   PRINT2600, (CV(I,J),J=1,I)
150   CONTINUE
200   CONTINUE
      IF(IFL(3).GT.0) CALL RKPASKR(A(2),X(1),IFL(3)-1,IFL(4),NPIN,RKR1,
     1 RKR2,GRKR)
      IF(IFL(3).GE.0) GOTO 205
      IRKR=-IFL(3)
      DO 204 K=1,IRKR
      READ 6000, GRKR(K),RKR1(K),RKR2(1)
204   CONTINUE
205   CONTINUE
      IF(IFL(5).GT.0) CALL PLOTFOT(TITLE,A(2),DSUBE,IFL(3),RKR1,RKR2,
     1 GRKR)
      WRITE(4,1001) TITLE
      WRITE(4,1001) LITCHER
      WRITE(4,*) DSUBE,A(2),RM1,RM2,Z1,Z2
      WRITE(4,*) X(2),X(1),YCO
      WRITE(4,5000) 1,ACUN,ACUN+1,(A(K),K=1,NOUN),X(1)
      WRITE(4,5000) 2,NOUN,NOUN+2,(B(K),K=1,NOUN),X(1),BDE
      WRITE(4,5000) 3,NOUN,NOUN+2,(E(K),K=1,NOUN),X(1),EDE
```

```
      WRITE(4,5000)  4,NOUN,NOUN+3,(C(K),K=1,NOUN),X(1),CDE,SIGPA
      IF(IFL(3).EQ.0)  GOTO  210
      IRKR=IABS(IFL(3))
      WRITE(4,1101)  10,IFL(3)+1
      WRITE(4,6000)  ((GRKR(K),RKR1(K),RKR2(K)),K=1,IRKR)
      WRITE(4,6000)  DSLOE,0.,5*A(2)
210   WRITE(4,1005)
      GO TO 1
       END
```

```
      SUBROUTINE KALMAN(YIJ,X,Y,Z,A,B,E,C,NDUN,NDIM)
      DIMENSION YIJ(NDIM),X(NDIM),Y(NDIM),Z(NDIM)
      DIMENSION A(NDIM),B(NDIM),E(NDIM),C(NDIM)
      REAL MACHEP
      MACHEP = 2.**(-47)
      DO1 I=1,NDUN
      X(I)=YIJ(I)
    1 A(I)=0.
      DO50 IT=1,30
      OMEGA = X(2)    ¢    BSUBE = X(1)
      CA = ABS((A(1)-OMEGA)/OMEGA) + ABS((A(2)-BSUBE)/BSUBE)
      A(1) = OMEGA    ¢    A(2) = BSUBE
      UE = 2.*BSUBE/OMEGA    ¢    UE2 = UE*UE
      UE3 = UE2*UE           ¢    UE4 = UE3*UE
      A1 = 2.*X(3)/OMEGA/UE2/3. - 1.
      CA = ABS((A(3)-A1)/A1) + CA
      A(3) = A1
        IF(NCUP - 4) 10,2,2
    2 A2 = 1.25*A1*A1 + 4.*X(4)/OMEGA/UE/3.
      CA = ABS((A(4)-A2)/A2) + CA
      A(4) = A2
        IF(NCUP - 5) 10,3,3
    3 A3 = (-5. + 3.*A2 + A1*(-10. + 13.*A2 - 7.5*A1*(1. + A1)) +
     1 4.*X(5)/OMEGA/UE3/3.)/5.
      Y(1) = BSUBE*.125*UE2*(15. - 9.*A2 + 15.*A3 + A1*(14. - 23.*A2 +
     1 10.5*A1*(1. + A1)))
      X(1) = YIJ(1) - Y(1)
      DA = ABS((A(5)-A3)/A3) + DA
      A(5) = A3
        IF(NCUP - 6) 10,4,4
    4 A4 = (A1*(35.*A3 + A1*(-56.25*A2 + 705.*A1*A1/32.)) + 8.5*A2*A2 +
     1 8.*X(6)/OMEGA/UE2)/10.
      Y(2) = OMEGA*UE2*(25.*A4 - 16.75*A2*A2 + A1*(-47.5*A3 + A1*(
     1 459.*A2/8. - 1155.*A1*A1/64.)))/16.
      X(2) = YIJ(2) - Y(2)
      DA = ABS((A(6)-A4)/A4) + DA
      A(6) = A4
        IF(NCUP - 7) 10,5,5
    5 A5 = (A1*(-21. + 45.*A2 - 105.*A3/4. + 25.5*A4 - 411.*A2*A2/8. +
     1 A1*(-225./8. + 945.*A2/16. - 435.*A3/8. + A1*(-141./4. +
     2 1509.*A2/16. - 3807.*A1*(1. + A1)/128.))) + A2*(8.5 + 22.5*A3 -
     3 51.*A2/4.) - 14.*A3 + 4.5*A4 - 7. + .8*X(7)/OMEGA/UE4)/7.
      Y(3) = BSUBE*UE3*.125*(175. + 190.*A3 - 112.5*A4 + 175.*A5 +
     1 A2*(-1613.5 - 357.5*A3 + 1005.*A2/8.) + A1*(285. + A2*(-459. +
     2 4677.*A2/8.) + 356.25*A3 - 397.5*A4 + A1*(2295./8. - 9639.*A2/16.
     3 + 5145.*A3/8. + A1*(288.75 - 14259.*A2/16. + 31185.*A1*(1. + A1)/
     4 128.))))
      X(3) = YIJ(3) - Y(3)
      DA = ABS((A(7)-A5)/A5) + DA
      A(7) = A5
        IF(NCUP - 8) 10,6,6
    6 A6 = 2.*(A1*(15.75*A5 - 483.*A2*A3/8. + A1*(-543.*A4/16. +
     1 4989.*A2*A2/64. + A1*(1953.*A3/32. + A1*(-2326.5*A2/256.
     2 + 23151.*A1*A1/1024.)))) + A2*(8.25*A4 - 75.*A2*A2/16.) +
     3 7.875*A3*A3 + 1.6*X(8)/OMEGA/UE3)/7.
      Y(4) = OMEGA*UE3*(245.*A6 - 271.25*A3*A3 + A2*(-442.5*A4 + 1707.*
     1 A2*A2/8.) + A1*(-682.5*A5 + 1533.75*A2*A3 + A1*(8535.*A4/8. -
```

```
    2 62813.*A2*A2/32. + A1*(-23865.*A3/16. + A1*(239585.*A2/128. -
    3 209055.*A1*A1/512.)))))/32.
      X(4) = YIJ(4) - Y(4)
      CA = ABS((A(3)-A6)/A6) + DA
      A(8) = AE
 10   CONTINUE
      IF(CA.LT.(FLOAT(NDUN)*PACHEP)) GOTO60
 50   CONTINUE
 60   CONTINUE
      A(1) = .25*OMEGA*OMEGA/ESUEE
      B(1) = A(1)  $  E(2) = A(2)
      B(3) = A(3) + 2.
      B(4) = A(4) + 3.*B(3) - 3.
      IF(NDUN-5) 111,103,103
103   B(5) = A(5) + 4.*B(4) - 6.*B(3) + 4.
      IF(NDUN-6) 111,104,104
104   B(6) = A(6) + 5.*B(5) - 10.*B(4) + 10.*B(3) - 5.
      IF(NDUN-7) 111,105,105
105   B(7) = A(7) + 6.*B(6) - 15.*B(5) + 20.*B(4) -15.*B(3) + 6.
      IF(NDUN-8) 111,106,106
106   B(8) = A(8) + 7.*B(7) - 21.*B(6) + 35.*B(5) - 35.*B(4)
     1 + 21.*B(3) - 7.
111   CONTINUE
      P = - A(3) + 1.
      P2 = P*P   $   P3 = P2*P   $   P4 = P2*P2
      P5 = P3*P2   $   P6 = P3*P3
      E(1) = A(2)/P2   $  E(2) = A(2)
      E(3) = P
      E(4) = (A(4) - 11./12. - P*(1.5 + 7.*P/12.))/P2
      IF(NDUN-5) 121,115,115
115   E(5) = (A(5) + 5./6. + P*(1.75 + P*(2.*E(4) + 7./6. + P*(2.*E(4)
     1 + .25))))/P3
      IF(NDUN-6) 121,116,116
116   E(6) = (A(6) - 13.7/18. - P*(1.875 + P*(17.*E(4)/6. + 119./72. +
     1 P*(5.*E(4) -2.5*E(5) + .625 + P*(13.*E(4)/6. - 2.5*E(5) +
     2 3.1/36.))))/P4
      IF(NDUN-7) 121,117,117
117   E(7) = (A(7) + .7 + P*(29./12. + P*(3.5*E(4) + 49./24. + P*(25.*
     1 (E(4)/3. - E(5)/6. + 1./24.) + P*(6.5*E(4) - 7.5*E(5) + 3.*E(6)
     1 + 3.1/12. + P*(5.*(E(4) - 2.*E(5))/3. + 3.*E(6) + .025)))))/P5
      IF(NDUN-8) 121,118,118
118   E(8) = (A(8) - 36.3/56. - P*(46.9/24. + P*(95.7*E(4)/24. +
     1 676.5/24. + P*(35.*(E(4) - .5*E(5) + .125)/3. + P*
     2 (299.*E(4)/24. - 14.375*E(5) + 5.75*E(6) + 71.3/144. + P*
     3 (35.*(.5*E(4) - E(5))/3. + 10.5*E(6) - 3.5*E(7) + .0875 +
     4 P*(1.0125*E(4) - 3.125*E(5) + 4.75*E(6) - 3.5*E(7) + 12.7/2016.
     5 )))))))/P6
121   CONTINUE
      RHO = 1. - X(2)*X(3)/X(1)/X(1)/6.
      RHO2 = RHO*RHO   $   RHO3 = RHO2*RHO   $   RHO4 = RHO2*RHO2
      RHO5 = RHO4*RHO   $   RHO6 = RHO3*RHO3   $   RHO8 = RHO4*RHO4
      TAU = X(2)*X(2)/X(1)/RHO2/4.
      S = 2.*TAU/X(2)   $   S2 = S*S   $   S3 = S2*S   $   S4 = S2*S2
      S5 = S2*S3   $   S6 = S3*S3   $   S7 = S4*S3   $   S8 = S4*S4
      C(3) = RHO   $   C(1) = TAU   $   C(2) = S
      IF(NDUN - 4) 210,204,204
204   C4 = 2.*(1. + S2*X(4)/TAU)/3.
```

```
      C(4) = C4
       IF(NOLN - 5) 210,205,205
205 C5 = (-5. + RHO*(10. + RHO*(-5.75 + 7.*RHO/6.)) - 3.*RHO2*(RHO - 1
    1 .)*C4 + 2.*S4*RHO8*X(5)/3./TAU)/5/RHO3
      C(5) = C5
       IF(NOLN - 6) 210,206,206
206 C6 = -C5 + (C4*(1. + 4.25*C4) + 2.*S3*X(6)/TAU)/5.
      C(6) = C6
       IF(NOLN - 7) 210,207,207
207 C7 = (-14. + RHO*(42. + RHO*(-139./3. + RHO*(25. + RHO*(-109./15. +
    1 + RHO)))) - 9.*RHO4*(RHO - 1.)*C6 + RHO3*(-28. + RHO*(30. - 9.*
    2 RHO/3.))*C5 + RHO2*(17. + RHO*(-34. + RHO*(17.75 - 13.*RHO/6.)) +
    3 45.*RHO3*C5 + 12.75*RHO2*(RHO - 1.)*C4)*C4 + .8*RHO8*S9*X(7)/
    4 TAU)/14./RHO5
      C(7) = C7
       IF(NOLN - 8) 210,208,208
208 C8 = -C7 + (3.*(C5 + C6) + 15.75*C5*C5 + C4*(16.5*(C5 + C6) +
    1 C4*(-3.25 - 75.*C4/9.)) + 1.6*S4*X(8)/TAU)/7.
      C(8) = C8
210 CONTINUE
      RETURN
       END
```

```
      SUBROUTINE ERRANS(CNVRT,FMU,NOUN,NOM1
      COMMON/YIJ/YIJ(14),X(14),Y(14),Z(14),YTMP(14),XT(14),YT(14),ZT(14)
      COMMON/ERRSTUF/ AJ(14,14),BJ(14,14),EJ(14,14),CJ(14,14),
     1 AV(14,14),BV(14,14),EV(14,14),CV(14,14),YV(14,14),SCRTCH(14,14),
     2 DA(14),CB(14),CE(14),DC(14)
      DIMENSION DLA(14),DRA(14),DLB(14),DRB(14),DLE(14),DRE(14),DLC(14),
     1 DRC(14)
      RSUBE(X) = SQRT(CNVRT/RHL/X)
      NCM1=NCUN-1
      DO 1 I=1,NOUN
    1 YTMP(I)=YIJ(I)
      DO  5 I=1,NOUN
      YTMP(I) = YIJ(I)*(1.+1.E-08)
      CALL KALKAN(YTMP,XT,YT,ZT,DLA,DLB,DLE,DLC,NOUN,NOM1)
      CLA(2)=CLB(2)=CLE(2)=CLC(2)=RSUBE(XT(1))
      YTMP(I) = YIJ(I)*(1.-1.E-08)
      CALL KALKAN(YTMP,XT,YT,ZT,DRA,DRB,DRE,DRC,NOUN,NOM1)
      DRA(2)=DRB(2)=DRE(2)=DRC(2)=RSUBE(XT(1))
      DO  4 J=1,NOUN
      AJ(J,I) = (DLA(J)-DRA(J))*5.E+07/YIJ(I)
      BJ(J,I) = (DLB(J)-DRB(J))*5.E+07/YIJ(I)
      EJ(J,I) = (DLE(J)-DRE(J))*5.E+07/YIJ(I)
      CJ(J,I) = (DLC(J)-DRC(J))*5.E+07/YIJ(I)
    4 CONTINUE
    5 YTMP(I) = YIJ(I)
      CALL JVJ(AJ,YV,AV,SCRTCH,NOUN,14)
      CALL JVJ(BJ,YV,BV,SCRTCH,NOUN,14)
      CALL JVJ(EJ,YV,EV,SCRTCH,NOUN,14)
      CALL JVJ(CJ,YV,CV,SCRTCH,NOUN,14)
      DO 10 I=1,NOUN
      CA(I)=SQRT(AV(I,I))
      CB(I)=SQRT(BV(I,I))
      CE(I)=SQRT(EV(I,I))
      CC(I)=SQRT(CV(I,I))
   10 CONTINUE
      DO 16 I=1,NOM1
      IP1=I+1
      DO 15 J=IP1,NOUN
      AV(I,J)=AV(I,J)/CA(I)/CA(J)
      AV(J,I)=AV(I,J)
      BV(I,J)=BV(I,J)/CB(I)/CB(J)
      BV(J,I)=BV(I,J)
      EV(I,J)=EV(I,J)/CE(I)/CE(J)
      EV(J,I)=EV(I,J)
      CV(I,J)=CV(I,J)/CC(I)/CC(J)
   15 CV(J,I)=CV(I,J)
      AV(I,I)=1.
      BV(I,I)=1.
      EV(I,I)=1.
   16 CV(I,I)=1.
      AV(NOUN,NOUN)=BV(NOUN,NOUN)=EV(NOUN,NOUN)=CV(NOUN,NOUN)=1.
      RETURN
       END
```

```
      SUBROUTINE JXJ(XJ,YV,XV,SC,NC,N)
      DIMENSION XJ(N,N),YV(N,N),XV(N,N),SC(N,N)
      DO 1 I=1,NO
      DO 1 J=1,NO
      XV(I,J)=0.
    1 SC(I,J)=0.
      DO 12 I=1,NO
      DO 12 J=1,NO
      DO 11 K=1,NO
   11 SC(I,J)=SC(I,J)+XJ(I,K)*YV(K,J)
   12 CONTINUE
      DO 22 I=1,NO
      DO 22 J=1,NO
      DO 21 K=1,NO
   21 XV(I,J)=XV(I,J)+SC(I,K)*XJ(J,K)
   22 CONTINUE
      RETURN
       END
```

```
      SUBROUTINE RKHNSKR(RSUBE,BSLBE,MAXV,INCREM,WMIN,FN,R),GV)
      COMMON/RKRYIJ/YNG(10),AG,YN1(10),NB,YOB
      COMMON/QUAD/NQ,XC(50),WC(50)
      DIMENSION FN(102),FX(102),GV(102)
2000  FORMAT(/10X*GAUSS-HERLER QUADRATURE FOR RKR CALCULATION USED *I3*
     1 POINTS*/)
3000  FORMAT(10X,*RMIN, RMAX, G OF V, F, AND G*/)
      PRINT2000,NQ
    1 IF(INCREM.EQ.0) INCREM=1
      NLEV = INCREM*(MAXV+1)
      CALL WRFIG(WMIN)
      CALL AENK(1,DUM,ESUBE)
      RINCVRS = 1./FLOAT(INCREM)
      V = -1.0
      PRINT 3000
      DO 9 ILEV = 1,NLEV
      V = V + RINCVRS
      W = V + .5
      CALL AENK(2,W,BSLBE)
      CALL KRNSKI(W,RN(ILEV),FX(ILEV),GV(ILEV),WMIN,RSUBE,ESUBE)
    9 CONTINUE
      END
```

```
      SUBROUTINE WHFIG(WPIN)
      COMMON/FKRYIJ/YNO(10),NG,YN1(10),N3,Y00
      DIMENSION YPP(10)
3000  FORMAT(/20X*WMIN FAILED TO CONVERGE.  FINISHED WITH*/1P,20X*WMIN =
     1 *E15.7,5X*AND THE LAST CORRECTION = *E15.7/)
      TINY = 5.E-15  $  WMIN = 0.
      DO 1 I=1,NG
    1 YPR(I) = FLOAT(I)*YNO(I)
      DO 3 IT =1,200
      F = FF = 0.  $  ICT = NG
      DO 2 I=1,NG
      F = WMIN*(YNO(ICT) + F)
      FP = YPR(ICT) + WMIN*FP
    2 ICT = ICT - 1
      F = F + Y00
      DELTA = F/FP
      WMIN = WMIN - DELTA
      IF(ABS(DELTA/WMIN)-TINY) 4,4,3
    3 CONTINUE
      PRINT3000, WMIN,DELTA
    4 RETURN
       END
```

```
      SUBROUTINE ABNK(IFL,N,BSLBE)
      COMMON/RKRYIJ/YN0(10),AG,YN1(10),NB,YOO
      COMMON/NETWEEN/ A(55),B(10)
      DIMENSION EIN(55)
      DATA EIN/1.,2.,1.,3.,3.,1.,4.,6.,4.,1.,5.,10.,10.,5.,1.,6.,15.,
     1 20.,15.,6.,1.,7.,21.,35.,35.,21.,7.,1.,8.,28.,56.,70.,56.,28.,
     2 8.,1.,9.,36.,84.,126.,126.,84.,36.,9.,1.,10.,45.,120.,210.,252.,
     3 210.,120.,45.,10.,1./
      IF(IFL-2) 100,200,200
  100 DO 1 J=1,NG
    1 YN0(J) = YN0(J)/BSUBE
      DO 2 J=1,NB
    2 YN1(J) = YN1(J)/BSUBE
      DO 3 I=1,NG
      DO 3 J=1,I
      IJ = (I*(I-1))/2 + J
    3 A(IJ) = EIN(IJ)*YN0(I)
      RETURN
  200 DO 5 I=1,NG
      B(I) = 0.  %  JCT = NG
      DO 4 J=I,NG
      JCTI = (JCT*(JCT-1))/2 + I
      B(I) = A(JCTI) + B(I)*W
    4 JCT = JCT - 1
    5 CONTINUE
      RETURN
       END
```

```
      SUBROUTINE KMNSKI(W,RN,RX),GV,WMIN,RSUBE,BSUBE)
      COMMON/RKRYIJ/YKC(10),NG,YN1(10),NB,Y00
      COMMON/GLAC/NGAUSS,XG(50),WG(50)
      COMMON/NBTWEEN/A(55),B(10)
3001  FORMAT(5X,2(F10.7,2X),F10.3,1P,2(2X,E15.7))
      F = G = 0.  $  WTOP = W - WMIN
      SQWTP = SQRT(WTOP)
      DO 2 I=1,NGAUSS
      XI = WTOP*.25*(XG(I)+1.)**2
      WP = W - XI
      BV = P = 0.  $  JCT = NG
      DO 1 J=1,NG
      P = B(JCT) - P*XI
    1 JCT = JCT - 1
      JCT = NB
      DO 4 J=1,NB
      BV = YN1(JCT) + BV*WP
    4 JCT = JCT - 1
      WT = WG(I)/SQRT(P)
      F = F +WT
      G = G + WT*BV
    2 CONTINUE
      F = SQWTP*F*RSUBE
      G = SQWTP*G/RSUBE
      RN = F*(SQRT(1. + 1./F/G) - 1.)
      RX = RN + 2.*F
      GV = 0.  $  JCT = NG
      DO 3 J=1,NG
      GV = (GV + YN0(JCT))*W
    3 JCT = JCT - 1
      GV = Y00 + BSUBE*GV
      PRINT3001, RN,RX,GV,F,G
      RETURN
       END
```

```
      BLOCK DATA RKRCC
      COMMON/QUAD/NQ,XC(50),WC(50)
      DATA NC/50/
C
      DATA XC/
C
     *606000045112447705429,606000030343674016144 8,606000737725344042658,
     *606001571134045030359,606002615613300362603,606004033505454063259,
     *606005440173650760263,606007230463555222425,606011201215770430258,
     *606013326331410526761 3,606015623531247472253,606020264322217606049,
     *606023063416544747579,606026013453244506728,606031066624564072548,
     *606034257022616506659,606037555724572657759,606105331373727006138,
     *606115111461623371209,606125034517650375173,606134541324556214 69,
     *606210547377557261023,606230262134353777769,606320226637177605448,
     *606500237016573144358,171277540761284644553,171417551140600173538,
     *171547515643424000329,171567230400220517218,171643272645322156538,
     *171652743260127402779,171662266631615406679,171671446404050771778,
     *171740222053205120179,171743520755161127123,171746711152313705238,
     *171751764324533271123,171754714361233030119,171757513455560171778,
     *171762154246530305553,171764451463672510148,171765765620073474 69,
     *171770547314122555269,171772337604127017378,171773744272323714468,
     *171775162164477415059,171776206643732747308,171777040052233735008,
     *171777474341037616123,171777732665330072139/
C
      DATA WC/
C
     *170757917226574057459,171067300516171121458,171153301772572137568,
     *171172716612671467262,171245063425464025058,171254466173007251058,
     *171263740437745474643,171273044044211 3 4578,171340771212646364478,
     *171344237125111167558,171347375105611415348,171352414677323160678,
     *171355313031656263013,171360051760467341373,171362454243341015229,
     *171364712316152575559,171366777653216602448,171370710204437332248,
     *171372437736121254 39,171374003561656714458,171375160455275446518,
     *171376144140714403639,171376734456334277773,171377330254430356269,
     *171377526350343424718,171377526350343423348,171377330254400355358,
     *171376734456334275739,171376144140714403508,171375160455375451179,
     *171374003561656714763,171372437773612122269,171370710204437333318,
     *171366777653216600219,171364712356152574648,171362454243341017378,
     *171360051760467341539,171355313031656262013,171352414677323230159,
     *171347375105611430329,171344237125111167178,171340771212646363768,
     *171273044044211326652,171263740457745474048,171254466173007255479,
     *171245063425464032439,171172716612671463078,171153301772572124018,
     *171067300516171115549,170757917226573663638/
C
      END
```

```
      SUBROUTINE PLOTPCT(MSG,RE,OE,IRKR,RKR1,RKR2,GRKR)
      COMMON/IGSZZZ/Z(200)
      COMMON/TKNAME/LT6/TXNAME/LTX/TKNAME/LTK/TTNAME/LTT
      DIMENSION R(1000),V(1000),LBLX(2),LBLY(2),MSG(8),NPAT(2,4)
      REAL RKR1(102),RKR2(102),GRKR(102),TKS(90)
      LOGICAL LIVE
      EXTERNAL FCNT2
      DATA INTPLT/0/
      DATA LBLX/*R (A*L1*S8*,*01*SU)      */
      DATA LBLY/*V (*LCM*U*,*4*-12*)      */
      DATA NPAT/*////*****//*,*//*****//*,*/////**/**,*/////**/**,
     1 */////*//**,*/////*////*,*/*/*/*/*/*,*/*/*/*/*/*/
1000  FORMAT(*PHIT ANY KEY*/*AND *RETURN**/*TO CONTINUE*)
1001  FORMAT(4A10)
      IF(INTPLT.EQ.1) CALL FRAME  $  IF(INTPLT.EQ.1) GO TO 50
      LIVE=.FALSE.  $  CALL TVINIT
      IF(LT6.NE.2HT6.AND.LTX.NE.2HTX.AND.LTK.NE.2HTK.AND.LTT.NE.2HTT)
     1 GO TO 40
      LIVE=.TRUE.  $  CALL CONNECT(4LFILM)  $  CALL CONNECT(5LTAPE9)
      CALL CONNECT(6LTAPE13)
   40 CALL MODES(Z,2,0) $ CALL SETSMG(Z,51,1.) $ CALL VECIG(Z,FCNT2,0)
      CALL SETSMG(Z,128,.25)  $  INTPLT=1
   50 CALL OBJ(TG(Z,15.,25.,100.,95.)  $  CALL SETSMG(Z,178,0.)
      X1=0. $ X2=5.*RE $ Y1=-.2*DE $ Y2=2.2*DE
      CALL SUBJE(Z,X1,Y1,X2,Y2) $ CALL GRIDG(Z,0.,0.,0.)
      CALL TICKGEN(X1,X2,20.,TKS,NXTK,XTK,NXXP)
      CALL TICKGEN(Y1,Y2,20.,TKS,NYTK,YTK,NYXP)
      CALL SETSMG(Z,102,1.)  $  CALL SETSMG(Z,103,1.)
      FMT=5.1 $ CALL LABELG(Z,0,XTK,0,FMT)
      FMT=7.0 $ CALL LABELG(Z,1,YTK,0,FMT)
      CALL SETSMG(Z,104,1.5)   $ CALL SETSMG(Z,105,1.5)
      CALL SETSMG(Z,178,1.)    $ CALL SETSMG(Z,45,2.)
      CALL LABELG(Z,0,XTK,1.0) $ CALL LABELG(Z,1,YTK,1.0)
      CALL SETSMG(Z,104,-1.5)  $ CALL SETSMG(Z,105,-1.5)
      NCHR=10
      DO 60 I=2,8
      IF(MSG(I).EQ.10H          ) GO TO 65
   60 NCHR=10*I
   65 CONTINUE
      CALL TXTLEG(Z,16,LBLX,16,LBLY,NCHR,MSG)
      CALL SETSMG(Z,45,1.)
      RINC=(X2-X1)/1000. $ DLET=(RE*.1-X1)*1000./(X2-X1)
      NDLET=IFIX(DLET) $ NPTS=1001-NDLET
      DO 105 NPT=1,4
      CUM2=VLVR(CUM1,NPT)
      RTS=RE*.1-RINC   $ NCAT=0
      DO 104 I=1,NPTS
      RTS=RTS+RINC
      VTS=VCPF(RTS,NPT)
      IF(VTS-Y1) 104,103,102
  102 IF(VTS-Y2) 103,103,104
  103 NCAT=NCAT+1
      R(NCAT)=RTS $ V(NCAT)=VTS
  104 CONTINUE
      CALL CASPG(Z,NCAT,R,V,NPAT(1,NPT),20.,30.,5)
  105 CONTINUE
      R(1)=X1 $ R(2)=X2 $ V(1)=V(2)=DE
```

```
      CALL LINESG(Z,2,R,V)
      IF(IPKR) 300,300,200
  200 DO 205 I=1,IRKR
      R(1)=RKR1(I) $ R(2)=RKR2(I) $ V(1)=V(2)=GRKR(I)
  205 CALL LINESG(Z,2,R,V)
  300 CONTINUE
      CALL EXITG(Z)
      IF(LIVE) WRITE(10,1000)
      IF(LIVE) READ(9,1001) NAPECUM
      RETURN
       END
```

```
      SUBROUTINE TICKGEN(MIN,MAX,MAXTICK,TICK,NOTICK,VALTICK,NEXP)
      DIMENSION TICK(50),MULTIPL(3)
      REAL MIN,MAX,MAXTICK
      DATA MULTIPL/1.,2.,5/
 1000 FORMAT(1PE8.1)
 2000 FORMAT(I3)
      RANGE = MAX - MIN
      ENCODE(8,1000,INTMO) RANGE
      NEXPCHR = SHIFT(INTMO,30)
      DECODE(3,2000,NEXPCHR) NEXP
      BIAS = 10**NEXP
      VALPRTK = ABS(RANGE/BIAS/MAXTICK)
      SCALE = .01
      DO 2 I=1,4
      DO 1 J=1,3
      TEST = SCALE*FLOAT(MULTIPL(J))
      IF(VALPRTK-TEST) 3,3,1
    1 CONTINUE
    2 SCALE = 10.*SCALE
    3 VALTICK = TEST*BIAS
      NTOP = INT(MAX/VALTICK) + 1
      NOTICK = 0
      DO 4 I=1,50
      TIKTEST = FLOAT(NTOP-I)*VALTICK
      IF(TIKTEST.GE.MAX) GO TO 4
      IF(TIKTEST.LE.MIN) GO TO 5
      NOTICK = NOTICK + 1
      TICK(NOTICK) = TIKTEST
    4 CONTINUE
    5 CONTINUE
      END
```

```
      FUNCTICN VCFR(RV,NRT)
      CCMMON/CLNCOF/A(56),NCUN
      DIMENSIOA LCT(4)
      CATA LCT/0,14,28,42/
C
C     ENTRY VOFR
       R=RV*RRE
       IF(NRT-2) 101,102,103
  101  X = R - 1.      $  GO TO 110
  102  X = 1. - 1./R   $  GO TC 110
  103  IF(NRT - 3) 104,104,105
  104  X = 1. - 1./R**F          $  XTRA = X  $  GO TO 110
  105  X = 1. - EXP(RMC*(1.-R))  $  XTRA = X
  110  F = 0.
       DO 111 I=NSTRT,NCUN
       II = NPLUS - I
  111  F = X*(F + A(II))
       VOFR = (1. + XTRA*F)*A(NO)*X**2
       RETURN
C
C     THIS  ENTRY INITIALIZES SEVERAL PARAMETERS TC BE USEC ABCVE
C
      ENTRY VOVR
       RRE=1/A(2)
       IF(NRT-3) 301,302,304
  301  NSTRT = 3  $  XTRA = 1.  $  GO TO 310
  303  F = A(31)  $  NSTRT = 4  $  GC TO 310
  304  RMO = A(45)  $  NSTPT = 4
  310  NPLUS=NSTRT+NOCUN+LCT(NRT) $ NO=1+LCT(NRT)
       VOFR = 7.
       RETURN
       END
```

APPENDIX II

This appendix is a synopsis of the program ERWIN (in honor of Erwin Schroedinger) which, like DUNPOT, is bereft of comment cards. The theory behind the algorithm and the mechanics of the program are briefly described, the formatting of the data input is outlined, and sample control card and input decks along with a program listing are provided.

For a simple $^1\Sigma$ state of a diatomic molecule, the radial equation is of the form:

$$-(\hbar^2/2\mu R)\frac{d^2}{dR^2}(R\psi) + (V(R)+(\hbar^2/2\mu R^2)J(J+1)-E)\psi = 0 \quad .$$

If we measure our reduced variable r in units of R_e and measure the reduced energy ε in units of B_e, and let the function $P = \psi/r$, the above equation reduces to

$$\frac{d^2}{dr^2}P(r) = (u(r)-\varepsilon)P(r) \quad ,$$

where

$$u(r) = V(R)/B_e + J(J+1)/r^2 \quad .$$

These reduced variables take the mass and equilibrium and internuclear distance out of the picture and have some other useful application. For one, the Bohr-Sommerfeld quantization becomes:

$$v + 1/2 = \frac{1}{\pi} \int_{r_-}^{r_+} \sqrt{u(r)-\varepsilon}\ dr \quad .$$

Moreover, the reduced well-depth, D_e/B_e, becomes the Harrison-Bernstein[1] well capacity parameter. The LeRoy-Bernstein[2] quantity, v_D, scales (within a factor of unity) as $(D_e/B_e)^{1/2}$, and a list of these scaling factors are given in Table I. The point here is to hopefully provide some insight into how the vibrational levels are spaced according to the well depth, independent of isotopic mass. It should be noted that the RKR f and g integrals are also simplified in these units.

The Numerov[3] solution to the radial equation assumes that $P(r)$ is known at r_i and r_{i-1}, and the function at r_{i+1} can be approximated by

$$Y_{i+1} = 2Y_i - Y_{i-1} + \delta^2(u_i-\varepsilon)P_i \quad ,$$

where $P_i \equiv P(r_i)$, etc., $Y_i = (1-\frac{1}{12}\delta^2(u_i-\varepsilon))P_i$, and $\delta = |r_i - r_{i-1}|$ (equally spaced r_i points). The use of Y_i instead of P_i in the difference equation reduces the error from δ^4 to δ^6.

In the Cooley procedure[3] for finding the vibrational energy from some initial guess, the wave function is set to some small number in the nonclassical region of the potential ($E_v < V(r)$), the wave function at the next point is estimated by the JWKB approximation, and the succeeding values at smaller r are calculated by the Numerov procedure until one arrives at the outer, absolute maximum,

or "matchpoint", of the wave function. The procedure is repeated starting from the inner nonclassical region until the outer, absolute maximum is achieved. The energy is systematically adjusted in order to improve the continuity of the derivative of the wave function at this matchpoint.

The notation used in the program code is actually that of Blatt[4], where $T_i \equiv \delta^2(u_i-\varepsilon)/12$. The intention is to incorporate some of his suggested modifications. Other future modifications should incorporate the higher order extension of the Numerov method outlined by Roothaan and Soukup[5]. At present, the program runs fast enough for our purposes, but the above modifications would facilitate the direct-fit discussed in Chapter III.

The program itself is written for the ad hoc purpose of calculating the vibrational energy levels and rotational constants for one potential only, where the parameters in the calculation are internally scaled by B_e and r_e. Although this scaling is aesthetically pleasing to this author, it should be modified for calculating Franck-Condon factors, where two potentials (and hence two sets of B_e and r_e) must be considered.

The potential used by the program is determined by the function routine VOFR(R), where R is in units of r_e. The routine must return the value of the potential in units of B_e. The routine also calculates the derivative through the entry VPRIME. A final entry, VUVR, is used at the beginning of the program to initialize the parameters used by the routine and returns the value of B_e to the main program

so that the program can output the energies in units other than B_e. The routine also calculates the centrifugal portion of the potential for $^1\Sigma$ states, i.e. the quantum number dependence is simply J(J+1). The function routine provided with the main program can calculate the potential energy for the Dunham, SPF, Thakkar and Huffaker series, but the modular form of this routine allows for substitution with a routine of any other functional form at linking time. An example is provided in the sample control card listing.

One of the weak points of the Numerov-Cooley algorithm is that the procedure converges on the energy level closest to the initial guess and pays no heed to the vibrational quantum number, v. A pre-processor, subroutine ENEW, estimates the energy level for a given v by iteratively solving the Bohr-Sommerfeld quantization condition mentioned earlier. This routine uses the auxiliary routine TP, which calculates the classical turning points for a given energy, and VOFR. The Gauss-Chebyshev quadrature points[6] used for calculating the Bohr-Sommerfeld integral and its energy derivative are tabulated, in octal, in BLOCK DATA CHEBYQD. The advantage of this pre-processor is that any energy guess can be given to this routine and, for a given v, an estimate correct to within 1% or less of the true value can be quickly made. In the event the iteration fails to converge, which occasionally happens when close to the top of the potential well, the routine returns the initial guess to the main program.

The subroutine, CASHION, is with a few minor modifications an unabashed copy of the function SCHR written by J. K. Cashion[7]. This is the Numerov-Cooley algorithm that determines the quantum mechanical

energy and wave function for the potential. It utilizes the subroutines TP, NRMLZ, and CALNODE. NRMLZ normalizes the converged wave function using a Simpson's rule integration. CALNODE, another Cashion creation, counts the number of nodes in the wave function in order to confirm that the energy for the correct v had been calculated.

Other subroutines are SETUPU, BSUBV, and EXTR. SETUPU calculates the array $\delta^2 u(r_i)/12$ used by CASHION. BSUBV calculates the rotational constant for each vibrational level by Simpson integration of ψ^2/r^2. EXTR is a dummy routine which can be replaced at link-time.

All input is read in through the main program ERWIN. Output is generated by ERWIN, ENEW, TP, and CASHION. Other I/O files in the program header card are ETCTRA, USW, and PSI. The first two of these files are unused and can be incorporated into a replacement routine for EXTR. PSI is a file to which the energies and wave functions may be written out (in binary) by routine CASHION.

Sample Control Decks

The following is for running on the 7600 with no program modifications:

```
(jobcard)
$ID=password
FETCHPS(JSWB,LGO,NEWN7S2)
LGO.
EXIT.
DUMP(0)
FIN.
END.
(7/8/9 card)
(data deck)
(6/7/8/9 card)
```

The next set compiles replacement files for the program's function routine, VOFR, and the subroutine EXTR. The latter routine will produce an auxiliary output file in the I/O file ETCTRA.

```
(jobcard)
$ID=password
FTN4,OPT=2,ROUND,B=VOFR.
FTN4,OPT=2,ROUND,B=EXTR.
FETCHPS(JSWB,ERWIN,NEWN7S2)
LINK,F=ERWIN,R=VOFR,R=EXTR,PP=[,,ETCTRA].
RETURN,ERWIN,VOFR,EXTR,FTN4LIB.
DISPOSE(ETCTRA=LP,T=[EXTRA/OUTPUT])
EXIT.
DUMP(0)
FIN.
END.
(7/8/9 card)
     (new VOFR function FORTRAN deck)
(7/8/9 card)
     (replacement FORTRAN subroutine for EXTR)
(7/8/9 card)
     (data deck)
(6/7/8/9 card)
```

The following is a description of the input structure and a sample input deck.

```
(ITITLE(I),I=1,8)
FORMAT(8A10)
```

One card of 80 characters, or fewer, labelling the data set.

```
NRT,NPR
FORMAT(16I5)
```

NRT: A flag determining which series potential is being used. The values 1,2,3, and 4 are for the Dunham, SPF, Thakkar, and Huffaker potentials, respectively. NRT is not used if a replacement function is used at link-time.

NPR: The number of potential parameters used in the potential function.

```
(A(I),I=1,NPR)
FORMAT(5E15.9)
```

These are the potential parameters used by function VOFR.

```
RCN,RCX
FORMAT(8F10.5)
```

These are the innermost and outermost values of r (in units of r_e) in which the potential is valid.

NEN,NPRIN,NCA,NGRID,IPRIN,NODE,NBV,NUMEROV.
FORMAT(16I5)

These are various integer flags and parameters. Their functions are:

NEN: The maximum number of iterations allowed to routine ENEW. If NEN=0, the pre-processor is not used.

NPRIN: Printing options in ENEW, which are:

= 0 : Only the converged energy is printed.

= 1 : Energies, corrections, etc., for each iteration are printed.

= 2 : Same as 1, except the classical turning points (in r_e) are printed for each iteration.

NCA: The maximum number of iterations allowed to CASHION. If 0, the routine is not employed.

NGRID: The number of grid points in the Numerov solution of the wave function. Maximum number is 5000, recommend more than 250.

IPRIN: Printing options for CASHION.

= 0 : Only the converged energy and the classical turning points are printed.

= 1 : Same as 0, except the energy, corrections, etc., are printed for each iteration.

NODE: Flag for the node counting routine.

= 1 : Number of nodes for each wave function are counted.

= 0 : The routine is skipped.

NBV: Flag for calculation of the rotational constant for each vibration level.

= 1 : B_v is calculated.

= 0 : Not calculated.

NUMEROV: Flag for printing out the wave functions (in binary) on I/O file PSI. Options are the same as NODE and NBV.

```
NV,NJ,TEO,TEPSWKB,TEPSNUM,TRN,TRX,TRTN,TRTX
FORMAT(2I5,3E10.4,4F10.5)
```

This data card is repeated for every energy level that is to be calculated.

NV: The vibrational quantum number.

NJ: The rotational quantum number.

TEO: Initial guess of the energy.

TEPSWKB: Convergence tolerance for ENEW. Energy units are the same at TEO. The energy units should be the same as that of B_e used in VOFR.

TEPSNUM: Convergence tolerance for CASHION.

TRN: Innermost point (in units of r_e) for the Numerov solution.

TRX: Outermost point for the Numerov solution.

TRTN: Inner classical turning point estimate for TE (in units of r_e).

TRTX: Outer classical turning point estimate for TEO.

Note: The above variables which have a "T" prefix must be given values for the first energy level. For the succeeding levels, if any or all of these variables are left blank, the refined values from the previous energy level calculation are used.

To terminate a data set and start a new one, insert a "-2" for NV and follow this card with the ITITLE card of the next data set. If a "-1" is inserted, a different series potential for the same molecule and the new data set should begin with the NRT, NPR card.

If no new data sets are to follow, insert a "-2" for NV and "STOP" for the title card, with the "S" beginning in the first column.

The following is a sample input deck to program ERWIN. The potential is the nominal Thakkar function for Ar_2. The "blank input" option described earlier is used extensively.

```
AR2/NOMINAL THAKKAR/TO E4
    3    6
31.228          .0597676        5.51476         -.20447         -.088769
.10585
.1          15.
   20    1   20 2000    1    1    1    0
    0    0 14.5       1.   E-02 1.   E-05 .7        3.          .85         1.3
    1    0
    2    0                                          4.
    3    0
    4    0                                          5.
    5    0                                          5.5
    6    0                                          6.
    7    0                                          10.
   -2
STOP
```

Note that the first two potential parameters above are ω_e and B_e as opposed to e_0 and r_e as outputted on file COFOUT by program DUNPOT.

REFERENCES

1. H. Harrison and R. B. Bernstein, J. Chem. Phys. 38, 2135 (1963).

2. R. J. LeRoy and R. B. Bernstein, J. Chem. Phys. 52, 3869 (1970); R. J. LeRoy, Molecular Spectroscopy 1 (a Specialist Periodical Report of the Chemical Society of London), edited by R. F. Barrow, D. A. Long and D. J.Miller (Chem. Soc., London, 1973) pp. 113-176.

3. J. W. Cooley, Math. Computation XV, 363 (1961).

4. J. M. Blatt, J. Comp. Phys. 1, 382 (1967).

5. C. C. J. Roothaan and G. A. Soukup, Int. J. Quantum Chem. 15, 449 (1979).

6. Handbook of Mathematical Functions (Ninth Printing), edited by Milton Abramowitz and Irene A. Stegun (Dover, New York, 1972) p. 889.

7. R. N. Zare and J. K. Cashion, Lawrence Radiation Laboratory Report UCRL-10881, July 1963, and R. N. Zare, UCRL-10925, November 1963: J. K. Cashion, J. Chem. Phys. 39, 1872 (1963).

Table I. Ratios of $(v_D+1/2)$ to the well capacity, $(D_e/B_e)^{1/2}$, for several model potentials.[a]

Potential	$(v_D+1/2)/(D_e/B_e)^{1/2}$
Muffin-Tin[b]	$(b/r_e)/\pi$
Sutherland-n	$[\pi(n/2-1)]^{-1}$
-6	0.15916
Lennard-Jones (m,n)	$\pi^{-1}(n-m)^{-3/2}(n^n/m^m)^{1/(2(n-m))}B(\frac{m/2-1}{n-m},3/2)$[c]
(12,6)	0.23858
Exp - 3[d]	0.94749
- 4	0.48178
- 5	0.32404
-6	0.24436
Morse	ρ^{-1} [e]

[a]Evaluated from the Bohr-Sommerfeld intergral for $E = D_e$ and $r_+ = \infty$.

[b]Square well with infinite inner wall, width of b, and outer "plateau" of D_e. r_e lies somewhere in the well.

[c]$B(x,y) = \Gamma(x)\Gamma(y)/\Gamma(x+y)$

[d]For Exp-n: $V(r) = D_e[\exp(2n(1-r))-2r^{-n}]$, r measured in units of r_e.

[e]ρ is the same as in the Huffaker-Morse potential of Chapter II.

```
      PROGRAM ERWIN(INPUT,OUTPUT,ETCTRA,JSW,PSI,
     1 TAPE3=ETCTRA,TAPE2=USW,TAPE1=PSI)
      COMMON/CHEBY/NCHEB,XCI(100),NCI(100),XCII(100),NCII(100)
      COMMON/CFISH/A(10),FOC,APR,NRT,FLN2
      COMMON/LCCLPOT/H,F,H2,RA,RX
      COMMON/PCTLUK/P(50000),U(50000)
      COMMON/PCTLUK/P(500000),U(500000)
      LEVEL2, P,U
      COMMON/CLTOFF/RCN,RCX
      COMMON/ETRA/XTR(50),ITR(50)
      DIMENSION ITITLE(8),NAME(4)
      DATA NAME/6HOUSHAP,3HSPF,7HTHAKKAR,8HHUFFAKER/
      DATA FLN2/0./
 1000 FORMAT(8A10)
 1010 FORMAT(16I5)
 1020 FORMAT(8F10.5)
 1030 FORMAT(5E15.9)
 1041 FORMAT(2I5,3E10.4,4F10.5)
 2000 FORMAT(1H1,40X8A10/)
 3000 FORMAT(/1H *NUMBER OF TERMS IN GAUSSIAN QUADRATURE =*I5/)
 3001 FORMAT(20X*USING THE *A10*POTENTIAL WITH*I5*  PARAMETERS*/)
 3002 FORMAT X*POTENTIAL IS VALID BETWEEN*F10.6* AND *F10.6/)
 3003 FORMAT(X*NEN    =*I5,10X*NPRIN =*I5,10X*NCA    =*I5,10X*NGRID =*I5,
     1 /1X*IPRIN =*I5,10X*NCCE   =*I5,10X*NBV    =*I5,10X*NUMERCV =*I5/)
 3004 FORMAT(//50X*FOR V =*I3* / J = *I3//* GUESS E = *F15.5* CM-1 AND E
     1PSILONS = *1P2(F10.3,X)/0PX*RANGE OF INTEGRATION BETWEEN *F10.6,
     2 * AND *,F10.4/* GUESS TURNING POINTS BETWEEN *F10.6* AND *F10.6/)
 3030 FORMAT(1P8(XE15.8))
    1 READ 1000,(ITITLE(I),I=1,8)
      IF(ITITLE(1).EQ.4HSTOP) STOP
      PRINT2000,(ITITLE(I),I=1,8)
      PRINT3000, NCHEB
    2 READ 1010, NRT, NPF
      PRINT3001, NAME(NRT), NPF
      READ 1030,(A(I),I=1,NPF)
      PRINT3030,(A(I),I=1,NPF)
      BSUBE = VUVR(DUMMY)
      READ 1020, RCN, RCX
      PRINT3002, RCN, RCX
      READ 1010, NEN, NPRIN, NCA, NGRID, IPRIN, NODE, NBV, NUMERCV
      IF(NUMERCV.GT.0) WRITE(1) ITITLE,NRT,NPF,A,NGRID
      PRINT3003, NEN, NPRIN, NCA, NGRID, IPRIN, NODE, NBV, NUMERCV
    3 READ 1041, NV, NJ, TEQ, TEPSWKB, TEPSNUM, TRN, TRX, TRTN, TRTX
      TFLN2 = FLN2  $  FLN2 = FLOAT(NJ*(NJ+1))
      IF(TEQ.NE.0.) EQ=TEQ
      IF(TEPSWKB.NE.0.) EPSWKB=TEPSWKB
      IF(TEPSNUM.NE.0.) EPSNUM=TEPSNUM
      IF(TRN.NE.0.) RN=TRN
      IF(TRX.NE.0.) RX=TRX
      IF(TRTN.NE.0.) RTN=TRTN
      IF(TRTX.NE.0.) RTX=TRTX
      IF(NV+1) 1,2,4
    4 PRINT3004, NV, NJ, EQ, EPSWKB, EPSNUM, RN, RX, RTN, RTX
      IF(NEN) 6,6,5
    5 CALL ENER(NEN,NPRIN,NV,E,EPSWKB,BSUBE,RTN,RTX,E)
      IF(NCA) 3,3,7
    6 E = EQ
```

```
7 IF(TRN.NE.0.OR.TRX.NE.0..OR.TFLN2.NE.FLN2) CALL SETUPU(NGRID)
  CALL GASIICN(IPRIN,NCA,NGRID,RTN,RTX,E,EPSNUM,BSUBE,NFLCNV)
  IF(NFLCN) 3,9,8
8 EQ=E
  NSTART=IFIX((RTN-RN)/H)   !  NSTOP=IFIX((RTX-RN)/H+.5)+1
  IF(NCCE.GT.0) CALL CALNCCE(NGRID,NODES,NSTART,NSTOP)
  IF(NBV.GT.0)  CALL BSUBV(NGRID,BSUBE,BV)
9 IF(NUMERCV.GT.0) WRITE(1) NV,NJ,NODES,BV,E,NFLCNV,P
  CALL EXTR(NGRID,NV,NJ,NODES,BV,BSUBE,E,EPSNUM,RTN,RTX,NFLCNV,
 *ITITLE)
  GO TO 3
   END
```

```
      SUBROUTINE ENEW(NCMOR,NPRIN,NV,EO,EPS,BSUBE,RTN,RTX,E)
      COMMON/CHEBY/NCHEB,XCI(100),WCI(100),XCII(100),WCII(100)
      COMMON/CCFISH/A(10),Y00,NFR,NRT,FLN2
      DIMENSION MARK(10)
      DATA MARK/10(1H*)/
      DATA PI/3.141592653589B/
2999  FORMAT(//30X*INITIAL GUESS OF E*/)
3000  FORMAT(2X*ITRN*6X*E*12X*CORRECTION*9X*INTEGRAL*9X*DERIVATIVE*/)
3001  FORMAT(X I5,1P4(2XE15.8))
3002  FORMAT(1F,/20X*FAILED TO CONVERGE.  GAVE E = *E20.13* ANYWAY*/)
3003  FORMAT(1F/10X10A1,3X*CONVERGED TO E = *E20.13,3X10A1/)
3004  FORMAT(/20X*>>>> E = V WAS NEGATIVE OR ZERO.  RESET E = EO. <<<<*
     1 /)
      VPH = FLOAT(NV) + .5      !      TPI = 2.*PI      !      E = EO/BSUBE
      EPSTEST = EPS/BSUBE
      PRINT2999
      IF(NPRIN.EQ.0) GO TO 1
      PRINT 3000
    1 CONTINUE
      DO 5 I=1,NCMOR
      CALL TPIE,RTN,RTX,NPRIN)
      RDEL = .5*(RTX-RTN)      !      RAV = .5*(RTN+RTX)
      RINT = RINP = 0.
      DO 2 K=1,NCHEB
      RC1 = XCI(K)*RDEL + RAV  !  RC2 = XCII(K)*RDEL + RAV
      EDIF = E - VOFF(RC1)
      IF(EDIF) 8,8,9
    9 GRAND1 = SQRT(EDIF)
      EDIF = E - VOFF(RC2)
      IF(EDIF) 8,8,10
   10 GRAND2 = SQRT(EDIF)
      RINT = RINT + WCII(K)*GRAND2
    2 RINP = RINP + WCI(K)/GRAND1
      RINT = RDEL*RINT/PI      !      RINP = RDEL*RINP/TPI
      DE = (VPH - RINT)/RINP
      IF(NPRIN) 4,4,3
    3 DERIN = DE*BSUBE
      EPRIN = (E)*BSUBE
      PRINT3001, I, EPRIN, DERIN, RINT, RINP
    4 IF(ABS(DE) - EPSTEST) 6,6,5
    5 E = E + DE
      EPRIN = E*BSUBE
      PRINT3002, EPRIN
      E = E*BSUBE
      RETURN
    6 CONTINUE
      EPRIN = E*BSUBE
      PRINT3003, MARK, EPRIN, MARK
      E = E*BSUBE
      RETURN
    8 E = EO
      PRINT3004
      RETURN
       END
```

```
      BLOCK DATA CHEBYCD
      COMMON/CHEBY/NCHEB,XCI(100),WCI(100),XCII(100),WCII(100)
      DATA NCHEB/100/
C
      DATA (XCI(I),I=1,50)/
C
     *171777737521710394319,171777733477142421479,171777632771342314069,
     *171777472071512271209,171777271066080242578,171777038037745507018,
     *171776527130466170418,171776164741373433378,171775564741466176385,
     *171775127331670487303,171774431246326616848,171773674502437234278,
     *171773101936363121529,171772506715051672285,171771362442471461138,
     *171770437166675075169,171767472424254445719,171766443240152240938,
     *171765337570505524629,171764271102471111678,171763134042176502438,
     *171761745114410711659,171760524767133675728,171757254166510046579,
     *171755753440006481369,171754423527234385375,171751304521423681301 8,
     *171751441072140039709,171750007747062032538,171746232443637206638,
     *171744631613241087359,171743106302320075198,171741341167217248705,
     *171677326302145576673,171673712771042244469,171670237664753025218,
     *171664631002440130725,171660767425152725219,171651752474677754675,
     *171651354200767042343,171645061640622376 05,171641611362374552218,
     *171573631151313237529,171563723571014633678,171554007056467344538,
     *171544044151471085459,171470136141726123279,171450127451143462075,
     *171360171261447241508,171240125241612303938/
C
      DATA (XCI(I),I=51,100)/
C
     *606637651535165477649,606417606516330540078,606327650326334316608,
     *606307641636051655279,606233733626306712659,606223778721310433609,
     *606214054206763144440,606204171662646540618,606136162641540322748,
     *606132271613715540340,606126423577010737603,606122602523010022253,
     *606117010352625052739,606113224677533764726 9,606107541130247525 18,
     *606104065600673553349,606100451475632201338,606036436610560532219,
     *606034671475457702739,60(033146164535710529,606031445334140571227,
     *606027770030715745329,606026336705637742178,606024732563541265078,
     *606023354250543422519,606022024337771326519,606020523611267731279,
     *606017253010674102133,606016032666376671 78,606014642735601275410,
     *606013596675336166168,606012404207272253238,606011334537625537328,
     *606010320535352332143,606007340611102702659,606006413335306316708,
     *606005527106272610613,606004762414465627 8,606004103275340543548,
     *606003346531451161769,606002650446107310525,606002211303661160168,
     *606001611303640434429,606001251064731160740 3,606000747740032270778,
     *606000500671717753523,606000300706265506608,606000014500643546372 8,
     *606000004300635356313,606000000405606723479/
C
      DATA (WCI(I),I=1,50)/
C
     *170540255610772300648,170660374356237174548,170750304623275013148,
     *170770366733760631339,171044206210131764258,171054176575123310048,
     *171064140673070742709,171074050473366727458,171141751002417667748,
     *171145654426771471259,171151534756657166108,171155370247371116733B,
     *171161174553750547143,171164750146710354409,171170470714410314279,
     *171174155046442325118,171177602622170440578,171241474110025735668B,
     *171243245715765541459,171244775641335407769,171246503022730704069,
     *171250164570327233663,171251622067602050038,171253232275015023348,
     *171254614605002164053,171256150430470770348,171257454725641211668,
     *171260731220751235059,171262154733107922629,171263347147037124029,
     *171264507364166401108,171265615117232013108,171266667522267032668,
```

```
*1712677063451603251109,1712766707755537770 9,1712716116377311731 2B,
*1712725073263603323 79,1712733423325525030 1B,1712741373047621547 8B,
*1712746757346135767 59,1712753756076722506 5,1712760363400116771 8,
*1712764376277711363 8,1712770014267030643 1B,1712773033524636074 8B,
*1712775452611326562 49,1712777470306371600 0B,1713400441577671161 7B,
*1713401045525564431 13,1713401247541404765 73/
C
 CATA (XCI(I),I=51,100)/
C
*1713401247541404765 08,1713401045525564431 1B,1713400441577671162 0B,
*1712777470306371600 19,1712775452611326562 59,1712773033524636074 8,
*1712770014267030643 29,1712764376277711363 8,1712760363400116771 9,
*1712753756076722506 9,1712746757346135767 7B,1712741373047621547 3B,
*1712733423325525030 59,1712725073263603323 49,1712716116377311731 69,
*1712706707755537770 39,1712677063451603251 58,1712666675222670327 4B,
*1712656111723203116 9,1712645073641664011 65,1712633471470271240 7B,
*1712621547331075226 7B,1712607312207512331 3B,1712593454729641211 76B,
*1712561954034077707 49,1712546146000021641 58,1712532322775015395 4B,
*1712516220676020501 39,1712501645703272337 59,1712465030211387044 59,
*1712447756413354105 8B,1712432457157554157 9,1712414741100257360 8B,
*1711776026221704410 35,1711741550464423253 2B,1711704787414103144 9B,
*1711647951467103145 73,1711611749507509472 1B,1711553762473711167 2B,
*1711519347556571663 29,1711485644267714714 48,1711417510021176701 4B,
*1710740504733667381 09,1710641436730707434 0B,1710141765751233103 4B,
*1710442026131746619 ,1707703667337505324 4B,1767503846232758146 2B,
*1706603743462372020 29,1705402556107723406 4B/
C
 CATA (XCII(I),I=1,50)/
C
*1777760114440415739,17 7770004720657162 68,1717775613401274787 9B,
*1717774025457651547 39,1717771644023026432 2B,1717767387736013660 8B,
*1717763728015275450 9,1717760165547516034 5B,1717754047626402303 9,
*1717747334414243354 79,1717742445024250247 8,1717734579550331136 4B,
*1717726552704076405 49,1717720156620443603 2B,1717711214574241327 3B,
*1717701710147612145 59,1717672044643230020 8,1717661646356466332 54B,
*1717651121164317353 29,1717640051312653513 29,1717626463360054241 8,
*1717614564410341220 19,1717602360233736742 08,1717567550237457454 8,
*1717554657470532531 09,1717541753564155773 3,1717529634163326645 8B,
*1717511621534003051 48,1717475343620630650 38,1717460630151161312 8B,
*1717443668522405703,1717426503670764422 69,1717411107130062747 9,
*1717376661623401172 19,1717326251635071440 8,1717267620076050600 38,
*1716641357501051211 49,1716604137400431142 78,1716546417061027567 8B,
*1716510415063642214 23,1716482150302044240 9,1716413457745475525 29,
*1715731345742705766 39,1715632201364256410 49,1715534522123501353 48,
*1715435564337203372 49,1714475024045647 3203,1714476142653704245 08,
*1713576947763542767 19,1711775646406713554 038/
C
 CATA (XCII(I),I=51,100)/
C
*6066002313710642307 69,6064201730014235016 8B,6063301635124073535 78,
*6063102753732130705 29,6062342213440574406 79,6062243256542764245 78,
*6062144576413521676 19,6062046432035072015 78,6061364320032320225 38,
*6061325527475733654 59,6061267362714135564 79,6061213607167502114 9,
*6061173503773466355 9,6061124202762656719,6061101517017271775 29,
*6061045152614270631 9,6061011161543766051 38,6060366706477150338 B,
*6060351274107133543,6060334113553247211 8,6060317147264616468 19,
*6060302434157147138 19,6060266156243774726 58,6060252143614451137 98,
```

```
*606023640242136223073,606022312030724524329,606021012275403203268,
*606017541754404103609,606016321366743656018,606015131441772353718,
*606013772246512426473,606012665661346042479,606011613142131445268,
*606010573313435477615,606007606763016563248,606006656320353645078,
*606005762115733417469,606005122507370137258,606004320212746264158,
*606003553327534275313,606003044336353442329,606002373501173547748,
*606001761223026174339,606001405275250233309,606001070100414176420B,
*606000613375473134563,606000375232012623053,606000214437630301708,
*606000077305712061529,606000017663337362048/
C
 DATA (WCII(I),I=1,50)/
C
*170577313101651023519,170677273332707476068,170757370747302700179,
*170777174526351526623,171047360417203616079,171057211713521165016,
*171067024315142223235,171076602271331201008,171143147475237360528,
*171146774476247120003,171152578236247172419,171153526245345442539,
*171162102246246162269,171165574776747425668,171171237031533225260,
*171174645560009376779,171240106005752544458,171241651764242212769,
*171243375043661623519,171245076451610351429,171246555551155452648,
*171250211516337561039,171251621517134514228,171253204753044524448,
*171254542653777762259,171256052446324776463,171257333371642337369,
*171260364720747707739,171261766142161703679,171261316557766075368,
*171264252710666652138,171265343107774021779,171266375725340445648,
*171267375546240635153,171270341775374626458,171271252251757670578,
*171272126212647327209,171272745313562736678,171273527246754722518,
*171274253545234645573,171274742136121701225,171275370367566411129,
*171275764247134467149,171276317360602145538,171276613547716650368,
*171277050657311225348,171277246571305641769,171277405207414476539,
*171277504252770636229,171277543704417426648/
C
 DATA (WCII(I),I=51,100)/
C
*171277543704417426649,171277504252770636028,171277405207414476538,
*171277246571305641773,171277050657311225359,171276613547716650378,
*171276317360602145543,171275764247134467153,171275372367566411138,
*171274742136121701229,171274253545234645628,171273527246754722528,
*171272745313562736709,171272126212647327219,171271252251757670625,
*171270341775074626479,171269375546240635168,171268343107774022029,
*171267375546240635148,171266252571066052148,171265136557766075408,
*171264176142161703739,171263064720747707749,171262333371642337418,
*171261605264032477659,171254542653770782308,171253204753044524478,
*171252162151713451423B,171250211516337561079,171246555551155452709,
*171245074451510331469,171243375043561623548,171241651764242213028,
*171240106100357254529,171174644556000537178,171171237031533225448,
*171165574775747425733,171162100246246162403,171153526245345442708,
*171152578236247172479,171146774476247120158,171143147475237360528,
*171107660227133120209,171067026315142223430,171057211713521652269,
*171047360417203616403,170777174526351527638,170757370747302700178,
*170677273332707502059,170577313101651023518/
  END
```

```
      SUBROUTINE TP(E,RTN,RTX,NPRIN)
      COMMON/CLTCFF/RCN,RCX
3000  FORMAT(7EX*R-INNER CONVERGED ON*I3* TO *F10.6)
3001  FORMAT(7EX*R-OUTER CONVERGED ON*I3* TO *F10.6)
      RTN1 = RTN      $      RTX1 = RTX
      DO 2 I=1,50
      IF(RTN1-RCN) 13,13,11
   11 IF(RTN1-1. ) 12,13,13
   12 DEL = (E-VDFR(RTN1))/VPRIME(RTN1)
      IF(ABS(DEL/RTN1) - 1.E-14) 3,3,1
    1 RTN1 = RTN1 + DEL
      ICT = I
    2 CONTINUE
   13 A = RCN      $      B = 1.
      DO 17 I=1,200
      ICT = ICT + 1
      RTN1 = (A+B)/2.
      IF((B-A)/RTN1-1.E-14) 3,3,14
   14 F = (E-VDFR(A))*(E-VDFR(RTN1))
      IF(F) 15,3,16
   15 B = RTN1
      GO TO 17
   16 A = RTN1
   17 CONTINUE
    3 RTN = RTN1
      IF(NPRIN-1) 5,5,4
    4 PRINT3000,ICT,RTN
    5 DO 7 I=1,50
      IF(RTX1-RCX) 19,20,20
   18 IF(RTX1-1. ) 20,20,19
   19 DEL = (E-VDFR(RTX1))/VPRIME(RTX1)
      IF(ABS(DEL/RTX1) - 1.E-14) 8,8,6
    6 RTX1 = RTX1 + DEL
      ICT = I
    7 CONTINUE
   20 A = 1.       $      B = RCX
      DO 24 I=1,200
      ICT = ICT + 1
      RTX1 = (A+B)/2.
      IF((B-A)/RTX1-1.E-14) 8,8,21
   21 F = (E-VDFR(A))*(E-VDFR(RTX1))
      IF(F) 22,8,23
   22 B = RTX1
      GO TO 24
   23 A = RTX1
   24 CONTINUE
    8 RTX = RTX1
      IF(NPRIN-1) 10,10,9
    9 PRINT3001,ICT,RTX
   10 RETURN
      END
```

```
      SUBROUTINE CASHION(IPRIN,NCMCR,N,RTN,RTX,E0,EPS,ESUBE,NFL)
      COMMON/LCCLPOT/HV,H,H2,RA,RX
      COMMON/PCTLUK/P(50000),U(50000)
$     COMMON/PCTLUK/P(50000),U(50000)
      LEVEL2, F,U
      DIMENSION MARK(100)
      DATA MARK/10(1H*)/
 1999 FORMAT(/30X*CCCLEY INTEGRATION RESULT*/)
 2000 FORMAT(2X*ITRN*9X*E*12X*CORRECTION*11X*F*13X*F-PRIME*7X*MATCHPOINT
    1*/)
 2001 FORMAT(1PXI5,4(2XE15.8)2XI6)
 2002 FORMAT(/10X10A1,3X*CONVERGED TO E = *1PE20.13,3X10A1/)
 2003 FORMAT(20X*THE TURNING POINTS ARE *F10.6* AND *F10.6/)
 2100 FORMAT(1P/20X*OCPS*  E SLOPED OVER TO *E15.2/)
 2101 FORMAT(20X*RENORMALIZE( AT M =*I5)
 2102 FORMAT(20X*OUTWARD INTEGRATION GAVE A ZERO AT THE MATCHPOINT ON IT
    1RN*I5)
 2103 FORMAT(/20X*FAILED TO CONVERGE.  E = *1PE20.13/)
      NFL=1
      PRINT1999
      IF(IPRIN) 2,2,1
    1 PRINT 2000
    2 CE = 0.     $   E = E0*HV/ESUBE    $   EPSTEST = EPS*HV/ESUBE
      OVFLO = 1.E+100      $      P1 = PN = 1.E-50
      DO 119 IT=1,NOMCR
       IN) = PN      $      SUMOUT = SUMIN = 0.
      TN = U(N) - E      $      TI = U(N-1) - E
      IF(TN) 100,100,101
  100 EPLIN = E*ESUBE/HV
      PRINT2100, EPPIN
      E0 = E*ESUBE/HV
      NFL=-1
      RETURN
  101 P(N-1) = P(N)*(TN/TI)**.25*EXP(SQRT(3.*TN)+SQRT(3.*TI))
      Y1 = (1.-TN)*PN
      Y2 = (1.-TI)*P(N-1)
      M = N - 2
  102 Y3 = Y2 + ((Y2-Y1) + 12.*TI*P(M+1))
      TI = U(M) - E
      P(M) = Y3/(1.-TI)
      IF(ABS(P(M))-OVFLO) 104,150,150
  150 PM = P(M)
      DO 103 K=M,N
  103 P(K) = P(K)/PM
      Y2 = Y2/PM      $      Y3 = Y3/PM
      PRINT 2101, M
  104 IF(ABS(P(M)) - ABS(P(M+1))) 107,107,105
  105 IF(M-5) 107,107,106
  106 Y1 = Y2      $      Y2 = Y3
      M = M - 1
      GO TO 102
  107 PMIN = P(M)      $      MTCH = M      $      YIN = Y2/PMIN
      MP1 = M+1
      DO 108 I=MP1,N
  108 SUMIN = SUMIN + P(I)*P(I)
      SUMIN = SUMIN/PMIN**2
      T1 = U(1) - E  $  T2 = U(2) - E  $  P(1) = P1
```

```
      Y1 = 0.  $  Y2 = (1.-T1)*P1  $  TI = T2
      ISTART = 2
      IF(T2.LE.0.) GO TO 109
      P(2) = P1*(T1/T2)**.25*EXP(SQRT(3.*T1)+SQRT(3.*T2))
      Y1 = Y2  $  Y2 = (1.-T2)*P(2)  $  TI = U(3) - E
      ISTART = 3
109   DO 112 I=ISTART,N
      Y3 = Y2 + ((Y2-Y1) + 1.5*TI*P(I-1))
      TI = U(I) - E
      P(I) = Y3/(1.-TI)
      IF(ABS(P(I))-OVFLO) 111,151,151
151   PI = P(I)
      DO 110 K=1,I
110   P(K) = P(K)/PI
      Y2 = Y2/PI      $      Y3 = Y3/PI
      PRINT2101, I
111   Y1 = Y2      $      Y2 = Y3
112   CONTINUE
      PMOUT = P(M)
      IF(PMCUT) 114,113,114
113   F = OVFLO      $      FPRP = -F
      CE = .001*E
      PRINT 2102, IT
      GO TO 116
114   YOUT = Y1/PMOUT      $      YM = Y2/PMOUT
      DO 115 I=1,M
115   SUMOUT = SUMOUT + P(I)*P(I)
      SUMOUT = SUMOUT/PMOUT**2
      F = (2.*YM - YIN - YOUT)/12. + TI
      FPRP = SUMIN + SUMOUT
      CE = F/FPRP
116   IF(IPRIN) 118,118,117
117   EPRIN = E*BSUBE/HV
      DPRIN = CE*BSUBE/HV
      PRINT2001, IT, EPRIN, DPRIN, F, YMM, NTCH
118   E = E + CE
      IF(ABS(CE) - EPSTEST) 120,120,119
119   CONTINUE
      E0 = EPRIN = E*BSUBE/HV
      PRINT2102, EPRIN
      NFL=0
      RETURN
120   CALL NPLZ(N,M,PMOUT,PMIN)
      EPRIN = E*BSUBE/HV      $      E = E/HV      $      E0 = E
      PRINT2002, MARK, EPRIN, MARK
      CALL TF(E,RTN,RTX,0)
      PRINT2003, RTN, RTX
      E0 = E*BSUBE
      RETURN
      END
```

```
      SUBROUTINE SETLFL(N)
      COMMON/LCCLPOT/HV,H,H2,RN,RX
      COMMON/PCTLUK/P(5000),U(5000)
$     COMMON/PCTLUK/P(50000),U(150000)
      LEVEL2, P,U
      H = (RX-RN)/FLOAT(N-1)
      H2 = H*H   $  HV = H2/12.
      R = RN
      DO 1 I=1,N
      U(I) = HV*VOFR(R)
    1 R = RN + I*H
      RETURN
       END
```

```
      SUBROUTINE NRMLZ(N,N,PNC,PNI)
      COMMON/LCCLPOT/PHO,H2,RH,RX
      COMMON/PCTLUX/P(50000),U(50000)
      COMMON/PCTLUX/P(50000),U(50000)
      LEVEL2, P,U
      E1 = E2 = O1 = C2 = 0.  $  PHO2 = PHO*PHO  $  PHI2 = PHI*PHI
      NM1 = N - 1  $  NP1 = N + 1  $  NM1 = N - 1
      DO 1 I=3,NM1,2
      O1 = O1 + P(I)**P(I)
      IP1 = I + 1
    1 E1 = E1 + P(IP1)*P(IP1)
      IF(N - N/2 - N/2) 2,2,3
    2 C2 = P(N+1)*P(N+1)
      MCNTN = N + 3
      GO TO 4
    3 C1 = O1 + P(N)**P(N)
      MCNTN = N + 2
    4 DO 5 I=MCNTN,NM1,2
      C2 = C2 + P(I)*P(I)
      IM1 = I - 1
    5 E2 = E2 + P(IM1)*P(IM1)
      TACKON = (P(1)*P(1) + P(2)*P(2))*H/2./PHO2
      C = O1/PHO2 + C2/PHI2
      E = E1/PHO2 + E2/PHI2
      SIMP = (P(2)*P(2)/PHO2 + P(N)*P(N)/PHI2 + 4.*O + 2.*E)*H/3.
      PNORM = SQRT(SIMP + TACKON)
      PNC = PNC*PNORM  $  PNI = PNI*PNORM
      DO 6 I=1,N
    6 P(I) = P(I)/PNO
      DO 7 I=NP1,N
    7 P(I) = P(I)/PNI
      RETURN
       END
```

```
      SUBROUTINE CALNCE(N,NCES,NSTART,NSTOP)
      COMMON/PCTLUK/P(50000),U(50000)
$     COMMON/PCTLUK/P(50000),U(50000)
      LEVEL2, F,L
      DIMENSION MARK(10)
      DATA MARK/10*(1H#)/
 2000 FORMAT(10X,10A1,3X,*NUMBER OF NODES = *I3,20X,10A1/)
      NCOES = 0
      DO 10 J=NSTART,NSTOP
      IF(P(J))    2,1,1
    1 IF(P(J-1)) 3,10,10
    2 IF(P(J-1)) 10,7,5
    3 IF(P(J+1)) 10,4,4
    4 IF(P(J-2)) 9,10,10
    5 IF(P(J+1)) 6,10,10
    6 IF(P(J-2)) 10,10,9
    7 IF(P(J+1)) 6,10,10
    8 IF(P(J-2)) 10,10,9
    9 NODES = NODES + 1
   10 CONTINUE
      PRINT2000,MARK,NCOES,MARK
      RETURN
       END
```

```
      SUBROUTINE BSUBV(N,BSUBE,BV)
      COMMON/LOCLPOT/HN,H,H2,RN,RX
      COMMON/PCTLUK/P(50000),U(50000)
$     COMMON/PCTLUK/P(500000),U(500000)
      LEVEL2, F,U
      DIMENSION MARK(10)
      DATA MARK/10*(1HE)/
 2000 FORMAT(10X,10A1,3X*ROTATIONAL BV   = *1PE28.13,3X,10A1/)
      BV = E = 0.  $  R = RN + 3.*H  $  D = (P(3)/(RN+2.*H))**2
      NM2 = N - 2
      TACKON = ((P(1)/RN)**2 + (P(2)/(RN+H))**2)*H/2.
      DO 1 I=4,NM2,2
      E = E + (P(I)/R)**2
      C = D + (P(I+1)/(R+H))**2
    1 R = R + 2*H
      BV = ((P(2)/(RN+H))**2 + 4.*D + 2.*E + (P(N)/RX)**2)*H/3. + TACKON
      BV = BSUBE*BV
      PRINT2000, MARK,BV,MARK
      RETURN
       END
```

```
      FUNCTION VOFR(R)
      COMMON/COFISH/A(10),Y00,ASR,NRT,FLN2
      DIMENSION AP(10)
C
C     ENTRY VOFR
       ANG = FLN2/(R*R)
       IF(NRT-2) 101,102,103
  101  X = R - 1.
       GO TO 110
  102  X = 1. - 1./R
       GO TO 110
  103  IF(NRT - 3) 104,104,105
  104  X = 1. - 1./R**R
       XTRA = X
       GO TO 110
  105  X = 1. - EXP(RHO*(1.-R))
       XTRA = X
  110  F = 0.
       DO 111 I=NSTRT,NPR
       II = NPLUS - I
  111  F = X*(F + A(II))
       VOFR = (1. + XTRA*F)*A1*X**2 + ANG
       RETURN
C
      ENTRY VPRIME
       ANGP = -2.*FLN2/(R*R*R)
       IF(NRT - 2) 201,202,203
  201  X = R - 1.
       GO TO 210
  202  X = 1. - 1./R      $      DXDR = 1./R**2
       GO TO 210
  203  IF(NRT - 3) 204,204,205
  204  X = 1. - 1./R**R      $      DXDR = R*(1. - X)/R
       XTRA = X
       GO TO 210
  205  X = 1. - EXP(RHO*(1.-R))      $      DXDR = RHO*(1.-X)
       XTRA = X
  210  F = 0.
       DO 211 I=NSTRT,NPR
       II = NPLUS - I
  211  F = X*(F + AP(II))
       VOFR = (2. + XTRA*F)*A1*X*DXDR + ANGP
       RETURN
C
C     THIS  ENTRY INITIALIZES SEVERAL PARAMETERS TO BE USED ABOVE
C
      ENTRY VUSR
       IF(NRT-3) 301,303,304
  301  BSUBE = A(2)      $      A1 = (A(1)/(2.*BSUBE))**2
       NSTRT = 3         $      XTRA = 1.      $      DXDR = 1.
       Y00 = 13.*A(4) - 1.75*A(3)**2 + (NRT-1)*2.*(1.-A(3))/3.
       GO TO 310
  303  R = A(3)          $      ESUBE = A(2)
       A1 = (A(1)/(2.*BSUBE*R))**2
       Y00 = (1. + R*(1. + 3.*A(4)*R))/9.
       NSTRT = 4
       GO TO 310
```

```
304   RHO = A(3)      1      A1 = (A(2)*RH3)**2
      ESUBE = A(1)/A1      1      NSTRT = 4
      Y80 = 3.*RHO**2*A(4)/8.
310   DO 311 I=NSTRT,NPF
311   AP(I) = FLOAT(I)*A(I)
      NPLUS = NSTRT + NPF
      VOFR = ESUBE
      RETURN
      END
```

```
      SUBROUTINE EXTR(N,NV,NJ,ACOES,3V,BSUBE,E,EPS,RTN,RTX,NFL,
     $ITITLE)
      DIMENSION ITITLE(8)
C
C     THIS IS A DUMMY SUBROUTINE.  REPLACE IT AT YOUR WHIM WITH
C     YOUR VERSION.  SUGGEST YOU COMPILE YOUR VERSION AND REPLACE
C     THIS ONE WITH A 'R=<BINARY FILENAME>' IN THE LINK CONTROL CARD
C
      RETURN
      END
```